Experiments with GMTI Radar Using Micro-Doppler

Benjamin W. Dilsaver

A thesis submitted to the faculty of
Brigham Young University
in partial fulfillment of the requirements for the degree of

Master of Science

David G. Long, Chair
D. J. Lee
Neal K. Bangerter

Department of Electrical Engineering

Brigham Young University

June 2013

ABSTRACT

Experiments with GMTI Radar Using Micro-Doppler

Benjamin W. Dilsaver
Department of Electrical Engineering, BYU
Master of Science

As objects move, their changing shape produces a signature that can be measured by a radar system. That signature is called the micro-Doppler signature. The micro-Doppler signature of an object is a distinguishing characteristic for certain classes of objects. In this thesis features are extracted from the micro-Doppler signature and are used to classify objects. The scope of the objects is limited to humans walking and traveling vehicles. The micro-Doppler features are able to distinguish the two classes of objects. With a sufficient amount of training data, the micro-Doppler features may be used with learning algorithms to predict unknown objects detected by the radar with high accuracy.

ACKNOWLEDGMENTS

TABLE OF CONTENTS

LIST OF TABLES

LIST OF FIGURES

CHAPTER 1.   INTRODUCTION

1.1   Motivation

A radar uses a radio frequency (RF) signal to measure characteristics about objects it detects within it's field of view. A radar can measure an object's range and Doppler. However, these measurements are generally not uniquely defining characteristics for classifying objects. This makes some of the radars' basic measurements difficult for use in classifying objects.

An additional measurement radar can provide is of the micro-Doppler signature of an object. Micro-Doppler comes from small movements the radar is able observe. The types of motion that generate micro-Doppler include vibration, rotation, swinging, and flapping. A moving object may include these motions as part of its movement. These motions combine to create an objects' micro-Doppler signature.

Because objects use different methods of travel, the micro-Doppler signature can be a differentiating characteristic that a radar can measure. Features can be extracted from the micro-Doppler signature. These features can then be used to identify or classify an object. The micro-Doppler signature allows a radar to be used to classify objects.

1.2   Thesis Statement

This thesis uses information collected by a simple radar and extracts more than just the range and Doppler about an object. Using the information in the micro-Doppler signature of an object, humans walking and traveling vehicles can be differentiated with a high degree of confidence.

1.3   Contributions

This thesis provides information on using the radar-derived micro-Doppler signature to classify humans walking and traveling vehicles. A simple set of micro-Doppler features is considered. This set of features is the micro-Doppler maximum, micro-Doppler variability, micro-Doppler bandwidth, and micro-Doppler span. This feature set is very simple and could be implemented for real-time processing applications.

Radar data is collected to analyze each of these features. The ability of the features to distinguish vehicles and humans walking is documented. The features are combined in a feature vector and are analyzed using a few common learning algorithms. The learning algorithm performance in classifying the results is evaluated and compared.

1.4   Thesis Organization

This thesis is organized into seven remaining chapters. Chapter 2 provides general background on radar theory. The chapter covers the measurement of an object's range and Doppler using radar. The chapter provides a brief overview of different types of radar systems and the radar signal processing used in the radar data analysis of this thesis.

Chapter 3 provides an introduction to measuring Doppler with high resolution. One application of high Doppler resolution is measuring micro-Doppler, which is also introduced along with different micro-Doppler profiles of motion. The scope of the thesis is presented as the study of micro-Doppler signatures of people and vehicles. Some hypothesis are made about the micro-Doppler signatures of these two classes of objects.

Chapter 4 covers the feature based extraction technique developed for extracting information from the micro-Doppler signature. The four micro-Doppler features created as part of this feature extraction are: micro-Doppler maximum, micro-Doppler variability, micro-Doppler bandwidth, and the micro-Doppler span. The features are extracted from a simulated dataset of a vehicle and a human walking. The features from the simulated data for each class of object are compared.

Chapter 5 details the radar data collection. Radar data was collected and organized into 41 datasets. These datasets consisted of various examples of a human walking and multiple types of traveling vehicles. The data is prepared for the micro-Doppler features to be extracted.

Chapter 6 analyzed the four features using the radar data that was collected in the experiment described by Chapter 5. The features are extracted from the 41 datasets and each feature is analyzed to measure how well it is able to distinguish humans walking from traveling vehicles.

Chapter 7 explores creating a feature vector from the four features and using that feature vector in various learning algorithms to compare the performance of different types of learning algorithms.

Chapter 8 concludes the thesis and suggests possible future work to be done.

CHAPTER 2.   BACKGROUND

2.1   Radar

Radar is a active sensing technique in which interactions of electromagnetic waves with physical objects are used to derive information about those objects. Electromagnetic energy is transmitted from an aperture, normally an antenna. That energy travels through the air as a wave and interacts with objects along its path. As the wave comes in contact with the objects, some of the energy is reflected back towards the radar system. The amount of the energy that is reflected is dependent on the characteristics of the object such as surface roughness and dielectric constant. A material with a high dielectric constant reflects more energy. A material with a greater surface roughness scatters more energy. The wave that is reflected from the object back to the radar is the sum of the surface roughness, dielectric constant, and the incident angle. Some energy reflected from the object propagates back toward the radar system as a received signal. The received waveform matches the transmitted waveform, except it has a time delay and a potential Doppler shift (explained in detail in Section 2.2). The time delay results from the travel time ("time of flight") to and from the object. This time corresponds to the object's range (distance) from the radar aperture.

The transmitted waveform ($s_t(t)$) produced by the radar) can be represented as the following:

$$s_t(t) = A_t \sin(2\pi f_0 t) \tag{2.1}$$

where A_t is the amplitude of the transmitted waveform and f_0 is the center frequency of the transmitted waveform in Hertz (Hz). The received signal from a single object can then be represented by

$$s_r(t) = A_r \sin(2\pi f_0(t - \tau)) \tag{2.2}$$

where A_r is the amplitude of the received signal and τ is the time delay in seconds,

$$\tau = \frac{2R}{c} \tag{2.3}$$

where R is the range, in meters, to the target and c is the speed of light in (m/s).

A typical function of the radar is to measure an object's range, R, from the radar. In order for the radar to measure this time delay and calculate range (see Eq. 2.3), the received signal is usually converted to a lower frequency. A lower frequency has many advantages such as the signal is less lossy, easier to process, and easier to digitize. Converting the signal to a lower frequency is known as down conversion. The signal is down converted using a mixer. Figure 2.1 depicts a mixer.
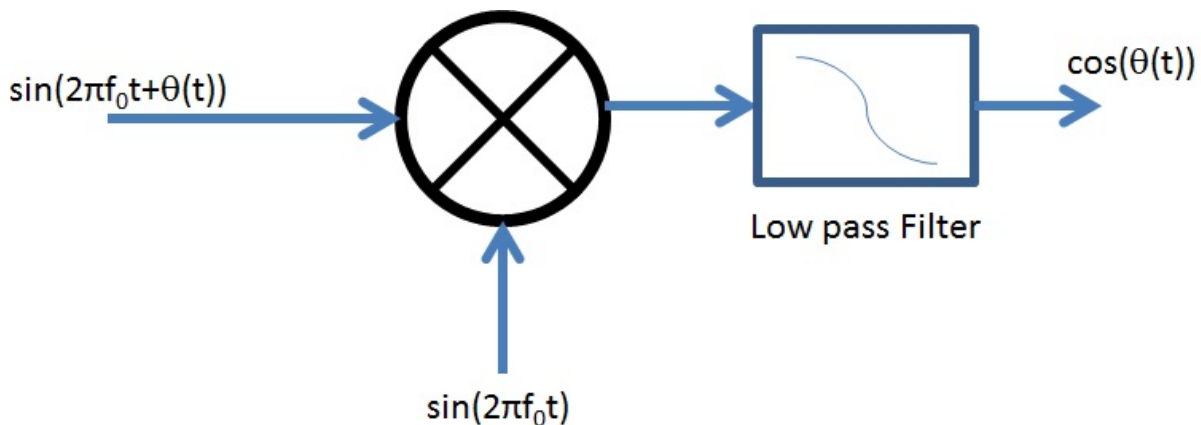
Figure 2.1: Diagram of a mixer. Transmitted and received signals are multiplied together and then the result is low pass filtered to produce the final output.

In the mixer the received signal is multiplied with the transmitted signal. The received signal enters the radar as a wave described by Eq. 2.2 and then is mixed with the transmitted signal, a wave described by Eq. 2.1. The following product-to-sum trigonometric identity can be used to compute the output of the mixer:

$$\sin(\theta)\sin(\varphi) = \frac{\cos(\theta - \varphi) - \cos(\theta + \varphi)}{2} \tag{2.4}$$

5

where θ and φ are angles. If θ and φ represent the transmitted and received waveforms, respectively, substituting the transmitted and received waveforms into Eq. 2.4 results in

$$
\begin{aligned}
\sin(2\pi f_0 t)\sin(2\pi f_0(t-\tau)) = \\
\frac{\cos(2\pi f_0 t - (2\pi f_0(t-\tau))) - \cos(2\pi f_0 t + 2\pi f_0(t-\tau))}{2},
\end{aligned}
\tag{2.5}
$$

which reduces to

$$
\sin(2\pi f_0 t)\sin(2\pi f_0(t-\tau)) = \frac{\cos(\tau) - \cos(4\pi f_0(t-\tau))}{2}.
\tag{2.6}
$$

The right-hand side of Eq. 2.6 is the cosine of the time shift added to the cosine of the time shift plus twice the carrier frequency. These two signals are separated by a large frequency difference: the first term is low in frequency; the second term is very high in frequency. To isolate the two signals a low pass filter is used, which eliminates the second term and preserves the low frequency first term and results in the following equation:

$$
\sin(2\pi f_0 t)\sin(2\pi f_0(t+\tau)) \approx \frac{\cos(\tau)}{2}.
\tag{2.7}
$$

This is the end result of mixing the transmitted signal with the received signal and preforming a low pass filter. This equation represents a simple relationship for calculating range as it is the *cosine* of the time delay due to the time of flight. A radar can measure an objects range by transmitting a signal and then receiving the echo from the object. Measuring an objects range is an essential function in locating and tracking objects.

2.2 Doppler

As with other waves (i.e., sound, light, etc.), electromagnetic waves produced by radar systems are subject to the Doppler effect. The Doppler effect is caused by changes in the distance between a wave source and an object due to movement of one or the other. As a result of these changes in distance, waves are compressed or expanded causing the apparent frequency of the wave to change. For example as a train passes by a stationary listener, the frequency of the train horn

seems to change from low to high frequency. These observed frequency changes are a result of the Doppler effect. A Doppler shift is induced by an object's relative movement, either toward or away from a wave source. The Doppler effect shifts the frequency of the received signal. Determining an object's position and velocity relative to a wave source requires multiple received signals over time since instantaneous Doppler shift is difficult to measure.

As previously noted the transmitted waveform can be represented by Eq. 2.1. In Eq. 2.2 the received waveform had a time delay, due to the range of the object. However, due to the Doppler effect the received wave can also have a Doppler shift. A received signal with a Doppler shift based on the object moving towards the radar or vise versa is given by

$$s_r(t) = A_r \sin(2\pi f_0(t - \tau_{radial}(t))) \tag{2.8}$$

where A_r is amplitude of the received signal, f_0 is the center frequency of the received signal in Hertz (Hz), and τ_{radial} is a time delay with radial velocity due to motion from either the object or radar. For a stationary object, τ is given by Eq. 2.3. However, a moving object has a radial velocity and induces a Doppler shift as it moves. Because range is now a transient term due to velocity, the range term R in Eq. 2.3 can be expressed by

$$R = R_0 + v_r t \tag{2.9}$$

where R_0 is the initial range in meters and v_r is the velocity in the radial direction given in meters per second and t is time in seconds. Equation 2.9 is the kinematic equation for range and can be substituted into the Eq. 2.3 for τ to produce

$$\tau_{radial}(t) = \frac{2R_0 - 2v_r t}{c}. \tag{2.10}$$

When this equation is then substituted into Eq. 2.8, the received signal, becomes

$$s_r(t) = A_r \sin(2\pi f_0(t - \frac{2R_0}{c} + \frac{2v_r t}{c})). \tag{2.11}$$

This received signal has a time delay due to the object's range and a Doppler shift due to velocity. Similar to the previous analysis, the received signal is multiplied by the transmitted signal in the down conversion process. If f_D, the Doppler frequency shift, is represented by

$$f_D(t) = \frac{2v_r t}{c} \tag{2.12}$$

and

$$\tau = \frac{-2R_0}{c}, \tag{2.13}$$

then Eq. 2.6 becomes

$$\sin(2\pi f_0 t)\sin(2\pi(f_0 + f_D)t + \tau) = \\ \frac{\cos(f_D + \tau) + \cos(4\pi(f_0 + f_D)t + \tau)}{2}. \tag{2.14}$$

This equation can then be simplified in a similar manner, as previously outlined, by low pass filtering the right-hand side. The result is

$$\sin(2\pi f_0 t)\sin(2\pi(f_0 + f_D)t + \tau) = \frac{\cos(f_D + \tau)}{2}. \tag{2.15}$$

Equation 2.15 is very similar to Eq. 2.7, derived in the previous section. Equation 2.7 was the analysis of a received radar signal of a single object separated from the radar by a range. When Doppler shift was added to the derivation, the end result is the range analysis with an additional term accounting for the object's Doppler shift.

2.2.1 Relationship between Doppler Shift and Radial Velocity

Radial velocity is directly related to the Doppler shift. Understanding this relationship clarifies how a radar is measuring velocity and what those measurements mean.

Radial Velocity

The frequency of the Doppler shift generated by a moving object is directly related to the velocity that the object is traveling in the radial direction. Figure 2.2 illustrates an object with

velocity vector comprised of radial and tangential components. The equi-range lines are concentric circles representing a single range to the radar. The radial velocity is the component of an object's velocity vector that is perpendicular to the equi-range lines. Tangential velocity is the velocity component that is tangential to the equi-range lines. If the object is traveling directly towards or away from the radar, then the tangential velocity component has zero magnitude. If an object is not traveling directly towards or away from the radar, then some component of the velocity is in the radial direction and some component is in the tangential direction.

Doppler frequency shift is directly related to the radial velocity by
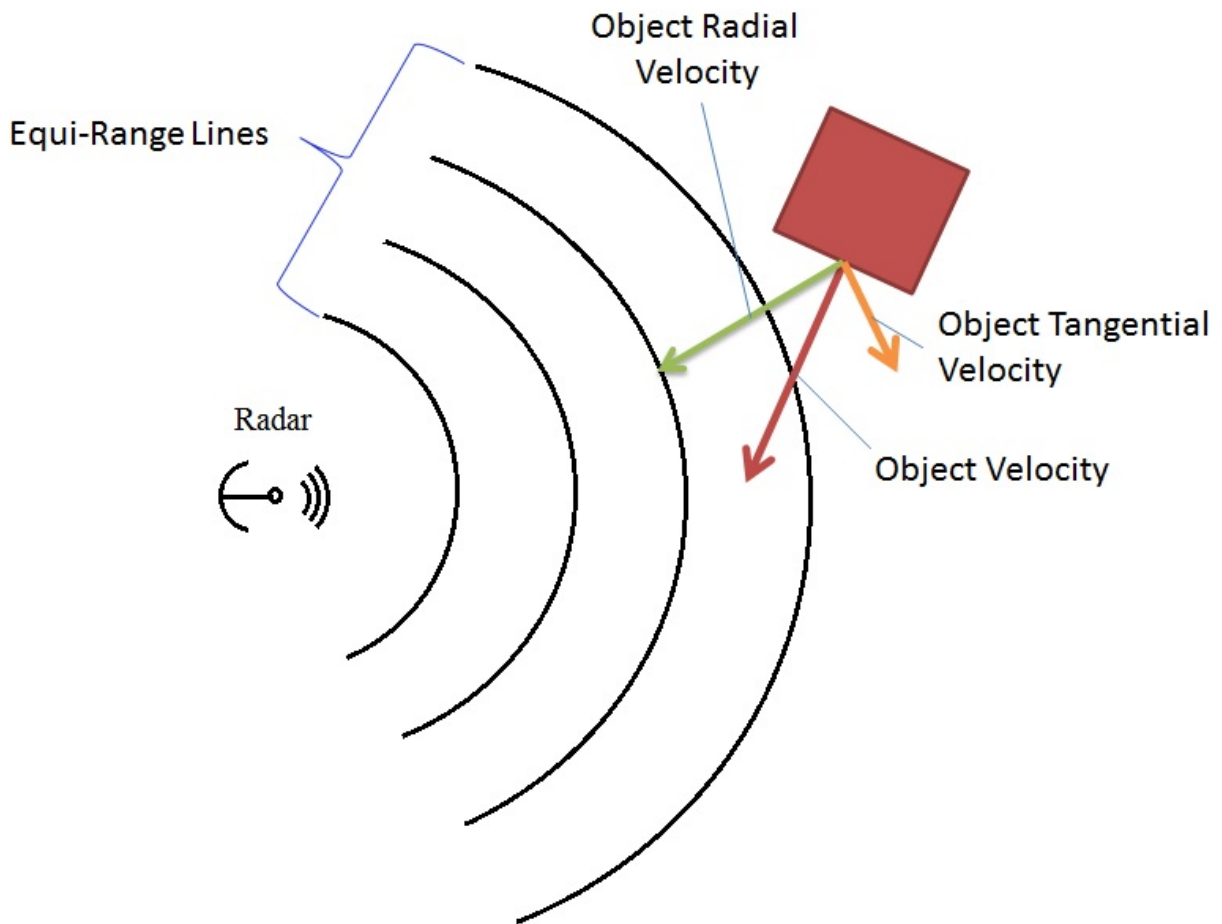
Figure 2.2: An object with a velocity vector, shown by the red arrow, traveling in proximity to a radar system. The object's velocity can be decomposed into a radial (shown by the green arrow) and tangential (shown by the orange arrow) component.

Table 2.1: Table of various targets, common speeds, and the Doppler shift associated with a particular speed for λ=3 cm.

Target	Speed(MPH)	Doppler Shift(Hz)
Person Walking	3.5	104.38
Person Running	15.0	447.35
Slow Moving Car	25.0	745.58
Fast Moving Car	60.0	1789.40
Bicyclist	20.0	596.46
Horse	5.0	149.12

$$F_D = +\frac{2v}{\lambda}. \tag{2.16}$$

Equation 2.16 was taken from [1] where F_D is the Doppler frequency, v is the radial velocity in meters per second (m/s), and λ is the wavelength of the transmitted signal in meters. This equation is used to calculate the Doppler frequency shift when the frequency of the transmitted wave and the object's velocity are known. This is helpful in predicting the Doppler frequency shift based on an anticipated radial velocity.

Using Eq. 2.16 with a wavelength of 3 cm, various Doppler frequency shifts can be calculated, assuming all velocity is in the radial direction. Table 2.1 summarizes the results. It can be seen, as the the speed increases so does the Doppler frequency shift.

In addition to measuring an objects range, radar systems can measure an object's velocity through the Doppler shift that is induced by the radial velocity. This is a key measurement the radar sensor provides.

2.3   Types of Radar Systems

There are many different types of radars. This section describes three different types of radar systems. Their mode of energy transmission defines them, and determines the type of information that can be gathered from the received signal. Some radars send out energy continuously while others send it out in a pulse or a packet of information. Pulsed radar systems are defined by

the pulse repetition interval (PRI). The PRI is the length of time between the start of one pulse to the start of the next pulse. The pulse repetition frequency (PRF) is 1/PRI. Figure 2.3 is a block diagram of a basic radar system. The radar signal is generated, amplified, and transmitted from an antenna. The signal is then received into an antenna, filtered, amplified, mixed down, and then digitized. This block diagram is similar for most radar systems. Three common types of radars are: continuous wave, interrupted continuous wave, and frequency modulated continuous wave.
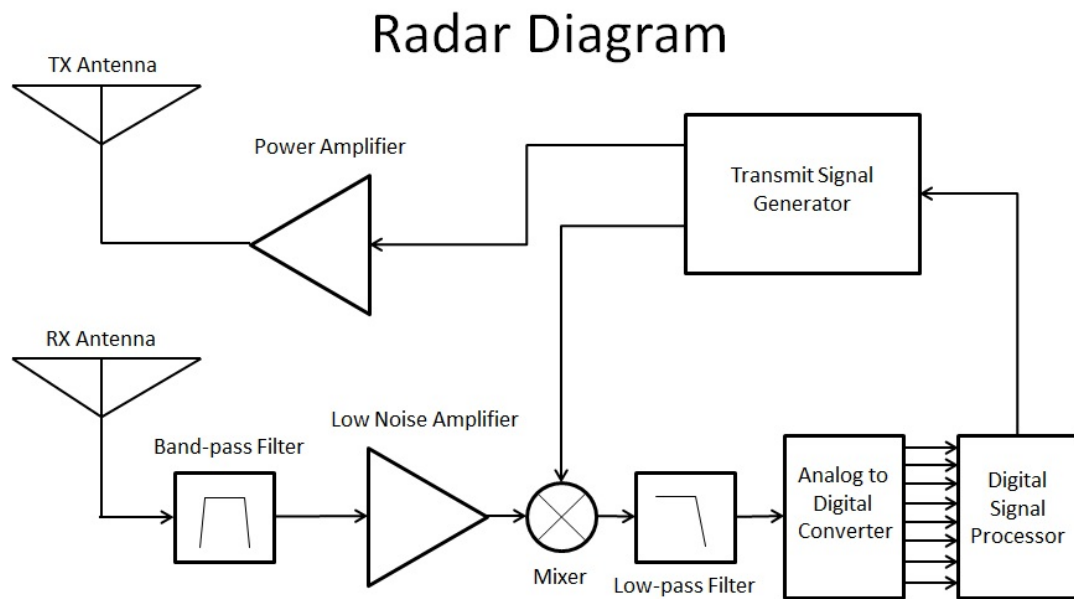
Figure 2.3: Block diagram of a typical radar system showing the individual components.

2.3.1   CW Radar

A continuous wave (CW) radar system transmits a single frequency continuously. Figure 2.4 is a plot of the representative signal. The plot shows the single frequency that is transmitted continuously. The signal is reflected off of an object and the reflected signal either decreases in
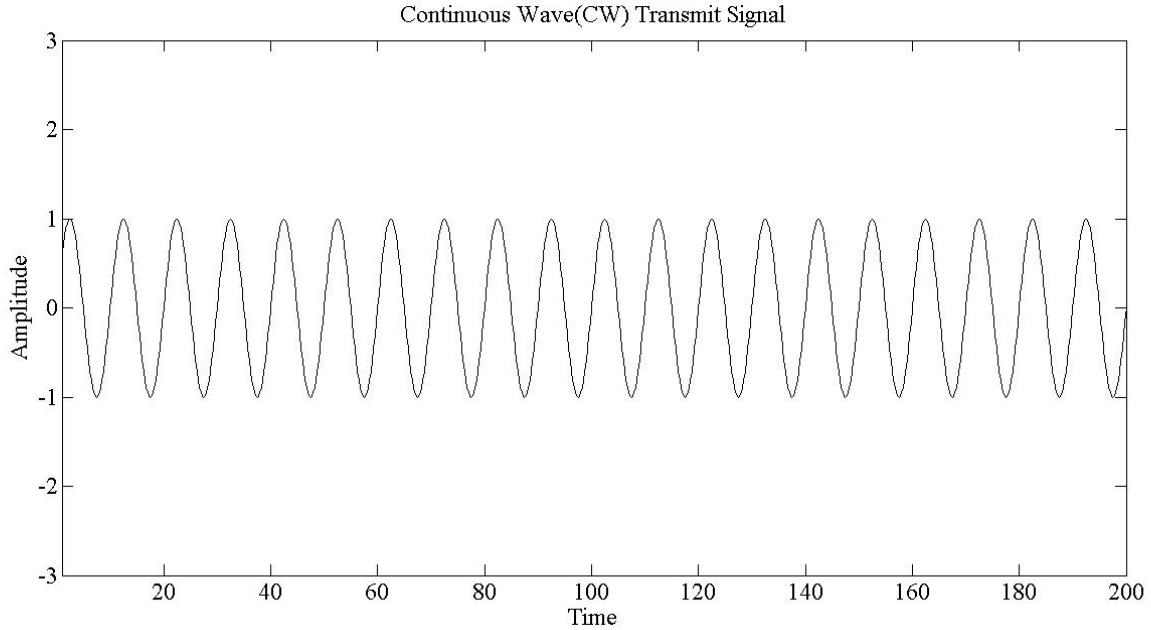
Figure 2.4: Continuous Wave radar signal. A single frequency transmitted continuously.

frequency, increases in frequency, or remains the same frequency as the transmitted signal. This frequency shift depends on the speed of the object the signal is reflected from. This type of radar system provides no range discrimination for an object, but does provide Doppler information. These radar systems are very limited in their functionality and information they provide. They are useful in law enforcement and for other speed tracking devices.

2.3.2   ICW Radar

Interrupted continuous wave (ICW) is similar to the CW radar system, except that the transmitted waveform is turned on and off periodically. Figure 2.5 is a plot of the representative ICW signal. Notice there is a portion of transmit signal followed by a space of no signal. Pulsing the signal on and off enables an object's range and Doppler shift to be discriminated. The range resolution, defined as the minimum range at which two targets can be uniquely identified, is dependent on the pulse length. The equation for range resolution is given by

$$\Delta R = \frac{c\tau}{2} \qquad (2.17)$$

12
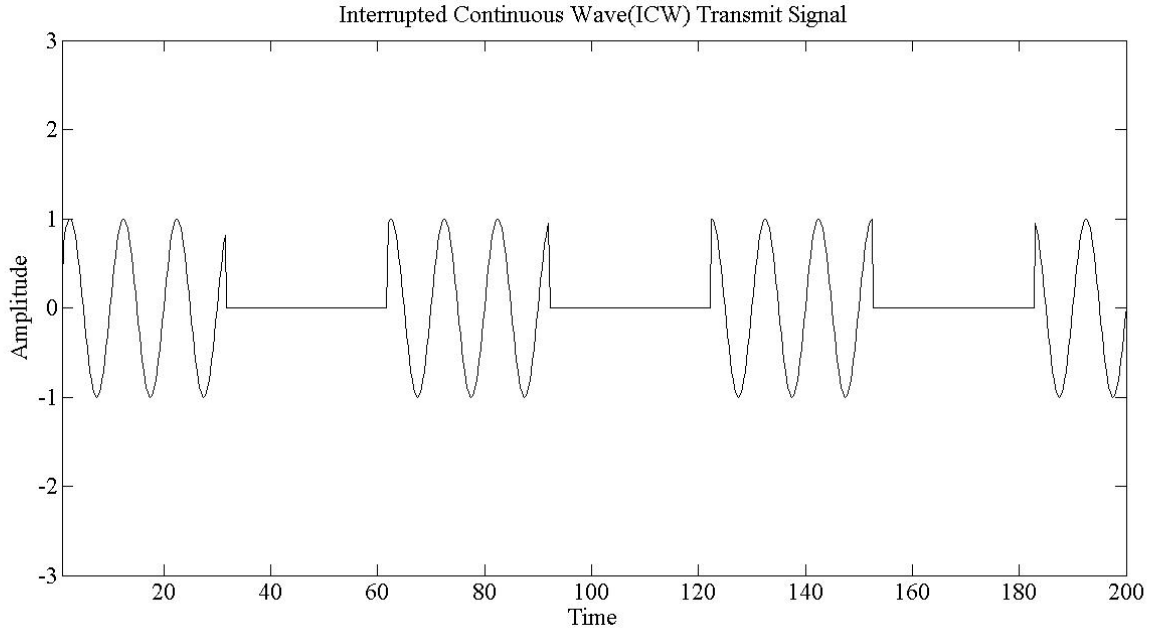
Figure 2.5: Interrupted Continuous Wave (ICW) radar signal. The transmit signal is pulsed on and off.

where ΔR is the range resolution in meters, c is the speed of light in m/s, and τ is the length of the pulse in seconds. The ICW radar system provides both range and Doppler information about an object.

2.3.3 FMCW Radar

Frequency modulated continuous wave (FMCW) is a type of radar system that changes frequency throughout the duration of the pulse. Typically the frequency is modulated linearly with time. The portion of the pulse in which the frequency is increasing is called an up chirp and the part of the pulse with decreasing frequency is called the down chirp. The main benefit of FMCW is that range resolution is independent of pulse length. Instead range resolution is related to the transmit frequency bandwidth. The range resolution is calculated using

$$\Delta R = \frac{c}{2\beta} \qquad (2.18)$$

13
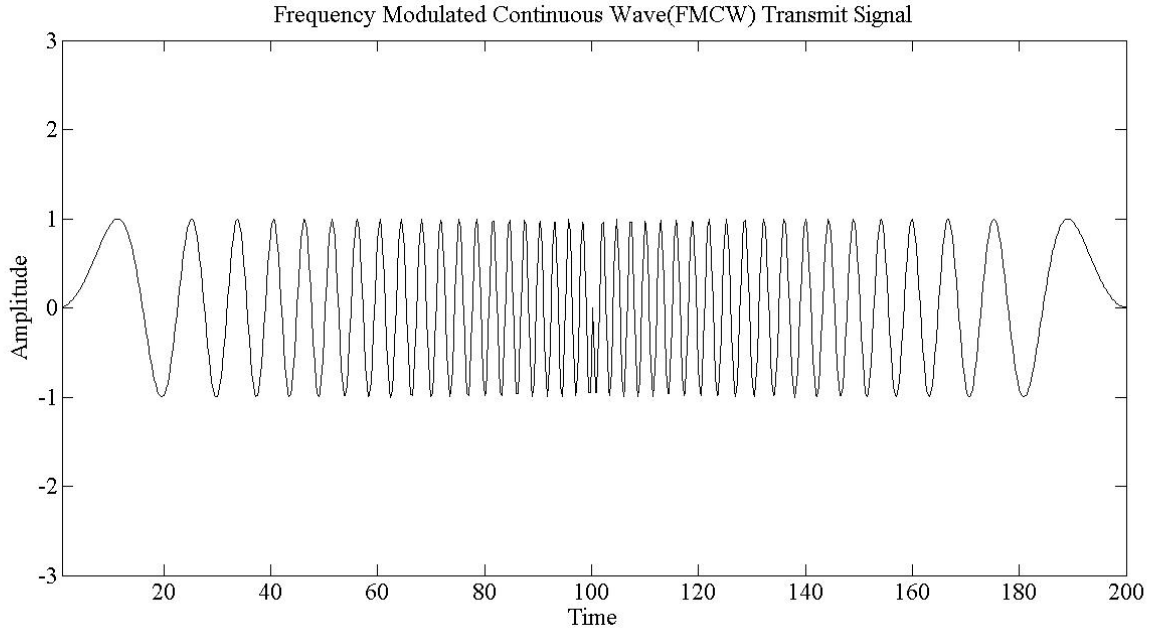
Figure 2.6: Frequency Continuous Wave (FMCW) radar signal. The transmit signal changes in frequency with time.

where ΔR is the range resolution in meters, c is the speed of light in m/s and β is the transmit bandwidth in hertz (Hz). This is significant because a FMCW radar system can have long or short pulses and still achieve equivalent range resolution.

2.4 Signal to Noise Ratio

A radar signal consists of two main components, the signal of interest and noise. The signal comes from a reflected object. The noise is unwanted and is produced by the radar components. A radar can detect the signal of interest if that signal has a greater amplitude than the noise. If the signal is lower than the noise level, the desired signal is difficult to detect. The measurement of the distance the signal is away from the noise is called the signal to noise ratio (SNR). A radar system with high SNR is able to detect signals better than one with low SNR. The SNR for a radar system measuring an object at a particular range can be calculated. First, the equation for the received signal power is

$$S = \frac{P_t G_t G_r \lambda^2 \sigma}{(4\pi)^3 R^4} \tag{2.19}$$

14

where P_t is the peak power transmit in watts, G_t is the gain of the transmit antenna, G_r is the gain of the receive antenna, λ is the signal wavelength in meters, σ is the radar cross section of the target in square meters, and R is the range to the target in meters. To calculate the noise of the radar system the following equation can be used

$$P_n = kT_o(F-1)B \tag{2.20}$$

where k is boltzmann's constant, T_o is the standard temperature (290° K), B is the instantaneous bandwidth of the receiver in Hz, and F is the noise figure of the receiver.

The SNR is the ratio of signal to noise. It can be found from the ratio of Eqs. 2.19 to 2.20. The resulting equation is

$$SNR = \frac{P_t G_t G_r \lambda^2 \sigma}{(4\pi)^3 R^4 kT_o(F-1)B}. \tag{2.21}$$

With a few key specifications about a radar system and if the range and size of the target are known, the SNR can be calculated. This analysis is useful in determining the minimum SNR that is required to detect a particular target at a given range. If the object is below the SNR detection threshold, it will be difficult for the radar to detect the signal. From Eq. 2.21 it can be seen that to increase SNR the are a few parameters that can be adjusted. This is assuming that the wavelength, target size, and range are all fixed. The SNR can be adjusted through the power transmitted, gain of the receive antenna, gain of the transmit antenna, the noise figure, and the signal bandwidth.

2.5   Radar Signal Processing

Signal processing forms the heart of most modern radar systems. The transmit waveform is generated using a digital to analog converter (DAC) and the received radar signal is digitized using an analog to digital converter (ADC). Previous generations of radar systems processed the signal using analog techniques. This was very difficult and not as flexible. Radar systems that use digital signal processing process the digital samples rather than the analog signal. The subset of digital signal processing for radar is referred to a radar signal processing. Radar signal processing has facilitated major advancements in our ability to use and process radar data. Radar signal

processing makes possible target detection, imaging, tracking, and all other techniques to extract information from radar data.

2.5.1 Moving Target Indicator

Moving target indicator (MTI) is a type of radar processing where moving objects containing a Doppler shift are separated from stationary objects. For this particular type of processing the stationary objects are considered clutter and are not of interest. There are two different time domains that this type of processing can be divided up into. One of the domains is called fast time while the other is called slow time. Each time accomplishes a certain purpose in obtaining information about the object of interest.

Fast Time Processing

Fast time processing is the processing that takes place on the pulse or the chirp. It is referred to as fast time because the processing time window is small. This processing step is also referred to as pulse compression. Fast time processing produces range information about the objects that are in the radar's FOV.

Slow Time Processing

Slow time processing is the processing that takes place on multiple pulses or chirps. Fast time is processing on a single chirp so any processing that takes place on multiple chirps is much slower and is referred to as slow time processing. Because this processing is done over a longer period of time it provides information on how objects are changing over time. The main purpose of slow time processing is to measure Doppler shift information.

2.5.2 Range Doppler Map

A range-Doppler map (RDM) is a way to visually represent radar data. Figure 2.7 is an example of a range-Doppler map. Range is across the x-axis. Objects that appear on the left side are at close range to the radar and objects that appear on the right side are at further ranges.

Doppler shift is on the y-axis. Objects that have no Doppler shift (i.e., they are not moving) are in the center of the RDM (orange region in Figure 2.7). Objects that are moving away from the radar have a positive Doppler shift and appear below the orange center region of the RDM. Objects that are moving towards the radar have a negative Doppler shift and appear above the orange center region of the RDM. As Doppler shift increases in frequency, the object moves further away from the center of the RDM. The intensity of the object's received return is usually represented by a color scale.

Range Doppler Map

Decreasing Doppler

Zero Doppler

Increasing Doppler

Increasing Range
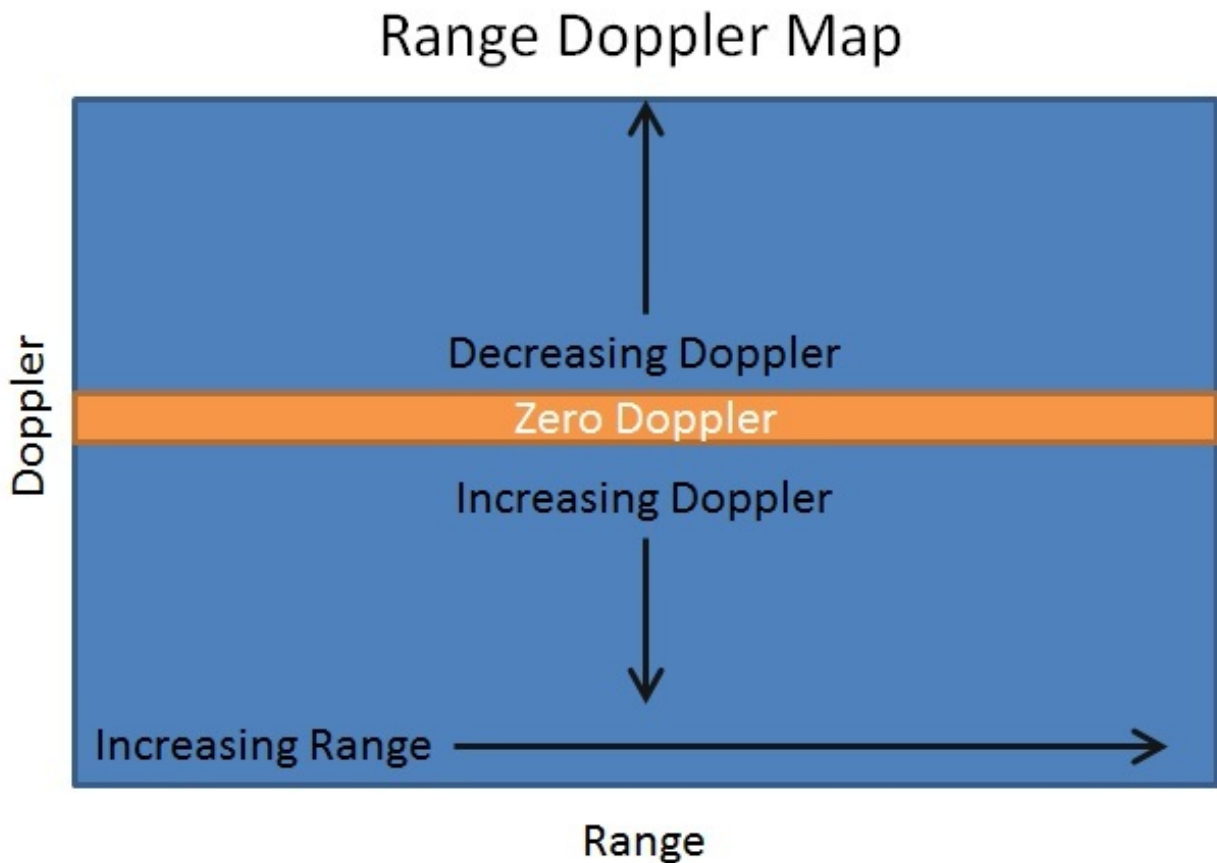
Doppler

Range

Figure 2.7: Description of a range Doppler map. The x-axis is range and the y-axis is Doppler. The center of the y-axis is zero Doppler shift. The positive and negative Doppler frequencies grow out from the middle.

2.5.3 Time-Frequency Analysis

Many signals have frequency content that changes with time, such as human speech. In order to get a more complete picture of such signals, both the time domain and the frequency domain must be used to analyze the signal. Time-frequency analysis utilizes both time and frequency domains to create a three-dimensional profile of the signal.

An illustration of the value of time-frequency analysis is considered below. Consider the chirp that is produced by a bat [2]. Figure 2.8 shows the time domain of the collected bat chirp data. The majority of the signal occurs between about 2 ms and 6.5 ms. This time domain plot reveals how the amplitude of the signal changes over time but shows very little about the frequency content of the signal. Figure 2.9 is a spectrogram of the same bat chirp. This spectrogram shows the frequency content of the entire bat chirp. From this graph we can see that the frequency content of the entire chirp ranges from about 30 kHz to 90 kHz. However there is no correlation in time to when these frequencies occurred. Using time frequency analysis we can generate the time-frequency plot of a recorded bat chirp in Figure 2.10. This graph shows how the frequency evolves with time and provides both frequency and time information simultaneously, which the time analysis and the frequency analysis by themselves are not able to.

One of the challenges of time-frequency analysis comes from the resolution of the two domains being analyzed, time and frequency. High resolution in the frequency domain results in low resolution in the time domain, and high resolution in the time domain results in low resolution in the frequency domain. This requires either a choice of a good resolution in either domain resulting in a poor resolution in the other domain or a balance of resolution in both domains. The choice of resolution depends on the analysis being preformed and the information that is desired.

Many radar signals are time-varying signals, and time-frequency analysis is a useful tool [3]. Time-frequency analysis is used in this thesis to extract information from such signals.

2.6   Chapter Summary

Using a radar system it is possible to measure information about certain objects. The primary measurement that a radar can make distances to objects (range) and objects radial velocity (Doppler). There are different types of radar systems including CW, ICW, and FMCW. In the next
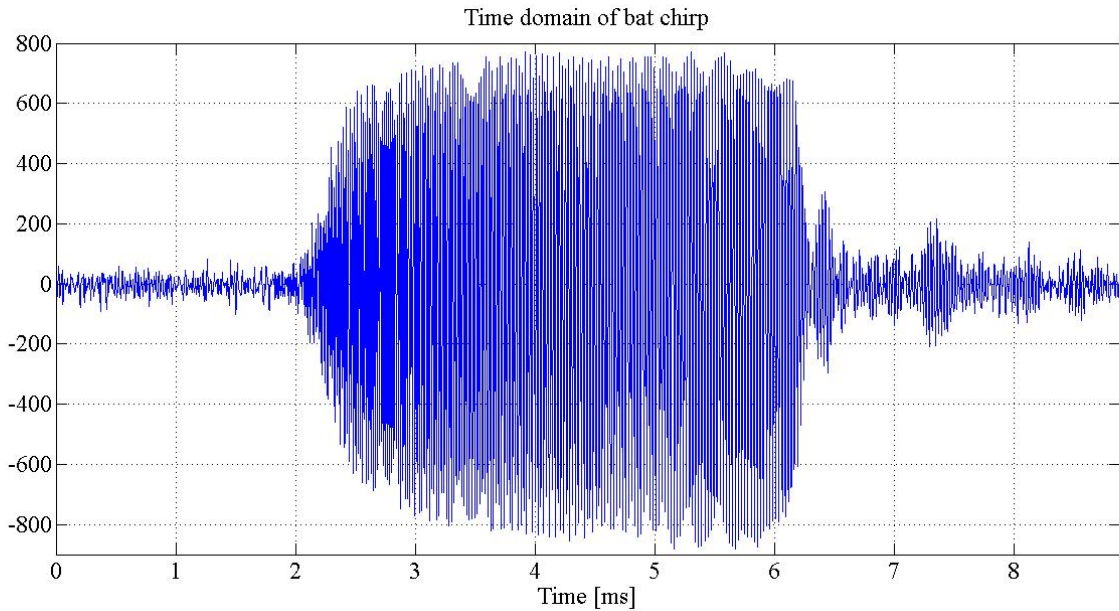
Figure 2.8: Plot of amplitude versus time of a bat chirp. From the graph we can see that the amplitude of the signal is high from 2 ms to 6 ms, relatively little can be inferred about the frequency content.
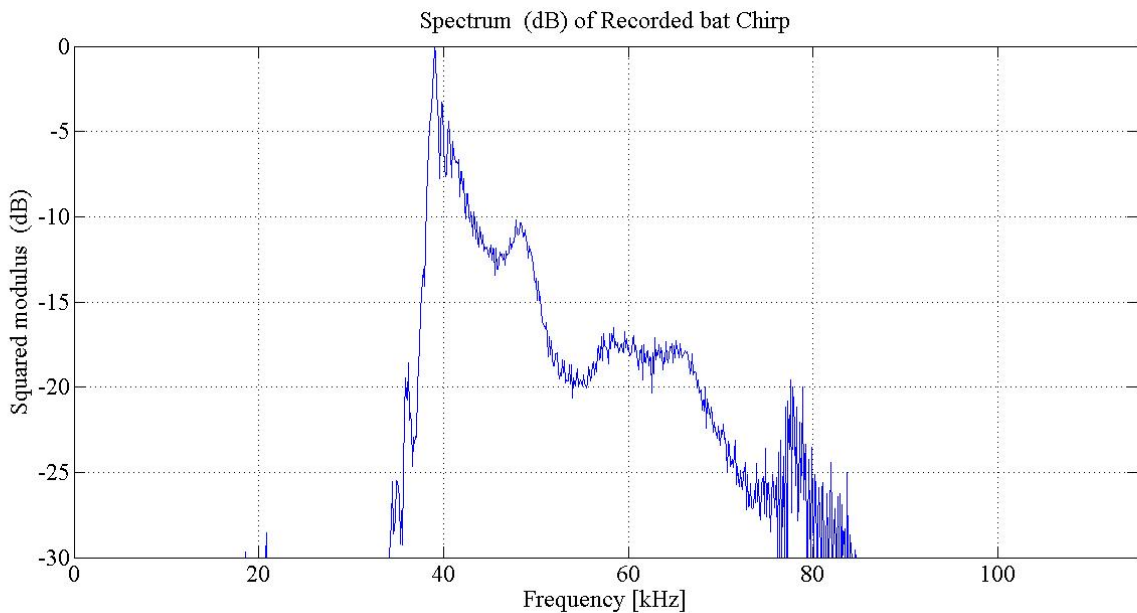
Figure 2.9: Spectrogram of a bat chirp. The bat chirp has a bandwidth that starts at 30 kHz and ends at 85 kHz. The lower frequency content has a greater amplitude, however the plot shows no correlation with time.
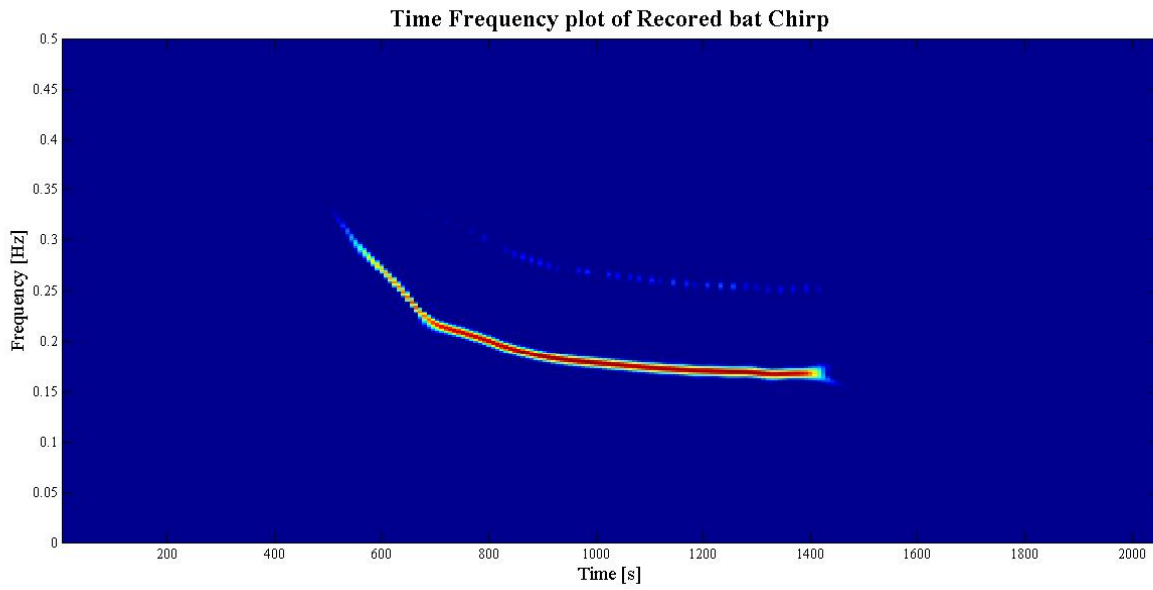
Figure 2.10: Time-frequency plot of a recorded bat chirp. This plot show both the time and the frequency information simultaneously.

chapter it will be shown how additional information about objects can be gathered from radar data using the object's micro-Doppler signature over time.

CHAPTER 3.   MICRO-DOPPLER

The previous chapter covered how range and Doppler information can be gathered about an object using a radar. This chapter explores increasing resolution in the Doppler spectrum and the additional data that can be gathered with high resolution micro-Doppler. Different micro-Doppler profiles that are likely to be seen by a ground based radar system are also explored.

3.1   Doppler Resolution

The ability to discriminate small variations in Doppler velocity from radar data is determined by the resolution of the Doppler spectrum. The Doppler spectrum resolution measures the change in signal frequency that can be discriminated by a radar system. If small differences in frequency can be differentiated, then Doppler resolution is high; otherwise Doppler resolution is low. Figure 3.1 illustrates the radar return of two objects that are separated in frequency. Ideally, the two points, separated by a small frequency difference, will be distinguishable as two unique points in frequency. The "bins" on the x-axis represent a span of frequency that is unambiguous. Radar returns from these two objects fall into the corresponding bins. Because the bins are so large, both the radar returns from both object 1 and object 2 are grouped in the same bin. This causes the targets to be indistinguishable from each other because their energy is combined and lumped into the same common bin. This is an example of low resolution. Figure 3.2 is a diagram of higher resolution in the frequency domain. Notice that the bin sizes are smaller and occupy less frequency space. Now most of the energy from object 1 goes in one frequency bin and the energy from object 2 goes in a different bin. Object 1 is now distinguishable from object 2 in frequency. This is an example of high resolution.

Frequency resolution is important in most signal processing applications. In radar signal processing it plays an important role in exploiting signals that are separated by a small frequency

difference. If the resolution is low then some of the fine details of the signal can be lost, making the information less valuable.
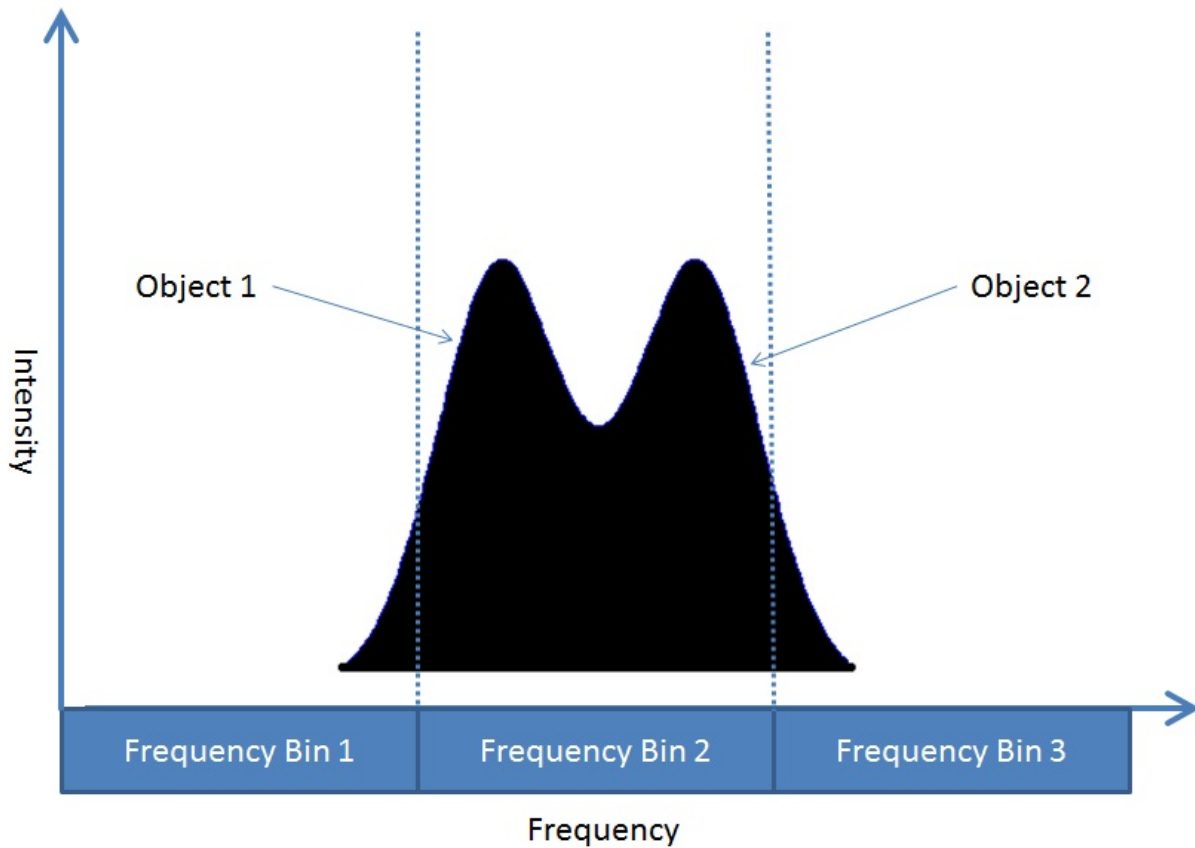
Figure 3.1: Diagram of low resolution. Note the large frequency bins on the x-axis. If the frequency bins are large it is difficult to discriminate between these two objects. In this example the signals from both object 1 and 2 are lumped into frequency bin 2.

3.1.1 Increasing Doppler Resolution

There are a number of ways to increase Doppler resolution when high resolution is desired. In cases where a FFT is used to analyze frequency content, increasing the number of samples input to the FFT can increase the frequency resolution. The output of the FFT has the same overall
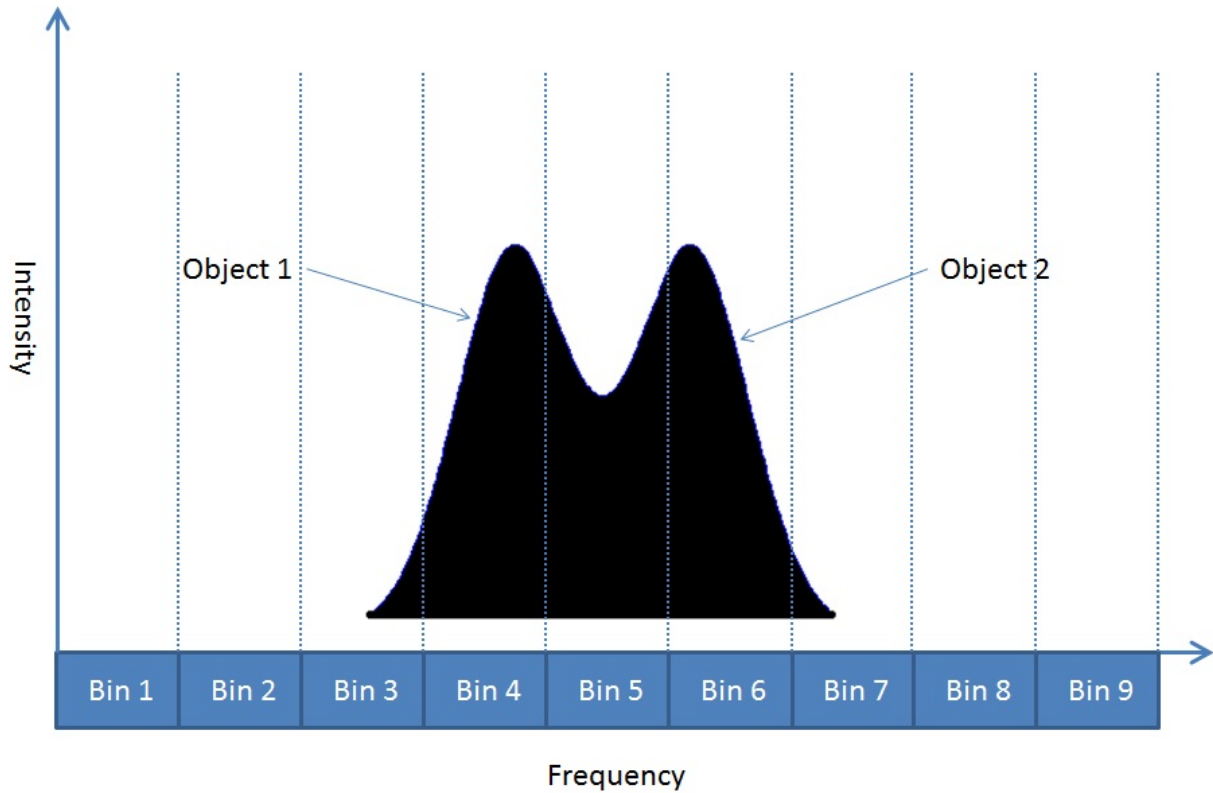
Figure 3.2: Diagram of high resolution. The frequency bins are smaller, making it possible to distinguish between the two objects. The signal from object 1 falls into frequency bin 4 and the signal from object 2 falls into frequency bin 6.

Table 3.1: Table of various N point FFTs and their respective resolution per FFT bin. Note this is for a radar system that we used in the above example with a 1KHz PRF.

Number of points in the FFT	Dopper Shift Per FFT point (Hz)	Doppler Shift per FFT bin (m/s)
32	31.25	0.46
64	15.63	0.23
128	7.81	0.11
256	3.91	0.05
512	1.95	0.03

frequency span, however each individual bin represents a smaller frequency range. There are a few drawbacks to increasing the number of samples. First, the FFT processing time increases as well.

Second, in some cases the amount of radar data available is not sufficient to increase the input into the FFT. However when sufficient samples are available, increasing the number of samples is a good option for increasing frequency resolution.

Doppler frequency resolution can be calculated using various input sample sizes. The equation to calculate the Doppler resolution is

$$\Delta F_{bin} = \frac{PRF}{2N} \tag{3.1}$$

where ΔF_{bin} is the frequency resolution of a bin in hertz (Hz), PRF is the pulse repetition frequency of the radar system, and N is the number of samples that are put into the FFT. Table 3.1 uses Eq. 3.1 to calculate frequency resolution for various input sample sizes. Table 3.1 shows that increasing the number of FFT input samples decreases the frequency span of each bin, which in turn increases the Doppler resolution. If certain resolution-specific Doppler features are desired, then the input to the FFT can be adjusted to achieve that resolution.

To illustrate the effect of input sample number has on the frequency resolution of radar data, we will consider the radar data of a person walking. The exact same data was processed five different ways using 32, 64, 128, 256, and 512 samples as inputs to the FFT. The results can be seen in Figs. 3.3, 3.4, 3.5, 3.6, and 3.7, which are the respective time frequency plots using the various inputs to the FFT. Notice that the first plot, Fig. 3.3, is fairly grainy in Doppler (y-dimension) since it is the lowest resolution. The bins are large and occupy a relatively large range of frequency. The general trend of the data is present however some of the finer details are blurred. This is a result of the low resolution. As more samples are added to the FFT the time frequency plots become clearer because of the increased resolution in the Doppler spectrum. In this example of a person walking, finer resolution allows for different features to be extracted that might not have been possible with low resolution.

3.2 Micro-Doppler

High Doppler frequency resolution is critical when analyzing micro-Doppler data. The term micro-Doppler refers to relatively small changes and variations in the Doppler spectrum. Micro-Doppler variations are caused by a variety of factors, but are primarily due to radial velocity
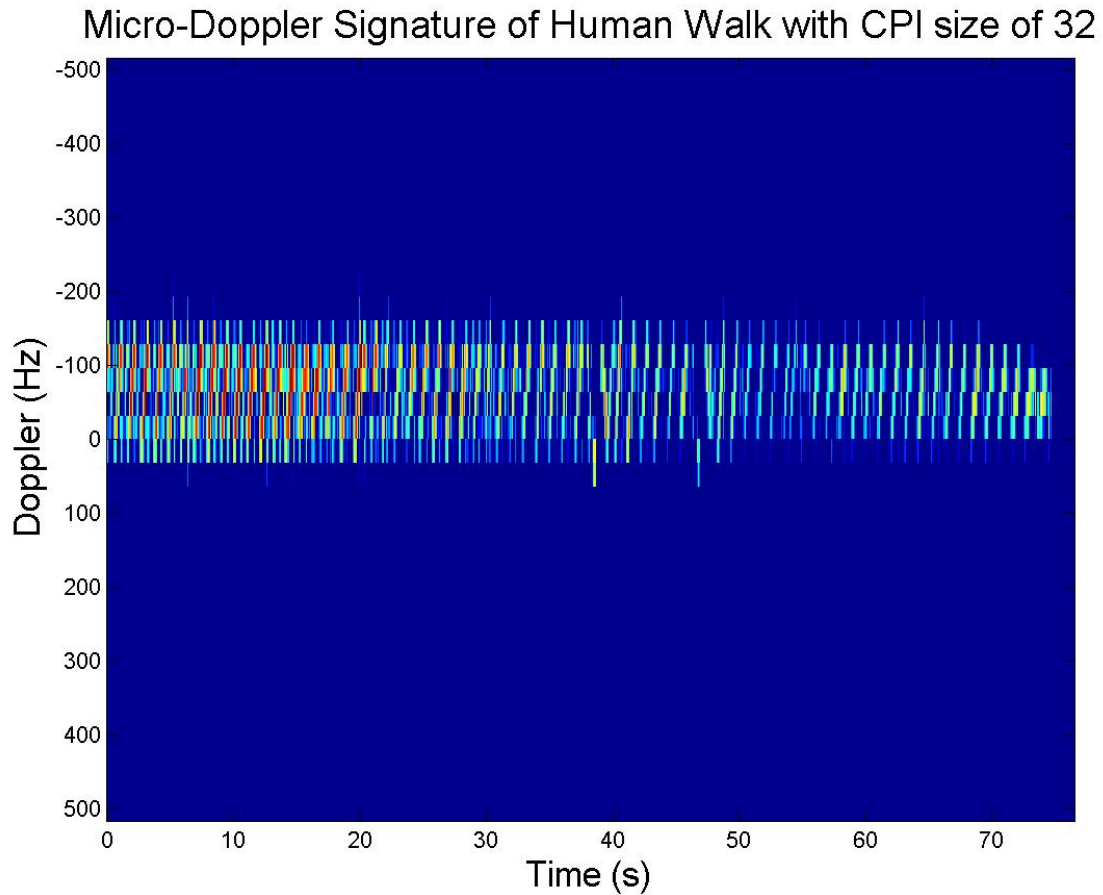
Figure 3.3: A time-frequency plot of a person walking with 32 samples used as an input to the Doppler FFT.

variation caused by small movements or "micro-motion." Radar is able to capture these micro motions to varying degrees. The radar system's ability to detect micro-Doppler depends on the target size, wavelength of the radar, and type of micro-Doppler motion. The micro-Doppler motion appears in the Doppler spectrum and in most cases varies with time. Micro-Doppler is usually associated with an object that has both a main return and some smaller features that contribute to the micro-Doppler signature. Micro-Doppler has been studied and researched heavily [4] [5] [6].

Micro-Doppler can be difficult to resolve because the Doppler shift of interest is very close to the strong return from the main body of an object. These small variations in Doppler can potentially be hidden in the main Doppler return. Different signal processing techniques can be used to extract the micro-Doppler information.

25
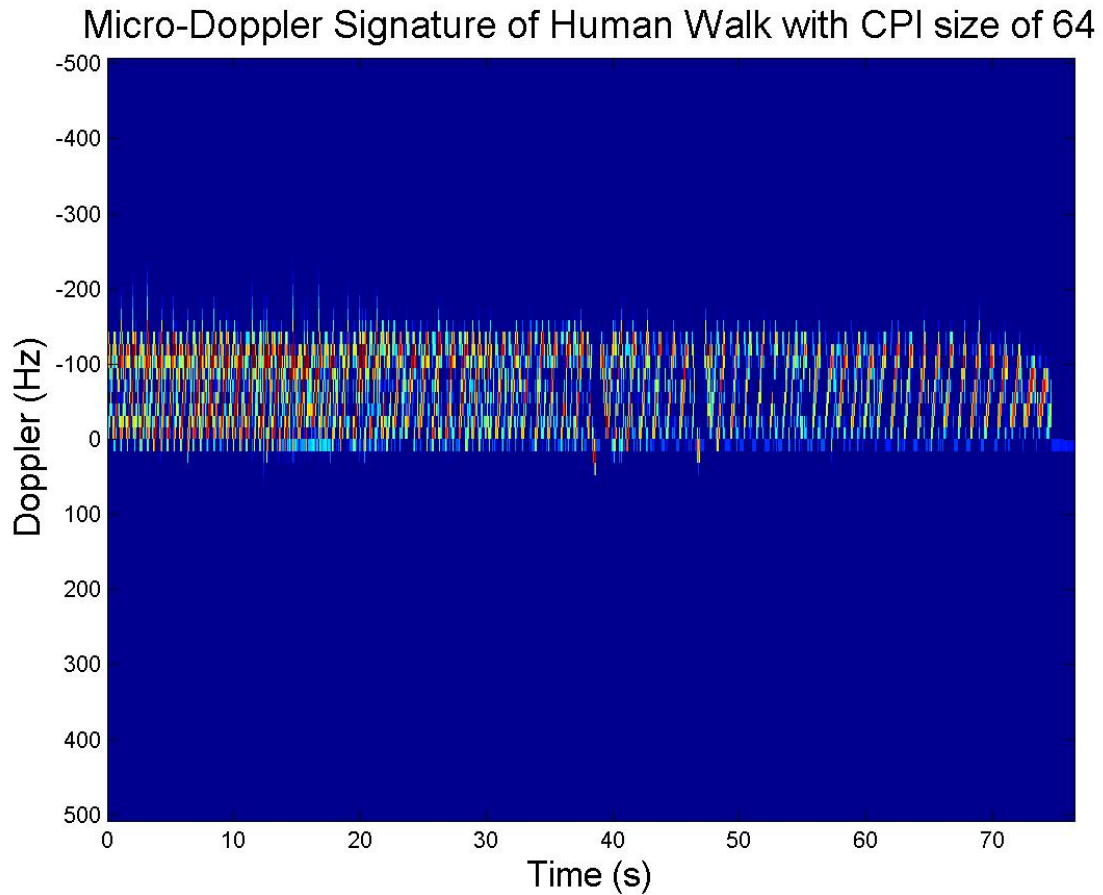
Figure 3.4: A time-frequency plot of a person walking with 64 samples used as an input to the Doppler FFT.

3.3 Micro-Doppler Motions

There are a several common motions that cause micro-Doppler, including vibration, rotation, articulation, and flapping.

3.3.1 Vibration

Vibration causes small motions leading to micro-Doppler that can be seen from the radar. Vibration causes varying degrees of displacement in an object. Radars can detect this vibration depending on the amount of displacement and the wavelength of the radar. Longer wavelength radars cannot as readily detect small displacements. However shorter wavelength radars can better detect

26
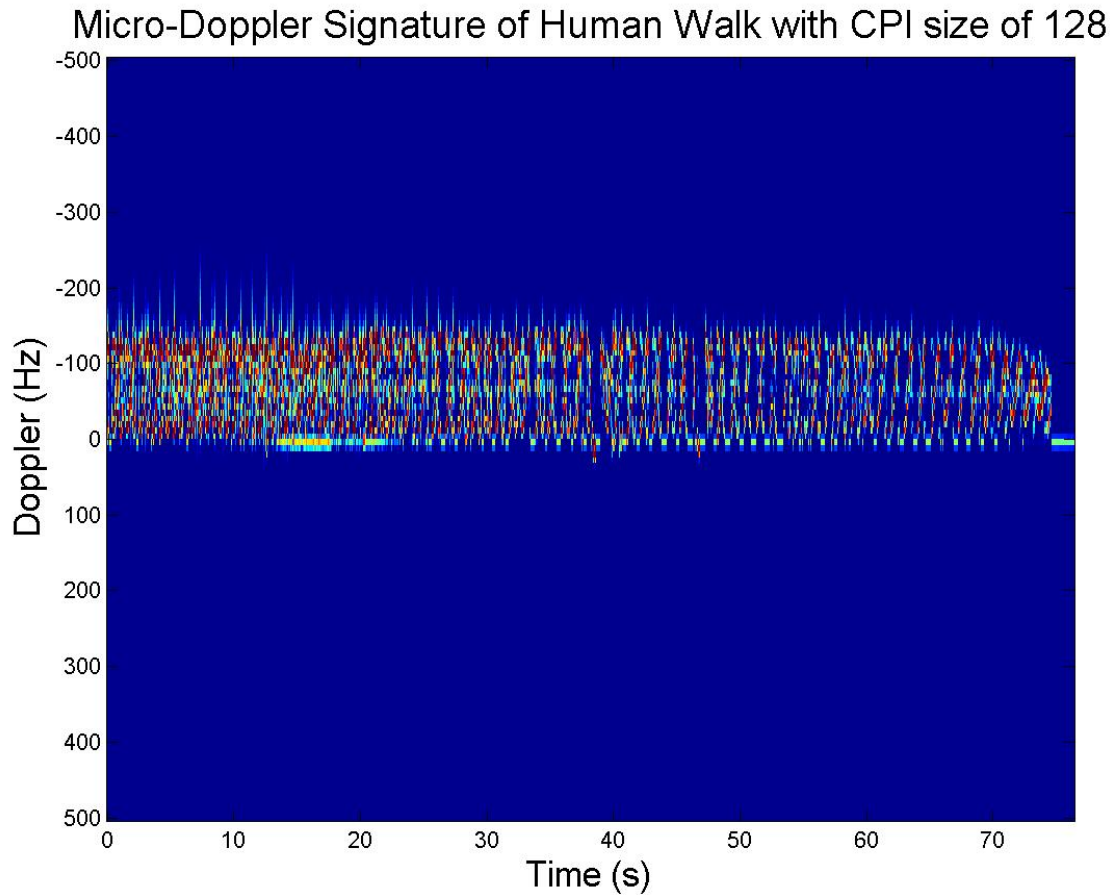
Figure 3.5: A time-frequency plot of a person walking with 128 samples used as an input to the Doppler FFT. Notice that the signal is slightly less grainy compared with Fig. 3.4

small displacements. Vibration in objects can be caused by a variety of mechanisms, commonly by engines in vehicles.

3.3.2   Rotation

Rotating objects also cause micro-Doppler. Rotation can come from helicopter blades, windmill turbines, or simply from the radiator cooling fan in a vehicle. As with most micro-Doppler, the detection of the rotation depends on the size of the rotating object, the frequency of the radar, and the speed of the rotation. If the rotation is at a constant rate, the the micro-Doppler signature is periodic. Figure 3.8 is a time-frequency plot of simulated helicopter blades [4]. The plot shows that as the blades are rotating a portion of the time they are moving towards the radar
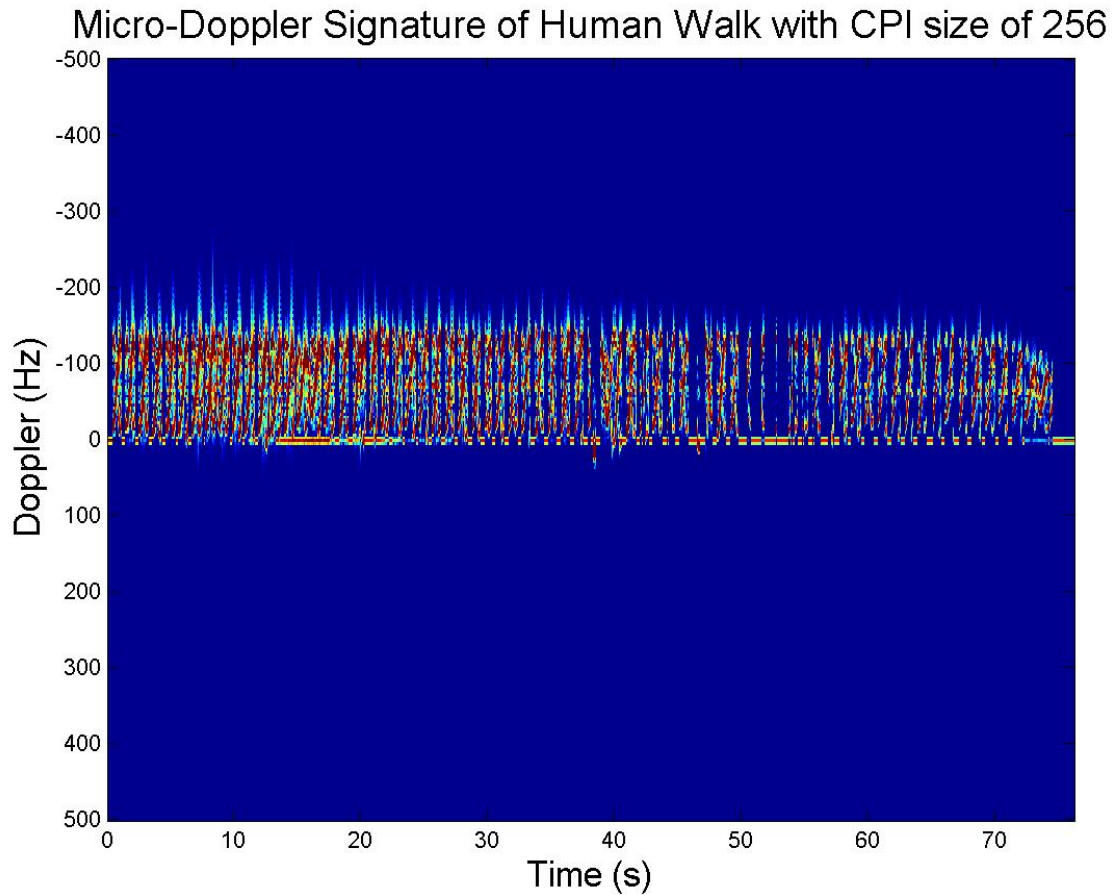
Figure 3.6: A time-frequency plot of a person walking with 256 samples used as an input to the Doppler FFT. The data has greater frequency resolution and improved visual resolution in the time-frequency plot compared to the previous plots.

and a portion of the time they are away away from the radar. The number of periodic waves corresponding to the different blades. Because the signature is periodic it can be inferred that the blades are rotating at a constant rate.

3.3.3 Articulation

This type of motion describes on object that swings back and forth. It can be generated by a pendulum or by the arms and legs on a human body. This type of motion is difficult to detect if the motion is tangential to the radar system and produces no radial velocity. Figure 3.9 displays simulated radar data of a pendulum that is swinging back and forth towards and away
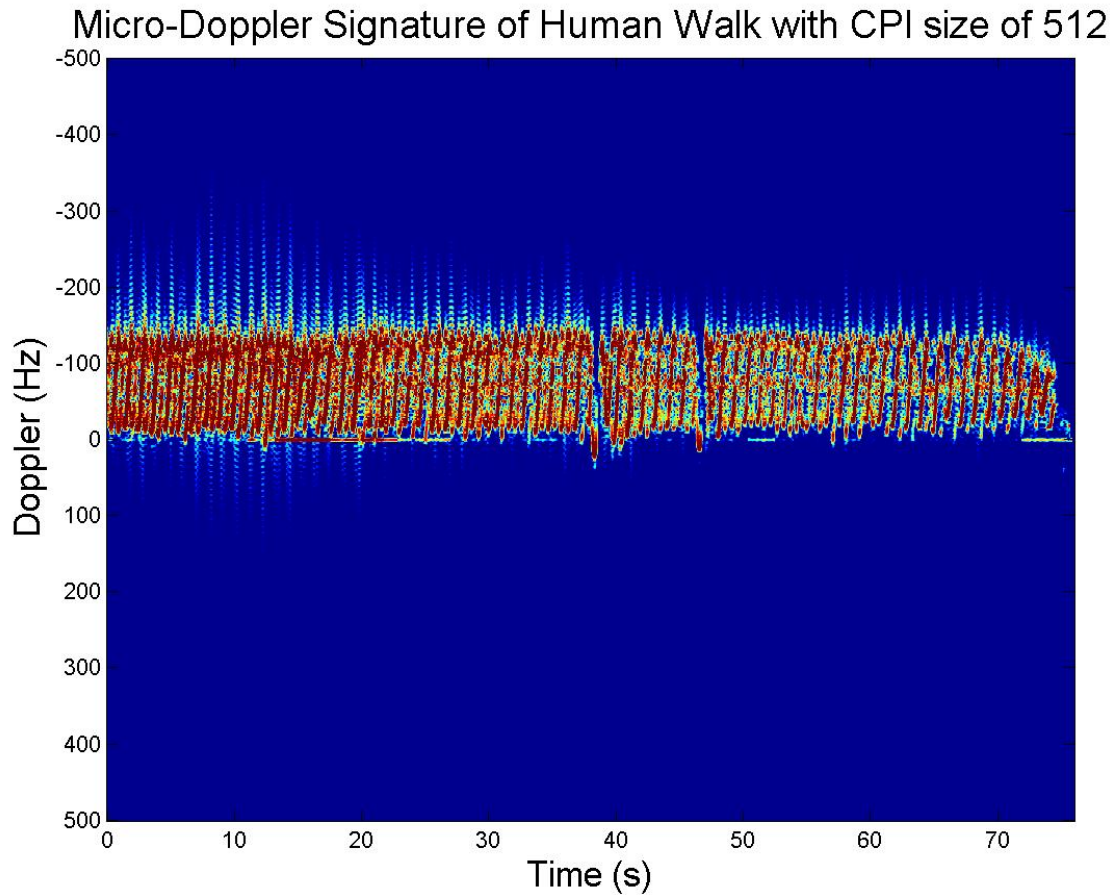
Figure 3.7: A time-frequency plot of a person walking with 512 samples used as an input to the Doppler FFT. This has the greatest frequency resolution out of the 4 plots presented here. Notice the detail the graph contains.

from a radar. From this plot it can be seen that as the pendulum swings towards the radar it has a negative Doppler velocity and as it swings away from the radar it has a positive Doppler velocity. This motion produces a triangular pattern over time as can be seen in the figure. This type of micro-Doppler motion could come from the arms and legs of animals and humans walking.

3.3.4 Flapping

Flapping is motion, produced by birds' wings as they fly. It is repetitive up and down motion. Figure 3.10 is a plot of the simulated radar data of a bird flapping its wings as seen by the

29
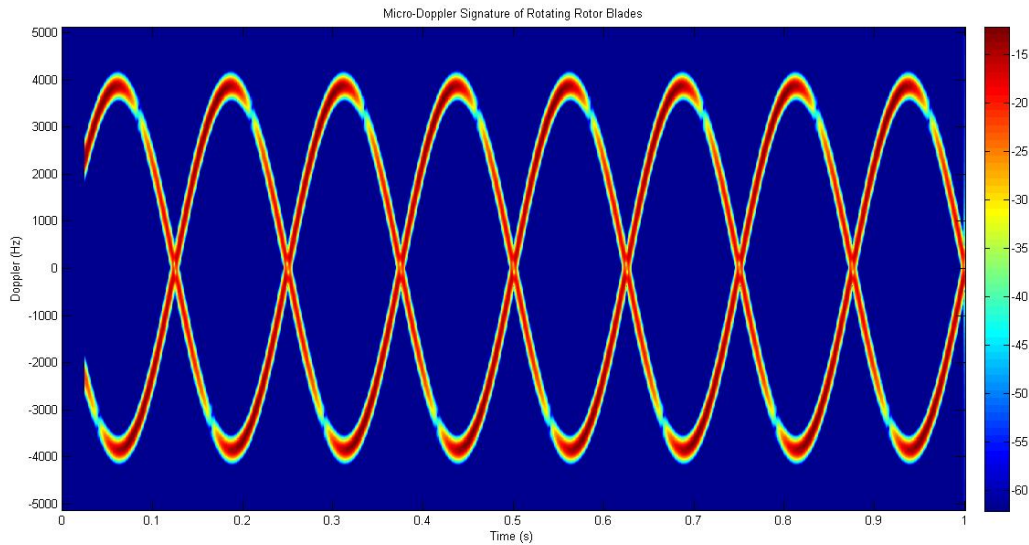
Figure 3.8: Time-frequency plot of a simulated helicopter blades rotating [4]. Notice there are two sets of periodic waves corresponding to various blades.
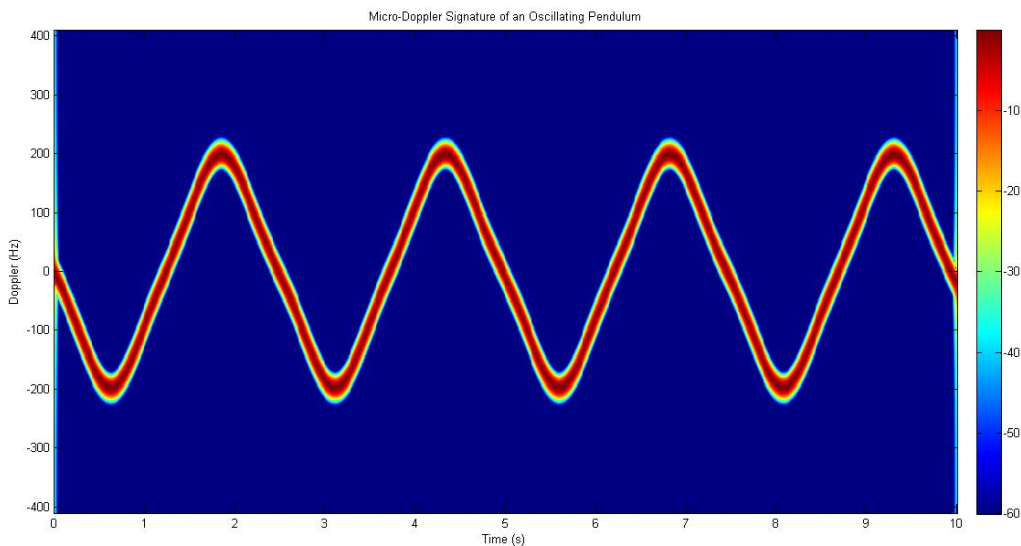
Figure 3.9: Time-frequency plot of simulated radar data of a pendulum swinging back and forth [4]. As the pendulum swings towards and away from the radar the Doppler shift changes from positive to negative producing the triangular waveform.

radar. The bird has a joint in the middle of the wing, so flapping produces two moving portions per wing that an be seen by the radar.
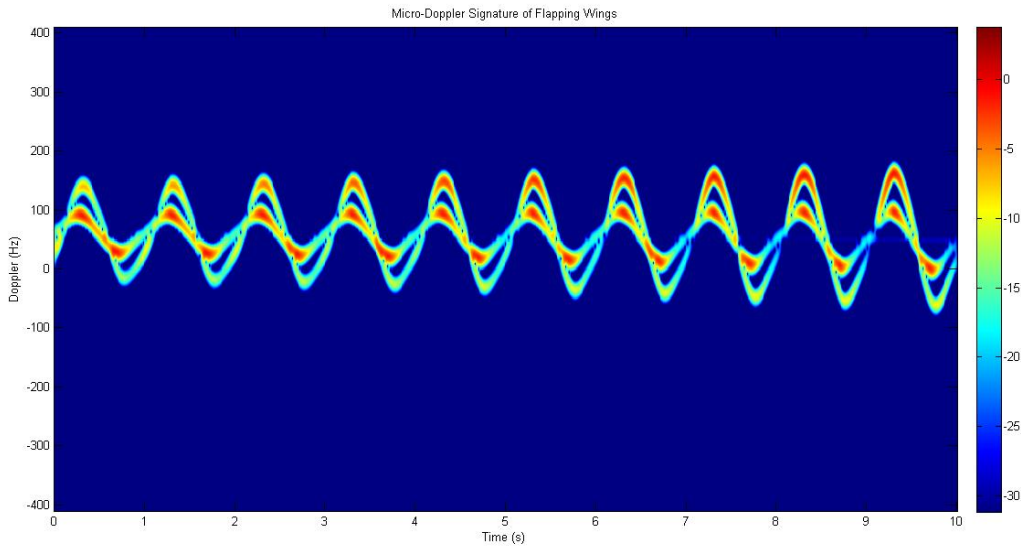
Figure 3.10: Time-frequency plot of simulated radar data of a bird's wing flapping [4]. Notice that there are 2 sets of motion both are quasi sinusoidal. One set of motion has a greater swing in Doppler and the other has a smaller swing. These two sets of motion correspond to the inner and outer sections of the wing as it flaps.

Vibration, rotation, articulation, and flapping are few of the types of common micro-Doppler motions. These motions are some of the fundamental motions by which objects move. There are many other motions that can produce micro-Doppler that were not listed. Complex motions produce complex micro-Doppler signatures and complicate efforts to identify individual motion components in the radar data.

3.4 Micro-Doppler Profiles

A radar system has the ability to gather information about an object in its field of view. At its most basic level the radar is able to measure distance to an object. In addition to distance, it is also able to infer some amount of information about the size of the object, the intensity of the backscatter, and the object's radial velocity. Using range, object intensity, and radial velocity one can make an educated guess about what type of an object the radar is viewing. However that

may or may not be enough information to classify the type of object. Some target classes are still ambiguous when using only the parameters previously stated. Additional information may be needed to classify a target beyond these basic parameters the radar measures.

Micro-Doppler can provide that additional information. Certain targets have a distinct micro-Doppler signature to the radar. These signatures are created by various parts of the object moving. The micro-Doppler signature of the object is a sum of all the micro-Doppler motions that the object contains. For example, the micro-Doppler signature of a person walking is the sum of the person's arm, leg and body motions: for a horse it is the sum of its leg, head, and body motions and for any other object it is the sum of all radial velocity sources. Capturing and analyzing the micro-Doppler provides useful information for uniquely classifying types of objects.

A few common micro-Doppler signatures are described here. These objects are detected by a ground based radar systems and it is useful to discriminate the objects.

3.4.1   Walking Human

The micro-Doppler of the human gait is very well documented [7] [8]. As a person walks, all parts of the body are in motion. Every moving part of a person has a different measurement of radial velocity. As a person walks, their feet and arms move a significant amount generating a large radial velocity. In contrast, a person's trunk or torso moves very little. This orchestra of moving parts of the human body creates a micro-Doppler signature that is uniquely human. Radar has the ability to detect and track this unique signature that comes from humans as they are in motion.

To get a better idea of what the micro-Doppler signature of a human walking is research has conducted with high speed cameras [7]. Data collected from high speed cameras records the speed of various parts of the body as a person walks and runs. Figures 3.11 and 3.12 summarize the measurements taken by the high speed camera. These figures show the velocities over time of the sternum, left hand, right hand, left knee, left toe, right knee and right toe. Figure 3.11 is of a human walking and Fig. 3.12 is of a human running. These plots show that the human gait is periodic and the right and left moving parts of the body have symmetric velocity characteristics. These plots also show the parts of the body measured occupy many velocities over a period of time.
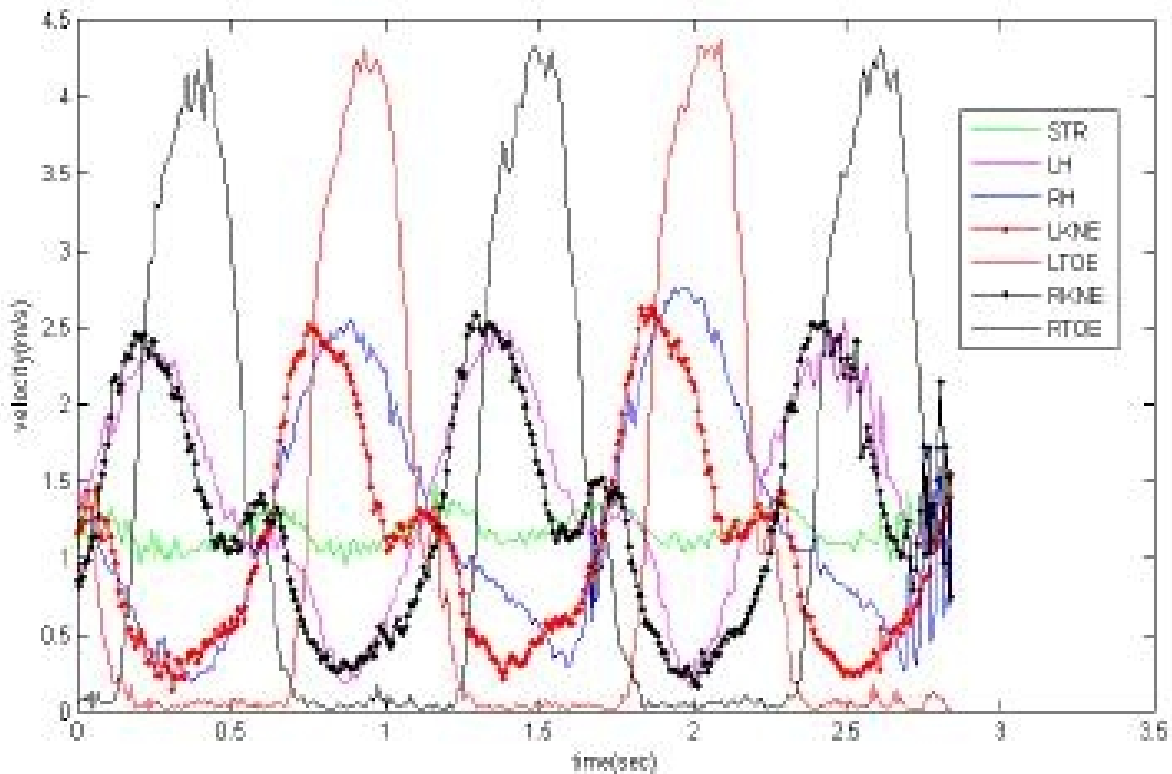
Figure 3.11: A plot of the various velocities of parts of the human body during walking [7]. The legend is defined by: sternum (STR), left hand (LH), right hand (RH), left knee (LKNE), left toe (LTOE), right knee (RKNE), and right toe (RTOE). The sternum has the least amount of velocity variation while the left and right toes have the most.

Information from the high speed camera produces an understanding of what the radar may be able to detect in the Doppler spectrum of a person walking. Because the micro-Doppler signature also is a measurement of velocity it would look very similar to both Figs. 3.11 and 3.12. Depending on the Doppler resolution and the angle of incidence, the radar can detect the body parts of a person as it is walking. A person walking would occupy a variety of Doppler frequencies and the trends in the data would be periodic as long as a person is moving at a constant rate. Those are some of the features that can be used to identify the micro-Doppler signature of a person walking. Some research has been done to model the radar signature of a person walking [4]. Figure 4.1 is a time frequency plot of simulated radar data of a human walking. Notice how similar it looks to the measured velocities of the different parts of the body.

33
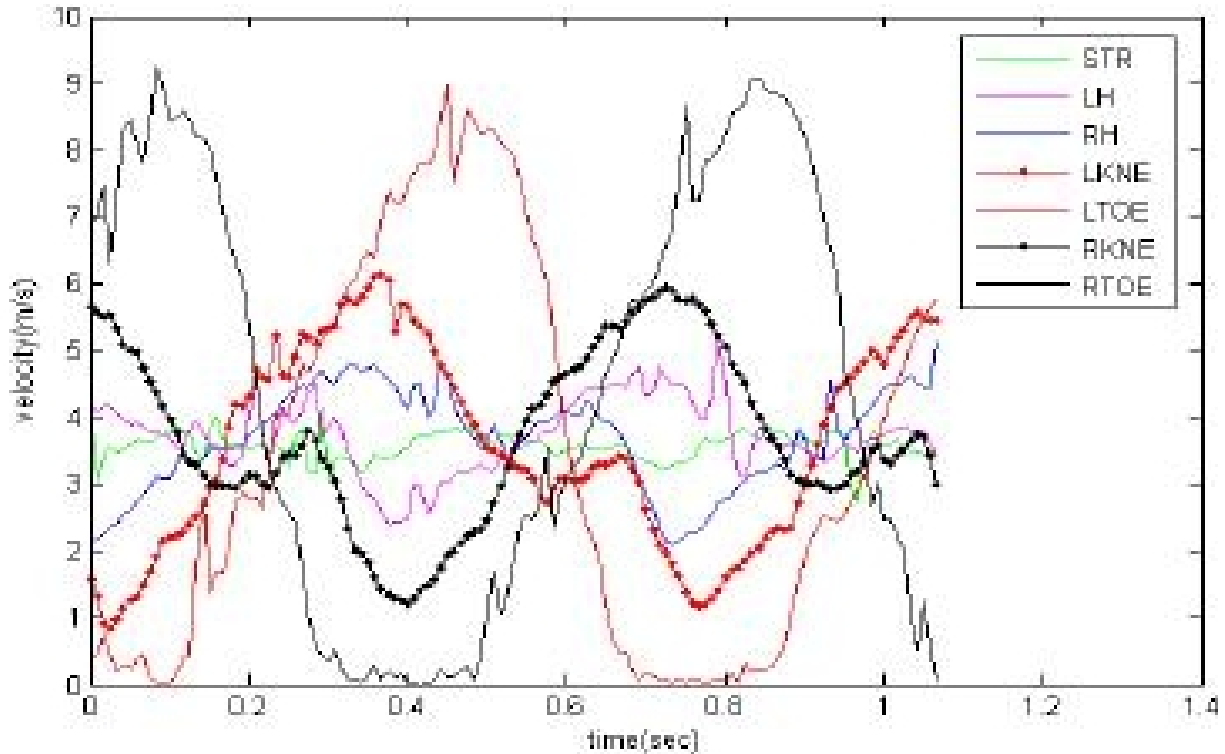
Figure 3.12: A plot of the various velocities of parts of the human body during running [7]. The legend is defined by: sternum (STR), left hand (LH), right hand (RH), left knee (LKNE), left toe (LTOE), right knee (RKNE), and right toe (RTOE). All of the velocities are faster and the period of the motion is also shorted in comparison to Fig. 3.11. A walking person's hands have a maximum velocity of about 4 m/s where a running person's hands have a maximum velocity of about 9 m/s.

3.4.2 Vehicle

A vehicle is another type of object detected by a ground based radar system. Each class of vehicle, ranging from large trucks to small cars have a different brightness to the radar system. Features contributing to the micro-Doppler signature include wheels, the radiator fan, vibrations from the engines, and any other moving objects on the vehicle. However since the main part of the vehicle has such a bright radar return in comparison to these smaller moving objects on the vehicle, the smaller objects are difficult to detect from the radar's perspective. With a very bright return from the main body of the vehicle and and very little returns from other velocities on the vehicle, the micro-Doppler signature is unique due to its lack of micro-Doppler motions.

34
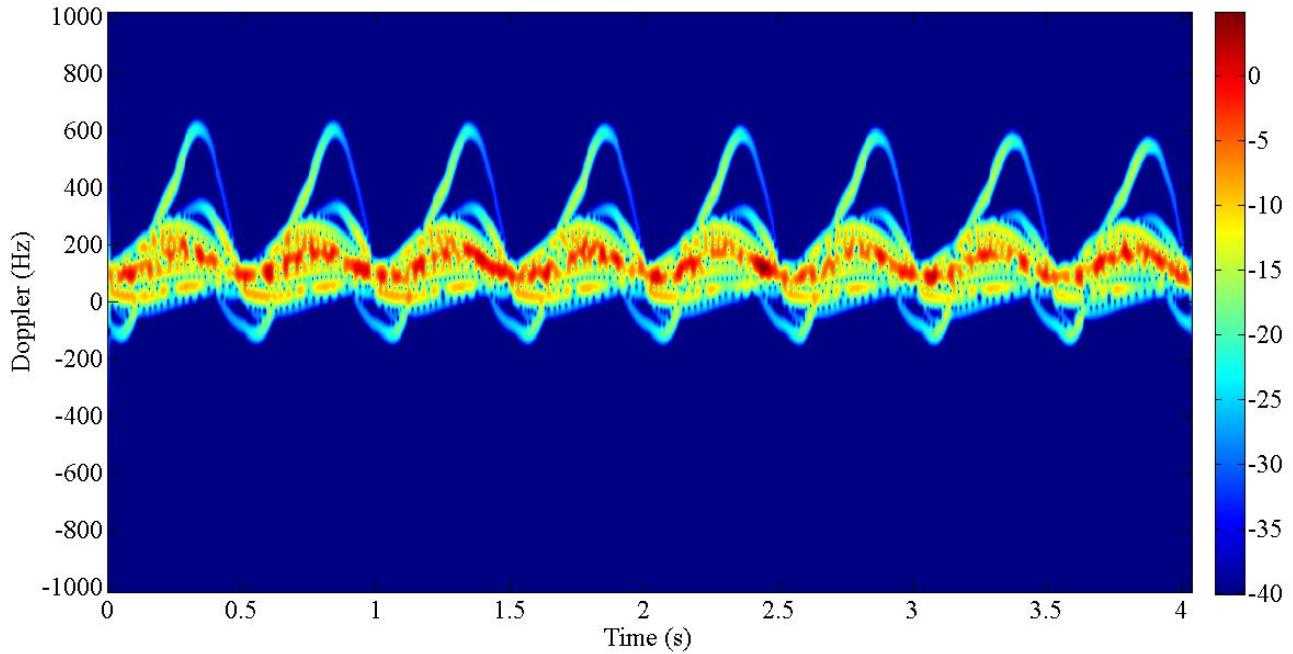
Figure 3.13: Simulated micro-Doppler signature of a human walking.

This lack of micro-Doppler is not the case with all vehicles. In the case of vehicles with tracks there is significant micro-Doppler motion and a micro-Doppler signature [9]. Figure 3.14 is a image of a M1A1 Abrams tank which is a tracked vehicle. In this image the tracks of the tank can be clearly seen. The tracks are usually quite large and can be seen from the radar. The velocity of the tracks are different from the main velocity on the vehicle. As the vehicle moves at a constant rate the tracks also move at a constant rate. Figure 3.15 is a example of the micro-Doppler signature of a tracked vehicle.

3.5   Chapter Summary

A radar with high resolution in Doppler can discriminate the Doppler spectrum. With the high resolution micro-Doppler can be measured. This is independent of the radar's range resolution. Micro-Doppler signatures of various objects provide additional information used to classify the object. Humans walking and vehicles have unique signatures and these signatures can potentially be used for classification.

Figure 3.14: An image of a tracked vehicle. This is the M1A1 Abrams tank [10].
.
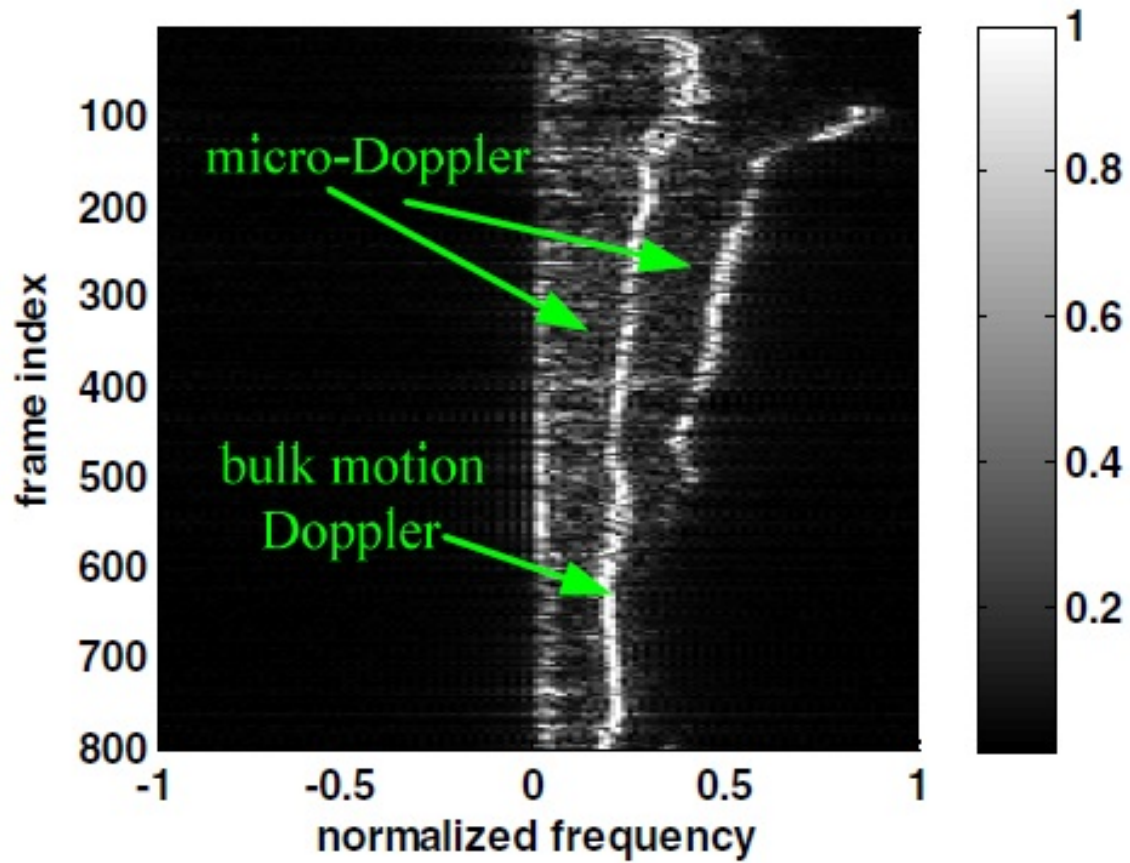
Figure 3.15: Micro-Doppler signature of a tracked vehicle [9]. This Micro-Doppler signature shows the main return from the bulk of the object and then two other lines in Doppler one on either side of the main return. This micro-Doppler is presumed to come from the vehicles' tracks.

CHAPTER 4.   ANALYZING MICRO-DOPPLER FEATURES

As shown in the previous chapter, the micro-Doppler signatures of objects give greater understanding to the sum of all radial velocity the object contains while in motion. The challenge comes in extracting information from the micro-Doppler signature to identify the object. There are many techniques used to analyze the micro-Doppler signature [11] [12] [13]. This chapter focuses on feature-based techniques that extract information from the micro-Doppler signature. In addition to presenting the features, two simulated micro-Doppler profiles are used to explore the results of the features.
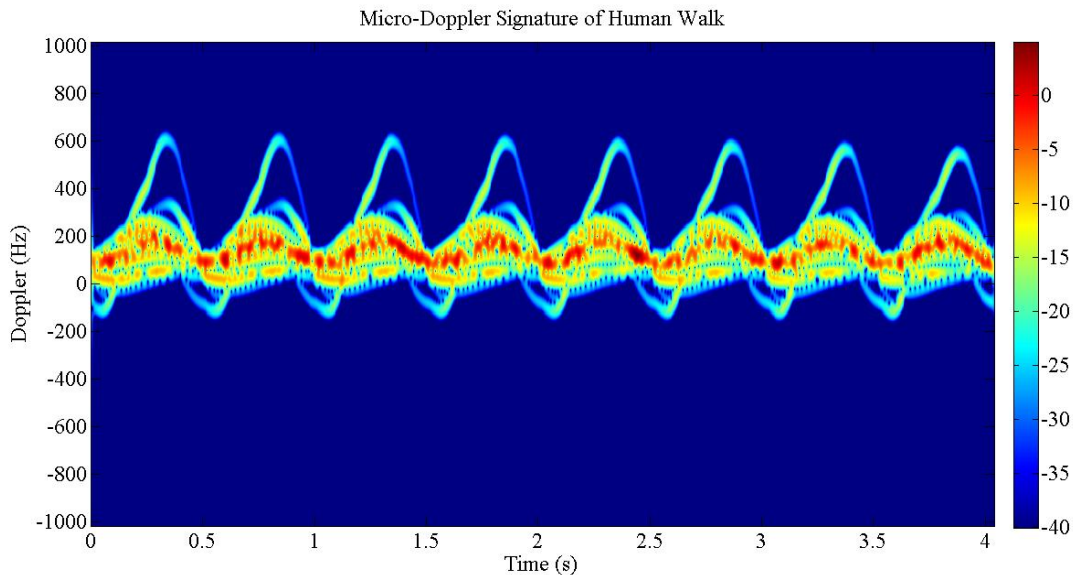
Figure 4.1: Simulated micro-Doppler signature of a human walking. The x-axis is time and the y-axis is Doppler frequency. The signature shows a high energy section in the frequency middle of the signature which is presumed to be the main trunk of a person. There is additional Doppler velocity faster or slower than the trunk which is presumed to come from the arms, legs, hands and feet.
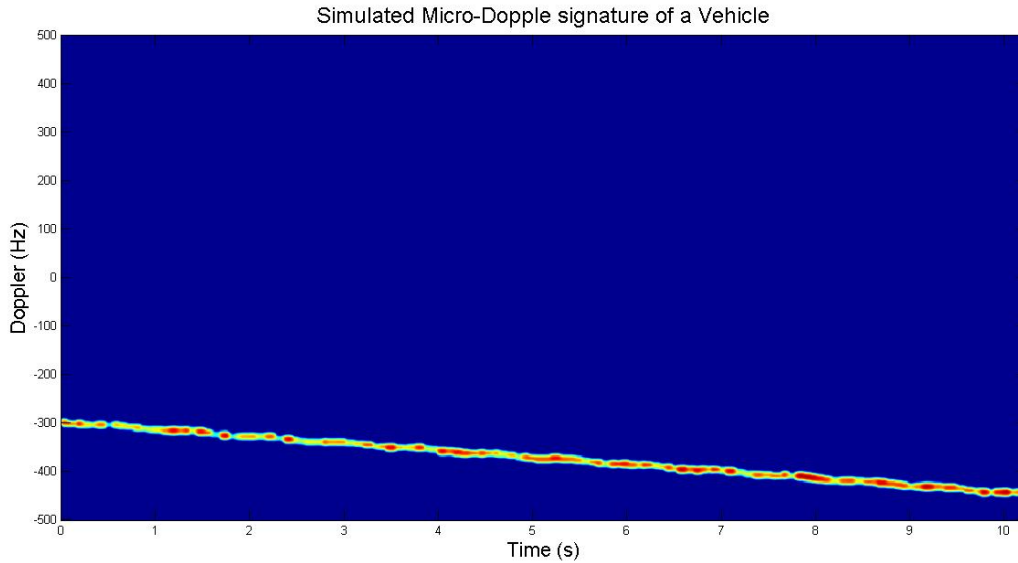
Figure 4.2: Simulated micro-Doppler signature of a vehicle accelerating from 10 mph to 15 mph.

4.1 Micro-Doppler Features

Selecting features to analyze an object's micro-Doppler signature is an important step in extracting information in feature based classification. Ideally, features selected are the most telling about a particular object or groups of objects. The types of objects analyzed and classified in this thesis are limited to vehicles traveling and humans walking. In selecting features for these two classes of objects, it is desired to have a single feature representing each of these objects with different values. In theory, if the feature value corresponds to a vehicle, the object is a vehicle and likewise, if the value corresponds to a human walking, the object is human. However, finding a single micro-Doppler feature to represent a group of objects or even a single object proves to be very difficult.

Because groups of objects share some characteristics, a particular micro-Doppler feature might describe a few objects well and others not so well. In lieu of a single micro-Doppler feature, multiple micro-Doppler features must be selected to accurately represent an object. The object is then described by combining all information from every feature. This approach is forgiving to some features that only provide limited information because the approach does not rely on a single feature but on the collective information obtained through all features. The following simple features selected are the attempt to describe humans and vehicles so that they can be differenti-

ated. The features selected are: Doppler maximum, Doppler variability, Doppler bandwidth, and Doppler span.

To estimate the results of these features simulated data is used for humans walking and vehicles traveling. A model of the micro-Doppler human walking is used to generate the simulated data [4]. For reference the data can be seen in Fig. 4.1. The second simulated dataset is of a vehicle accelerating from 10 mph to 15 mph. This dataset was generated for the purposes of this thesis. For reference the data can be seen in Fig. 4.2.

4.1.1   Doppler Maximum

It is noted that humans walking and vehicles can travel at different speeds. The velocity can potentially be a measurement that differentiates humans from vehicles. To measure this feature from the perspective of the micro-Doppler signature the Doppler maximum feature was created.

The Doppler maximum is defined as the point in time and Doppler frequency containing the highest amplitude. It is a measurement of frequency bin not amplitude. The Doppler maximum is calculated using a few steps. First, the short time Fourier transform is calculated on the object's time profile using the following:

$$X(m, \omega) = \sum_{n=-\infty}^{\infty} x[n]w[n-m]e^{-j\omega n} \tag{4.1}$$

where $x[n]$ is the samples in time of the object and $w[n]$ is a window function. $X(m, \omega)$ is the object's Doppler frequency spectrogram. It is calculated as often as an object is detected by the radar. To calculate the Doppler maximum, the following equation is used

$$N_{FD} = \arg\max_{m \in \mathbb{R}} |X(m, \omega)|^2 \tag{4.2}$$

where N_{FD} is the frequency bin location in the spectrogram of the maximum. This point represents Doppler frequency shift with the greatest amplitude observed by the radar. This point is generally near the center of the micro-Doppler frequency span of an object. The measured Doppler maximum can be decomposed into two parts. The first is due to the bulk velocity of the object. The

second is the contributions from the object's micro-Doppler. In communication terms the bulk velocity represents the carrier and the micro-Doppler represents the modulation.

The Doppler maximum is calculated for the simulated data sets described earlier. Figure 4.3 is the time-frequency plot of a human walking with the Doppler maximum plotted in black. The lower plot is the Doppler maximum. The simulated time-frequency plot shows the different features of a human walking. The upper plot shows the mass of the human and then some of the other features of the human walking such as the arms, legs, hands, and feet. These features can be seen in the time-frequency plot as deviations from the main portion of Doppler that have either more or less Doppler shift than the main Doppler return. From the Doppler maximum in the lower plot, it can be seen that the Doppler maximum is not the main mass of a person the entire duration of the dataset. At times an arm or leg or some other part of the body dominate the Doppler. Those points in time are the peaks in the data. Figure 4.4 is the time-frequency plot of a vehicle with the Doppler maximum plotted on top in black. The lower portion of the plot is the Doppler maximum plotted in isolation. A vehicle has fewer features that cause the micro-Doppler to spread out. As a result the Doppler maximum of a vehicle has few peaks compared to the human walking.

The Doppler maximum may thus be a useful feature for classifying objects. Similar objects travel at similar speeds. Humans have a bounded range of speed towards or away from the radar that can be measured through the Doppler maximum. Vehicles have a much broader range of speed. The slower portion of a vehicles' speed range overlaps a human's speed range which may cause some ambiguity in using this feature to differentiate humans walking and vehicles traveling.
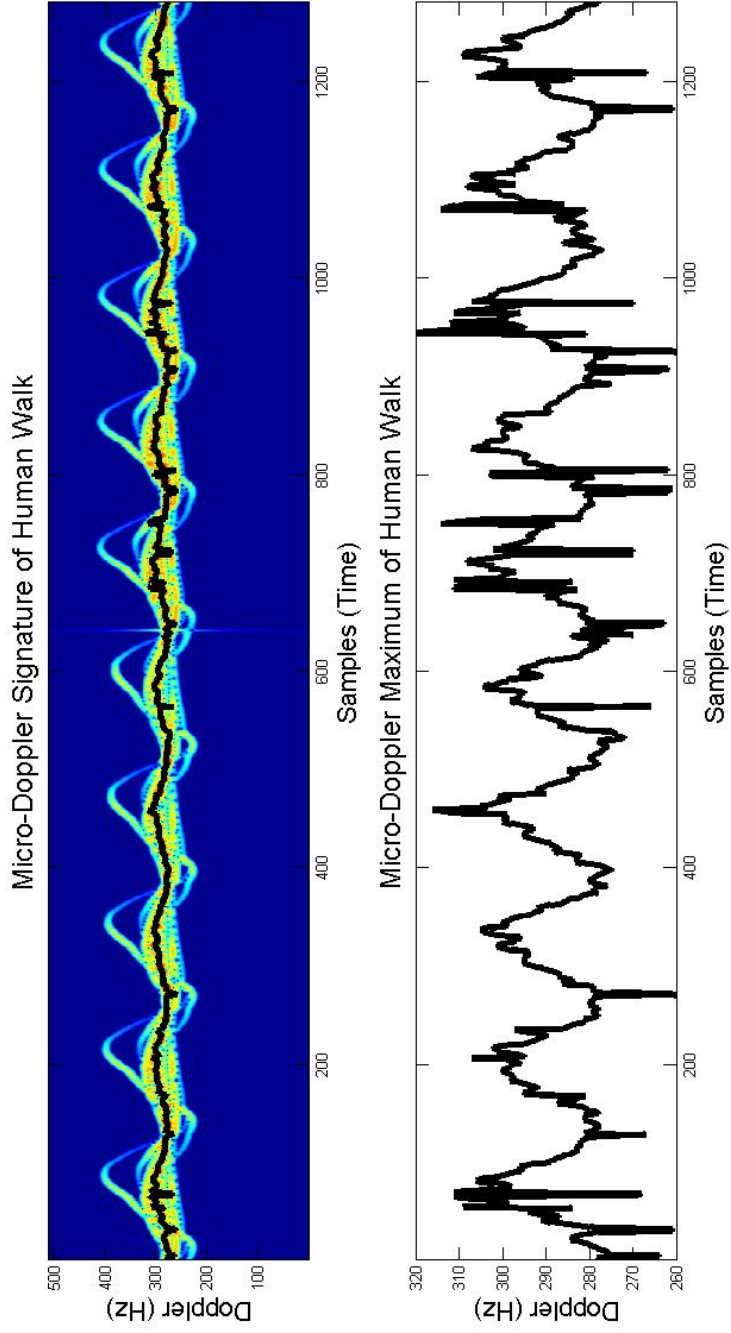
Figure 4.3: Upper plot is the simulated micro-Doppler signature of a human walking. The Doppler maximum is plotted as the black line. This represents the maximum amplitude in time and Doppler shift for this object. The lower plot is the Doppler maximum plotted in isolation.
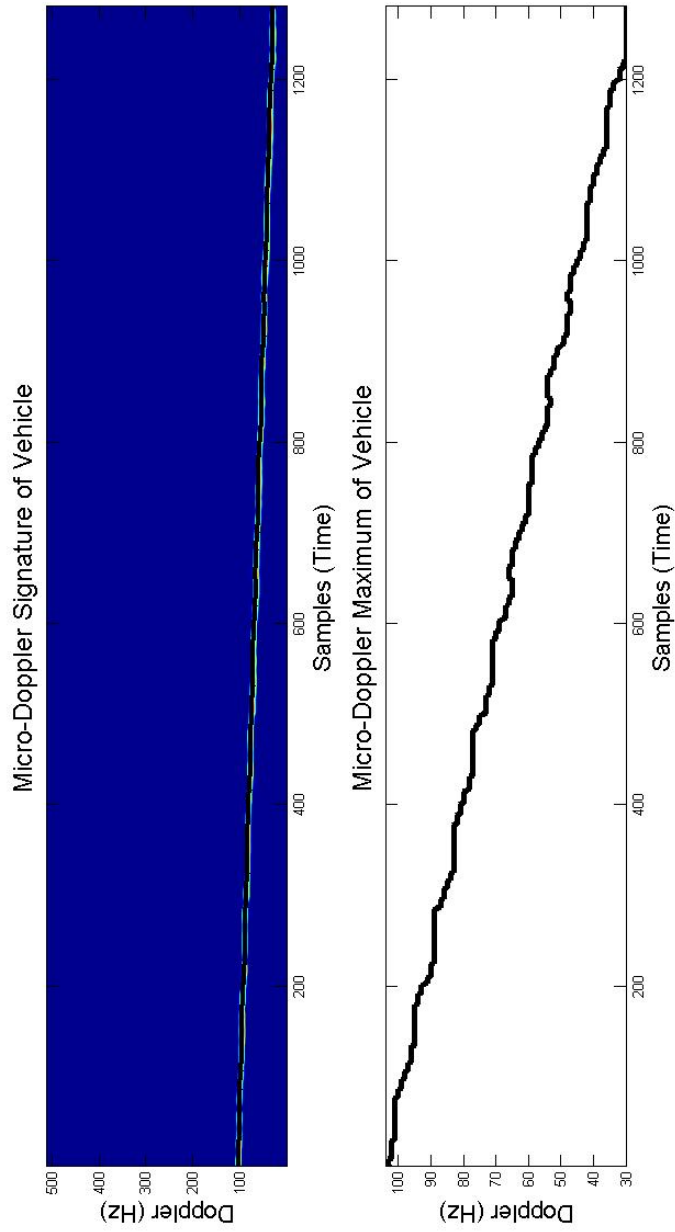
Figure 4.4: Simulated micro-Doppler signature of a vehicle accelerating from 10mph to 15mph. The upper plot is the the time-frequency plot with the Doppler maximum is plotted as the black line. The lower plot is the Doppler maximum plotted in isolation. This represents the maximum amplitude in time and Doppler shift for this object.

4.1.2 Doppler Variability

The time-frequency data of vehicles traveling and humans walking exhibits some differences. One of those differences is how the Doppler maximum changes over time. Doppler variability is a feature created to measure the variability in the Doppler maximum observed in vehicles and humans.

As seen with the Doppler maximum found using the simulated radar data, certain objects have peaks due to the radar return of different contributions of the object in the micro-Doppler signature. The peaks are observed in the human walk but not observed in vehicles. Doppler variability is a way to measure these peaks seen in the Doppler maximum. Doppler variability is calculated in a few steps. First, the variance is calculated using the following:

$$\sigma_N(n) = \sum_{i=1}^{2}(x_i - \bar{x}) \tag{4.3}$$

where x_i is the input vector and $\bar{x}$ is defined as follows,

$$\bar{x} = \frac{1}{2}\sum_{i=1}^{2}x_i. \tag{4.4}$$

This is the general equation for variance with a fixed vector length of 2. To calculate the variance, the Doppler maximum described in the previous section is used as the input vector x_i. The final step is to apply a maximum hold on the resultant vector, to allow the maximum value to persist over a window of time. This is calculated using

$$\sigma_{Doppler}(n) = \max_{k \in n-\frac{t}{2}:n+\frac{t}{2}} \sigma_N(k) \tag{4.5}$$

where t is an even integer representing the length of a time window and $\sigma_{Doppler}$ is the final result and the Doppler variability. The variance peaks have a short duration so the max hold forces variance values that are great in amplitude to persist over the specified time window width t.

The upper half of Fig. 4.5 is the time frequency plot of a human walking with the Doppler maximum plotted in black. The lower half of the plot is the variance with Doppler variability. In comparing the top and bottom graphs it can be seen where the Doppler maximum contains peaks and the variance also contains peaks. One can also see how those peaks contribute to the Doppler

44
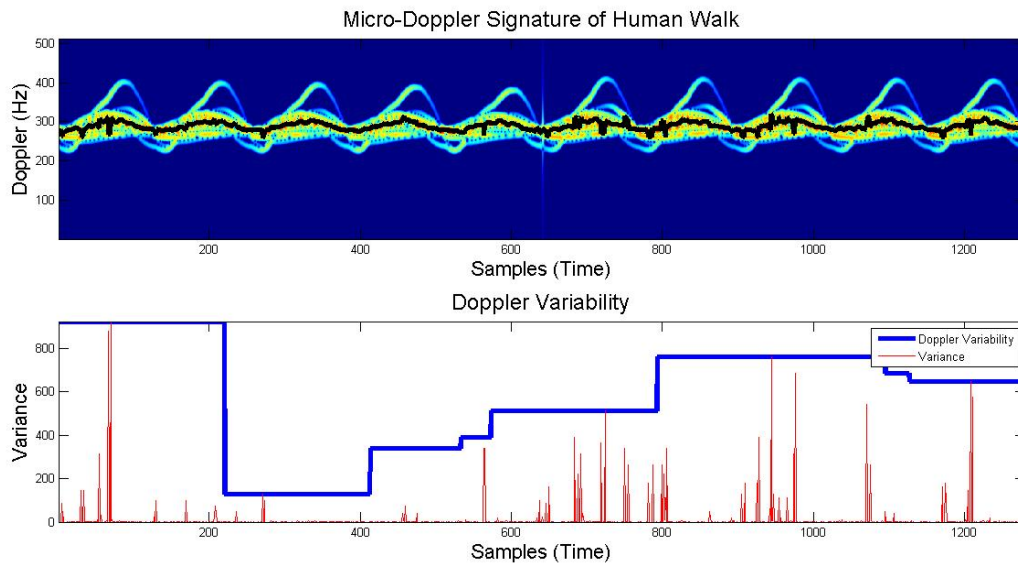
Figure 4.5: The upper plot is the simulated micro-Doppler signature of a human walking with the Doppler maximum is plotted as the black line. The lower plot is the variance of the Doppler maximum in red and the Doppler variability plotted in blue. Where there are peaks in the Doppler maximum in the upper plot the lower plot also increases.
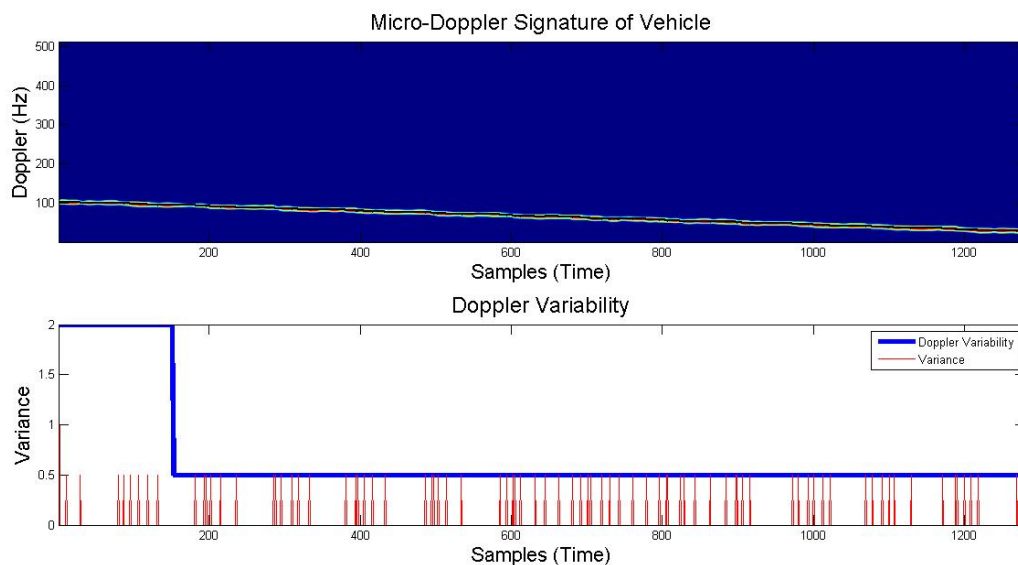
Figure 4.6: Simulated micro-Doppler signature of a vehicle accelerating from 10 mph to 15 mph with Doppler maximum is plotted as the black line. The lower plot is the variance of the Doppler maximum in red and the Doppler variability plotted in blue.

variability seen in blue. The upper half of Fig. 4.6 is the time-frequency plot for the simulated vehicle data. The lower half of the plot is the variance and the Doppler variability. In the vehicle data the peaks are shallow and the Doppler variability is much smaller in comparison with the human walking.

Doppler variability is selected as a feature because it appears to be a good measure of the number of unique physical objects that comprise a micro-Doppler signature. This is based on the observations in the two simulated datasets and the known behavior of each object.

4.1.3 Doppler Bandwidth

Another observed difference between the micro-Doppler profiles of humans walking and vehicles is the amount of Doppler energy spread over a single instance in time. A human walking has a lot of energy spread over frequency in Doppler, presumably from the hands, feet, arms, and legs all moving at different velocities as the human walks. A vehicle has very little energy spread over frequency in Doppler. The Doppler bandwidth is a feature created to measure the Doppler frequency spread of an object.

Doppler bandwidth is defined as the width of the micro-Doppler signature of an object. It is calculated using the following sets of equations. First a binary threshold is applied to the Doppler spectrogram using the following

$$b(m) = \begin{cases} 1 & |X(m,\omega)|^2 > \frac{2}{k}\sum_{i=1}^{k}|X(i,\omega)|^2 \\ 0 & otherwise \end{cases} \tag{4.6}$$

where $X(m,\omega)$ is the short time Fourier transform of the Doppler spectrum and $b(m)$ is the resultant binary threshold vector. Data points in the spectrogram above the threshold are given a one while the rest are given zeros.

Figures 4.7 and 4.8 are the simulated data sets after the binary threshold is computed. Notice how the threshold is an outline of the higher amplitude data in the previous time-frequency plot. This step of thresholding is similar to edge detection in image processing. After the binary threshold has been computed, the Doppler bandwidth is computed by finding the largest width for every instance in time. The thresholding simplifies this step and the bandwidth is found by
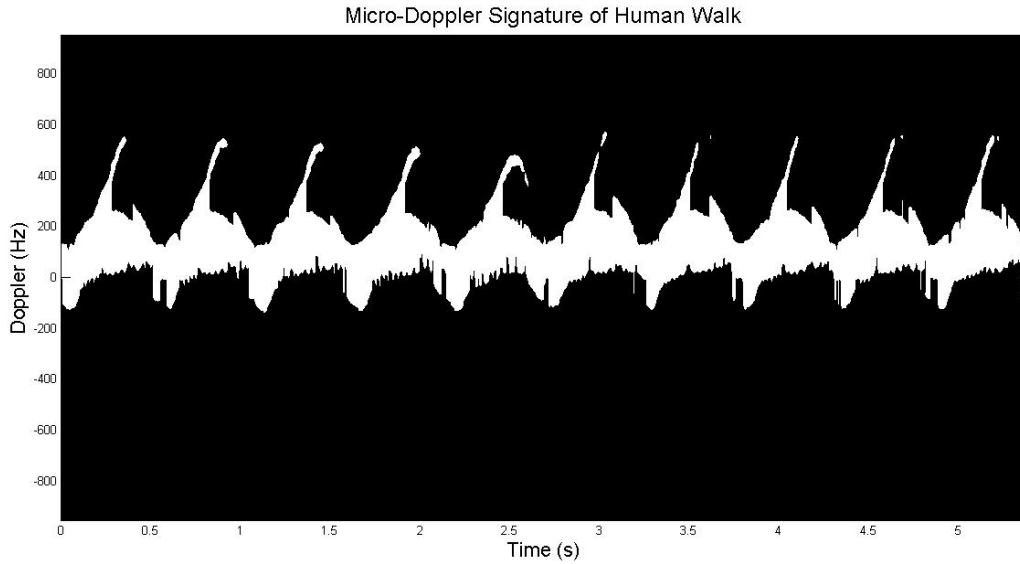
Figure 4.7: Simulated micro-Doppler signature of a human walking. A binary threshold has been applied to the time-frequency data. The data points with the greatest amplitude are seen in white. Compare to Fig. 4.1
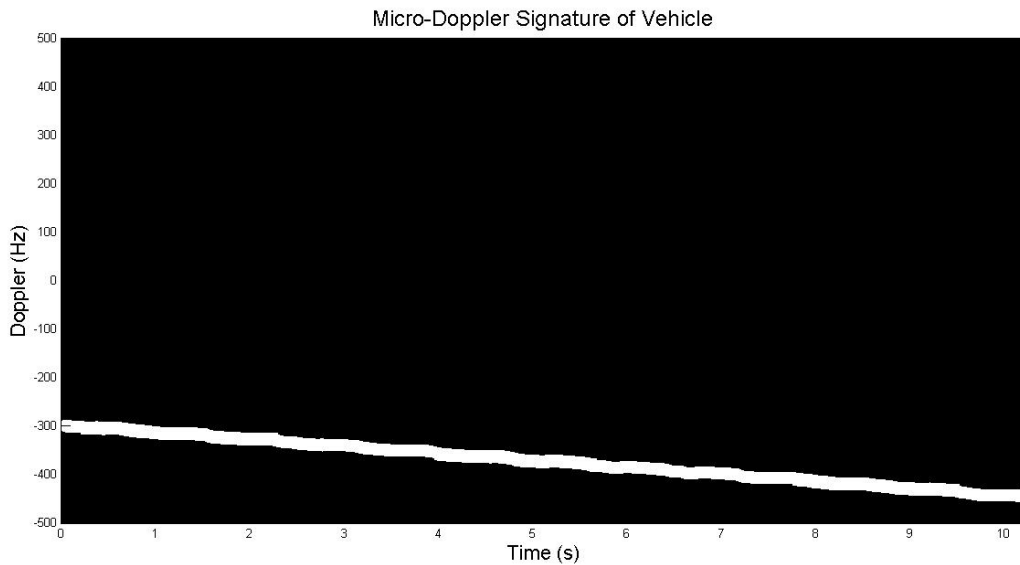
Figure 4.8: Simulated micro-Doppler signature of a vehicle accelerating from 10 mph to 15 mph. A binary threshold has been applied to the time-frequency data. The data points with the greatest amplitude are seen in white.

searching the binary threshold for the longest row of ones. Figures 4.9 and 4.10 show the simulated datasets after the largest width is found. The white line plotted on top of the time-frequency plot is the Doppler bandwidth. Notice the slight difference between the binary threshold and the Doppler bandwidth. This is a because the algorithm is searching for a contiguous group of ones.
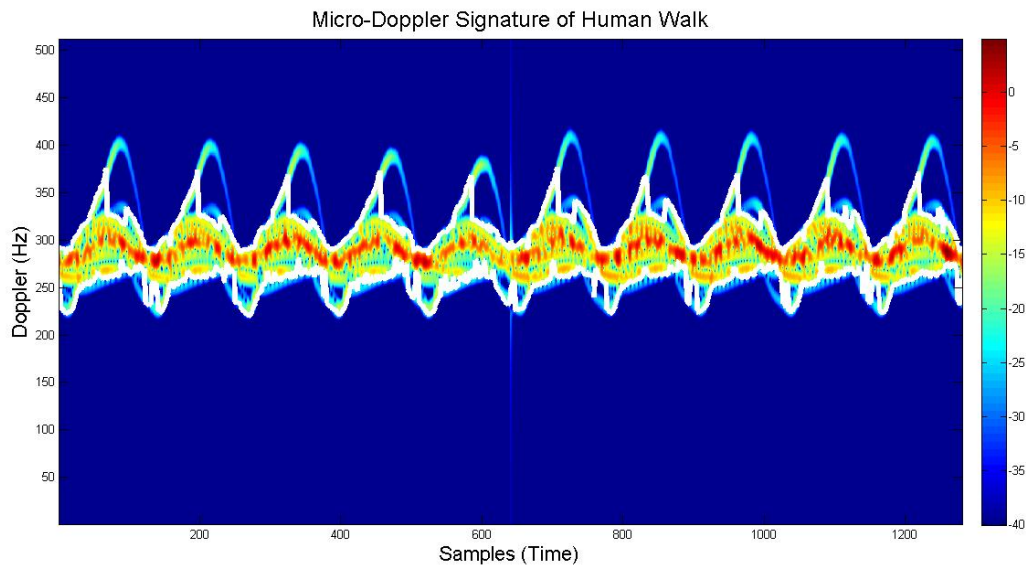
Figure 4.9: Simulated micro-Doppler signature of a human walking. The Doppler bandwidth is the distance between the white lines.

Doppler bandwidth appears to be able to provide a measurement where humans and vehicle will have differences. Different objects are expected to have a different range of radial velocity, particularly if the objects method of travel or motion differs from each other. This is seen from the simulated radar data of the human walking and the vehicle. Those objects move differently and thus appear to have different bandwidths. The Doppler bandwidth is an attempt to measure the range of radial motion.

4.1.4 Doppler Span

Differences between humans walking and vehicles traveling are readily apparent using the Doppler maximum. There may be more information in the Doppler maximum data than just the variability. As seen with the Doppler bandwidth, humans walking and vehicles occupy differing
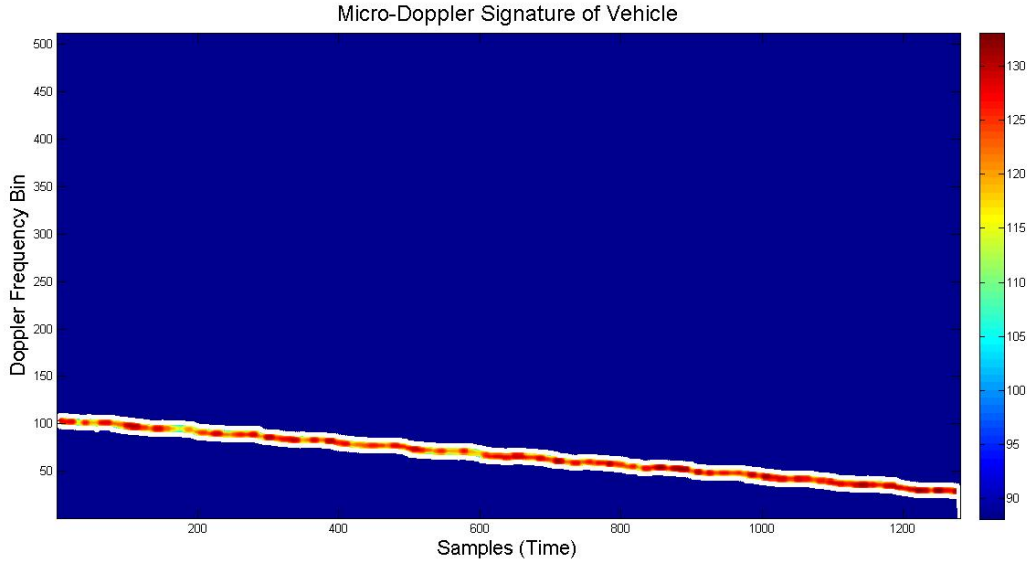
Figure 4.10: Simulated micro-Doppler signature of a vehicle accelerating from 10 mph to 15 mph. The Doppler bandwidth is the distance between the white lines.

amounts of Doppler energy because of the differing range of radial velocities. The Doppler span is a feature created to measure the Doppler frequency span in the Doppler maximum data. Doppler bandwidth uses the spectrogram and a threshold while the Doppler span uses the Doppler maximum data covered earlier in this chapter. It is defined as the distance between points of greatest amplitude that have the least amount of Doppler shift to the greatest amount of Doppler shift over a given window of time. It can be calculated using the following:

$$Span(n) = \max_{k \in n-\frac{w}{2}:n+\frac{w}{2}} N_{FD}(k) - \min_{k \in n-\frac{w}{2}:n+\frac{w}{2}} N_{FD}(k) \tag{4.7}$$

where N_{FD} is calculated using Eq. 4.2 and w is an even window size. The window size dictates the length of data over which the minimum and maximum will be found.

Figure 4.11 is a plot of the Doppler maximum (N_{FD}) surrounded by the Doppler span for the simulated data of the human walk. The lower limit is plotted with the red line and the upper limit in green. The lower portion of the plot is the Doppler span calculated from the upper and lower limits. Figure 4.12 is a similar plot however this plot is the simulated data for the vehicle traveling. In comparing the two plots it can be seen that the Doppler span for the human walking, in

49
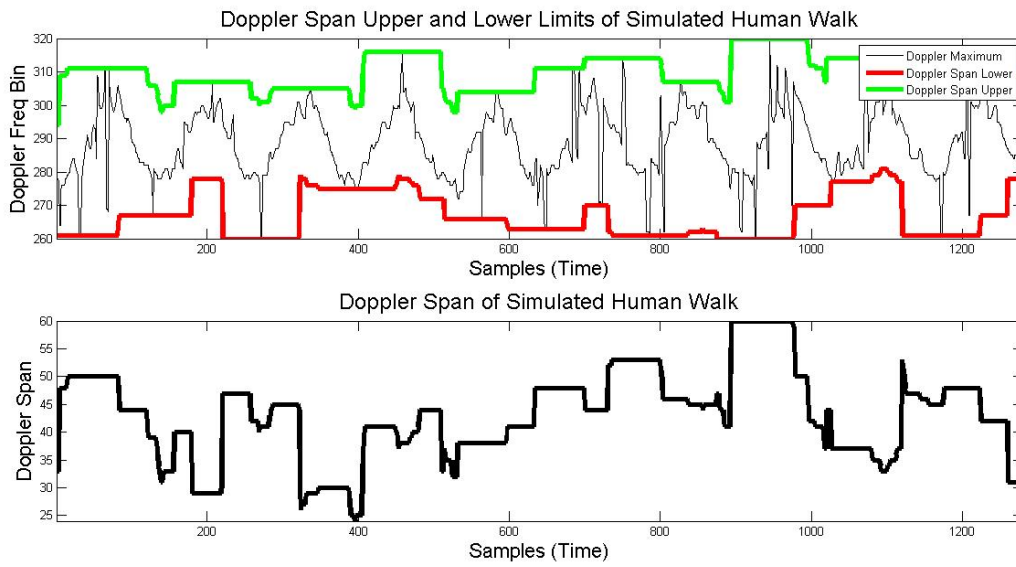
Figure 4.11: Simulated micro-Doppler signature of a human walking. The upper plot is the Doppler maximum plotted as the black line while the upper limit of the Doppler span is the green line and the lower limit of the Doppler span is the red line. At a single time sample the distance between the upper and lower bounds in the Doppler span. The lower plot is the calculated Doppler span.
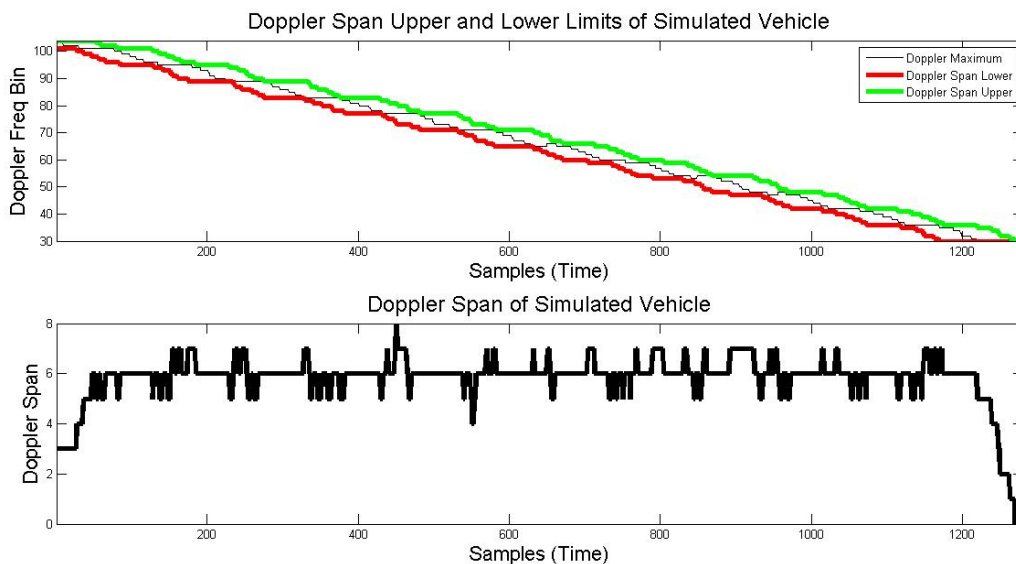
Figure 4.12: Simulated micro-Doppler signature of a vehicle accelerating from 10 mph to 15 mph. The upper plot is the Doppler maximum is plotted as the black line while the upper limit is the green line and the lower limit is the red line. At a single time sample the distance between the upper and lower bounds in the Doppler span.

general, is wider than the span for the vehicle. This may be due to the total range of micro-Doppler velocity that a human has versus a vehicle.

4.2 Chapter Summary

The four features selected to analyze the micro-Doppler signatures of humans walking and vehicles are Doppler maximum, Doppler variability, Doppler Bandwidth, and Doppler span. Most of these features developed as a result of analyzing and comparing the time-frequency plots of the two classes of objects. These features were analyzed using two simulated data sets and seem to result in measuring differences in these two classes of objects. Table 4.1 summarizes the four micro-Doppler features used in this feature based analysis of the micro-Doppler signatures of humans walking and vehicles and their possible physical measurement.

Table 4.1: Listing of the four features being analyzed with their possible physical measurement.

Micro-Doppler Feature	Measurement
Doppler Maximum	General speed of the object
Doppler Variability	Number of unique physical contributors
Doppler Bandwidth	Range of velocity for physical contributors
Doppler Span	Range of velocity for physical contributors

CHAPTER 5.   DATA COLLECTION AND PROCESSING

The previous chapter covered the set of micro-Doppler features chosen for the purpose of differentiating humans walking from vehicles. The selected features were analyzed using simulated data. This chapter covers how actual radar data was collected for the purpose of analyzing the micro-Doppler features of actual humans walking and vehicles. This chapter also covers the initial processing on the collected data.

5.1   Data Collection

The micro-Doppler features selected in the previous chapter are analyzed using simulated radar data. It appears from the initial results the features are adequate at measuring some of the differences between humans walking and vehicles. Having simulated data is only as good as the model used to generate it and the models used do not account for real world conditions. To preform a complete study of the micro-Doppler features, actual radar data was collected.

5.1.1   Radar System

An experimental radar system was used to collect the radar data. The radar system was built for the purpose of collecting data for this thesis. It was constructed using commercial off-the-shelf parts along with some custom components. The system operates at C-band, generally from 7.95 GHz to 8.00 GHz. This frequency is high enough to detect the micro-Doppler of interest. The system used high gain horn antennas to maximize the SNR. Figure 5.1 is the block diagram for this experimental radar system. The radar system successfully captured and stored raw data.

Figures 5.2, 5.3, and 5.4 show the radar. These images show the various components of the radar system such as the horn antennas, cabling, and electronics. The radar electronics are placed on a metal plate mounted on a tripod and was transported to different sites for data collection.
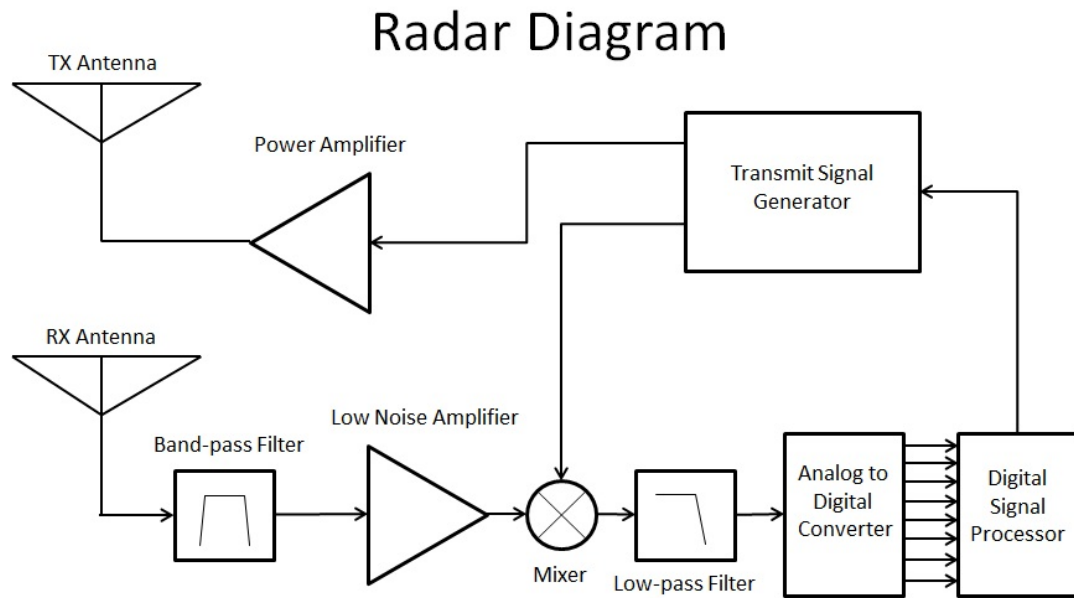
Radar Diagram

Figure 5.1: Block diagram of the experimental radar system used to collect data for this thesis.

5.1.2   Method of Data Capture

A controlled experiment was conducted to collect the data. The radar had a clear line of sight to the test objects. The experiment was designed so the object of interest was the only moving object in the radar's field of view (FOV) at the time of the data collection. This allowed the experiment to be controlled, simplified the signal processing, and allowed the micro-Doppler signature to be more readily extracted.

Once the site was selected to preform the data collection, the radar was set-up and powered on. The system was verified operational and the data collection commenced. Recording of the radar raw data started when the object of interest entered the radar's FOV and the recording stopped when the object left the radar's FOV.

Figure 5.2: Data collection radar sitting on a tripod. Side view of the horn antennas and the cables.

5.1.3 Description of Data

It was desired to collect radar data of humans walking and vehicles in a variety of scenarios in order to establish a database for analysis of the micro-Doppler signatures. Radar data for a human walking was collected on a cooperative person. The person was separately recorded walking towards and away from the radar system. Figures 5.5 and 5.6 show the two main trajectories of the human walking as they moved through the radar's FOV. Radar data for vehicles was collected on a variety of different vehicles. The vehicles also followed similar trajectories as outlined by Figs. 5.5 and 5.6.

Table 5.1 gives a summary of all data collected. It shows the number of data files, the type of object, and the trajectory. Forty one data files were collected, 19 were vehicles and the remaining 22 were a human walking.

Figure 5.3: Back view of the data collection radar sitting on a tripod showing many of the coaxial and power cables required to run the system.

Table 5.1: Listing of the data sets collected.

Number of Datasets	Object Type	Object Trajectory
13	Vehicle	Trajectory 1
6	Vehicle	Trajectory 2
11	Human	Trajectory 1
11	Human	Trajectory 2

These data files are intended to provide a simple test of the radar's measurement capabilities of humans walking and vehicles traveling. Every case could not be considered; however, it is hoped that the collected data is sufficient for an initial evaluation of the features.

Figure 5.4: Front view of the data collection radar sitting on a tripod. The high gain horn antennas can be seen at the front of the radar.

5.2   Data Processing

Processing is required to extract features from the collected data. After processing the raw data, the features can be readily extracted. The processing is divided up into 3 steps: pre-processing, range and Doppler processing, and generating a time-frequency profile.

5.2.1   Pre-Processing

The data recorded by the radar system was raw samples from the ADC. In addition to the raw data, meta-data was also recorded which contained details about the test object and test setup. The raw data is stored in large chunks containing some amount of unwanted data at the beginning
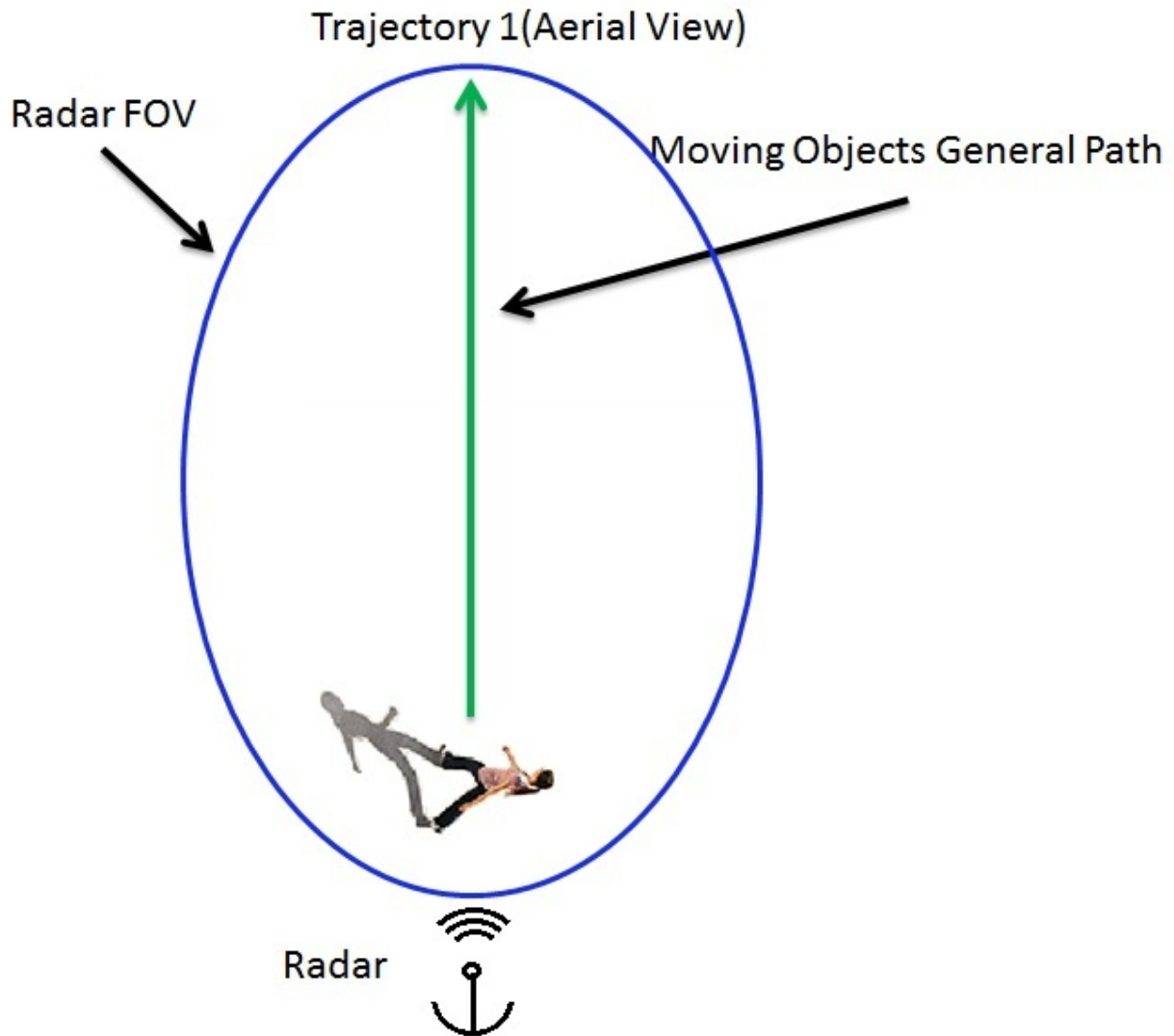
Figure 5.5: Trajectory 1 of an object during data collection. In this trajectory the object travels directly away from the radar.

and end of the data recording. Also, some of the recordings contained two separate scenarios separated by some amount of time.

The first step in analyzing the micro-Doppler signature is to clean the raw data captured. The sections of data at the beginning and end of the data recordings containing no information are removed and the data recordings containing multiple scenarios are separated into individual data files. This is done using a data viewer written in Matlab. The data is visualized using a Range Doppler map (RDM). RDMs are explained in detail in Chapter 2. The index into the raw data is
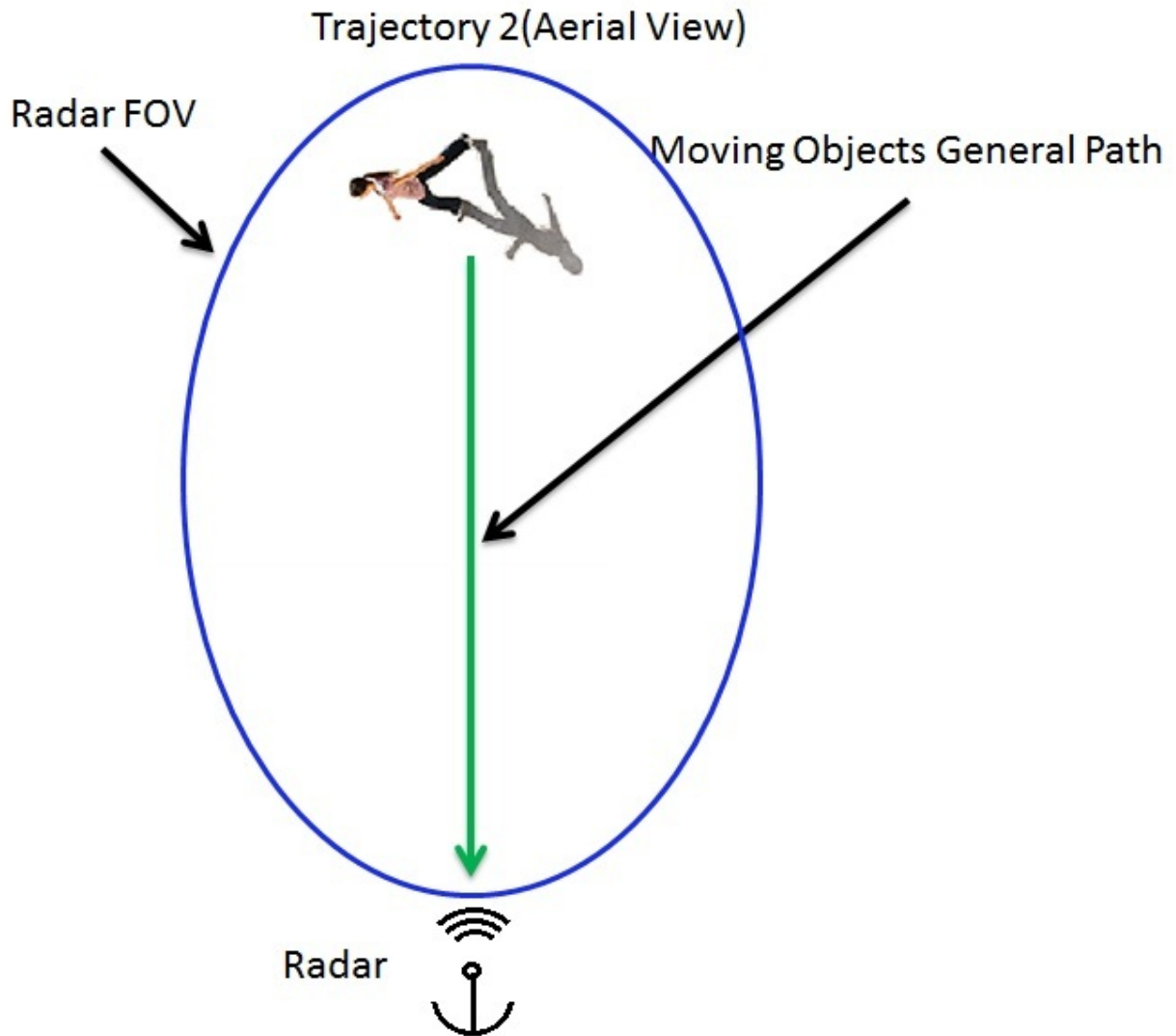
Figure 5.6: Trajectory 2 of an object during data collection. In this trajectory the object travels directly towards the radar.

displayed along with the RDM. Once the object of interest is visually located in the RDM the start index is recorded. The stop index is recorded in a similar manner when the test object is no longer visible in the RDM. Using the start and stop indexes a smaller data subset is generated. The clean data set has no dead time at the beginning and end of the file and contains a single test object.

The raw radar data was processed into 41 clean data sets. The data is then ready for the range and Doppler processing.

5.2.2 Range and Doppler Processing

After the data is cleaned, the range and Doppler processing is preformed. This processing step extracts the test objects range and the Doppler spectrum. The data is first range compressed to obtain the objects' range information. Then the Doppler information is extracted. To extract the Doppler information 512 chirps are used to create a CPI. A chirp is defined as the portion of the data captured while the output frequency of the radar is increasing. A CPI is defined as the coherent processing interval which is the amount of chirps over which the signal will be integrated. A CPI size of 512 was chosen to maximize the Doppler resolution based on earlier experimentation. However, with a CPI of 512 the time resolution is sacrificed. In order to maximize the time resolution a sliding window is used to select which 512 chirps are used to create the CPI. Using this technique of a long CPI with a siding window provided the highest resolution possible in time and also in frequency. Figure 5.7 shows how two CPIs are generated with shared data in the middle due to the sliding window.

A CPI is processed to create a RDM, from which the object is detected. Detecting the object is simplified because of only one object of interest moving in the radars' FOV at a time. Once the object is detected the Doppler profile is isolated in preparation for the next processing step.

5.2.3 Time-Frequency Doppler Profile

After the range and Doppler processing, the final processing step is to generate the time-frequency Doppler profile of the test object. The range and Doppler processing produces a Doppler profile. Each of the object's Doppler profiles for each instance in time are assembled. This step is how the time-frequency plot is generated. After this step is complete the data is then ready for feature extraction.
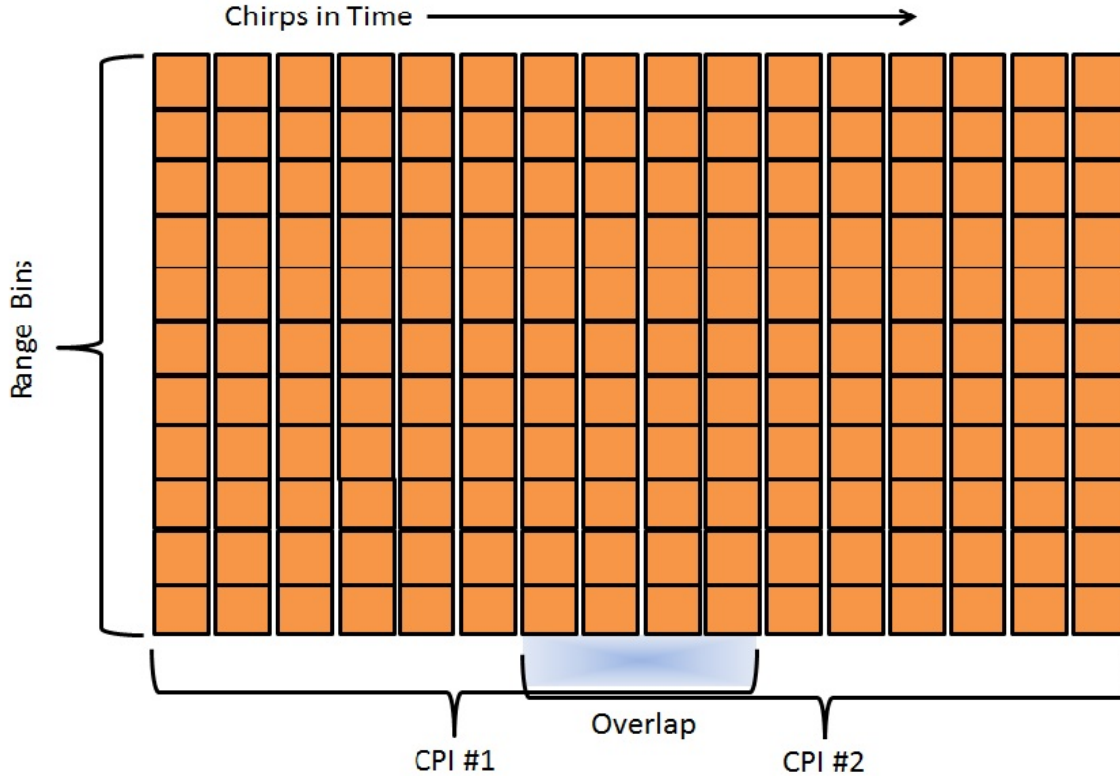
Figure 5.7: Illustration of the sliding window used to select the samples for the CPI.

5.2.4   Data Processing Summary

Figure 5.8 summarizes the data processing steps. The data is first cleaned, then the range and Doppler processing takes place followed by the generation of the time frequency profile. Once this processing is complete the data is ready for feature extraction.

5.3   Chapter Summary

In order to complete a study of the micro-Doppler signatures of vehicles and humans walking actual radar data was collected by an experimental radar system. The collected radar data was preprocessed and separated out into individual files which resulted in 19 vehicle datasets and 22 human walking datasets. Range and Doppler processing an time-frequency analysis was preformed on these clean datasets.

Figure 5.8: Summary of the data processing flow. This represents the steps taken prior to feature extraction.

CHAPTER 6.   MICRO-DOPPLER FEATURE RESULTS

The previous chapter covered how radar data was collected for the purposes of this thesis and the initial processing of data prior to the features being extracted. This chapter covers the analysis of the features after they are extracted from the radar data. This chapter also contains a brief analysis of each feature.

6.1   Doppler Maximum

As stated earlier, the Doppler maximum is a micro-Doppler feature chosen to analyze the signature of an object. The Doppler maximum is a measure of the velocity of an object. The Doppler maximum is extracted from each of the 41 datasets collected on the experimental radar system. It is extracted from the time-frequency profile of each dataset using the method previously outlined.

Figure 6.1 is a representative time-frequency plot of a human walking. The upper plot is the time-frequency plot with the Doppler maximum plotted in black and the lower plot is the isolated Doppler maximum. The structure of the time-frequency profile is similar to the simulated data analyzed previously. The Doppler maximum also behaves similar to the Doppler maximum extracted from the simulated data. The Doppler maximum is near the slower moving centroid of the signature while for brief moments the Doppler maximum measures either a higher or lower velocity. These discontinuities in the Doppler maximum are presumed to be a result of the motion effects from arms, hands, feet or legs. This behavior can be observed in Fig. 6.2 with the peaks and valleys in the Doppler maximum over time.

Figure 6.2 is a plot of a traveling vehicle from a representative dataset. The upper plot is the time-frequency plot with the Doppler maximum plotted in black and the lower half is the isolated Doppler maximum. This representative dataset is not unlike the simulated data analyzed previously. Both share similar time-frequency profiles and the Doppler maximum is also similar.
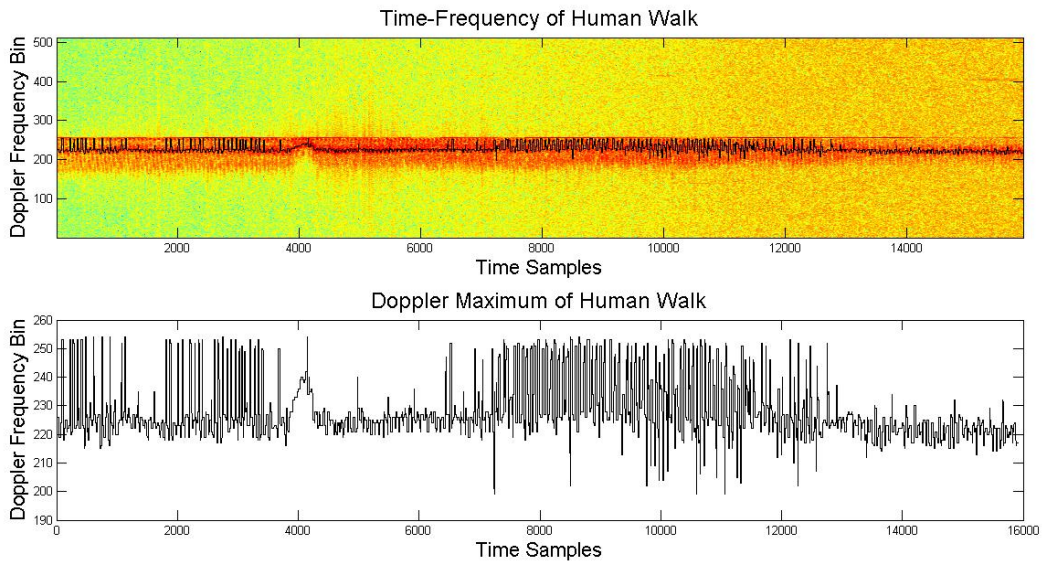
Figure 6.1: The upper plot is the time-frequency plot of a human walking with the Doppler maximum plotted in black. The lower plot is the Doppler maximum plotted in isolation. This is a representative dataset of a human walking.
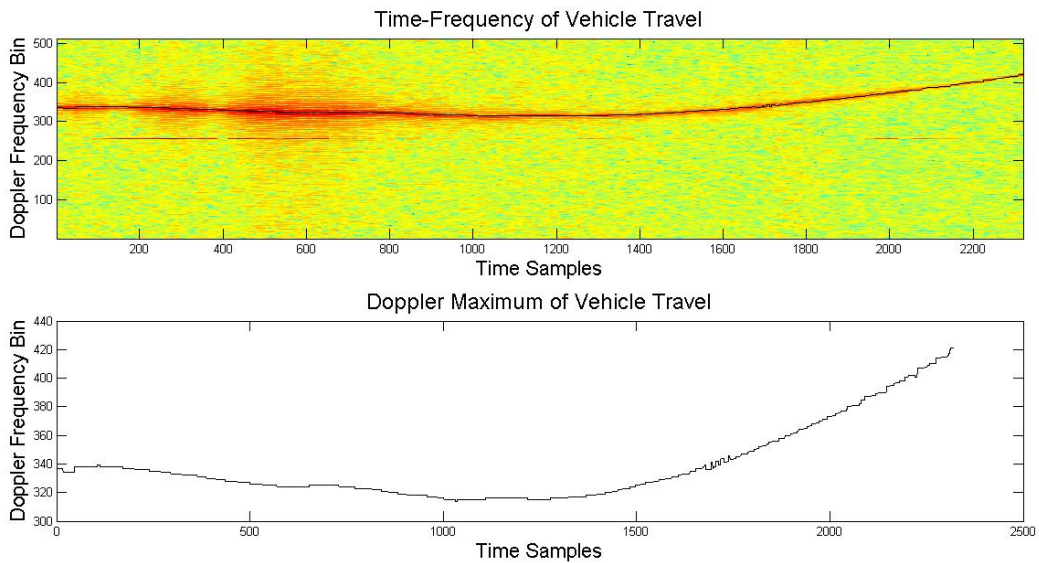
Figure 6.2: The upper plot is the time-frequency plot of a vehicle traveling with the Doppler Maximum plotted in black. The lower plot is the Doppler maximum. This is a representative dataset of a vehicle traveling.

In general, the time-frequency profile of the vehicle seems to be quite simple, which results in the Doppler maximum also containing very little structure or variance.
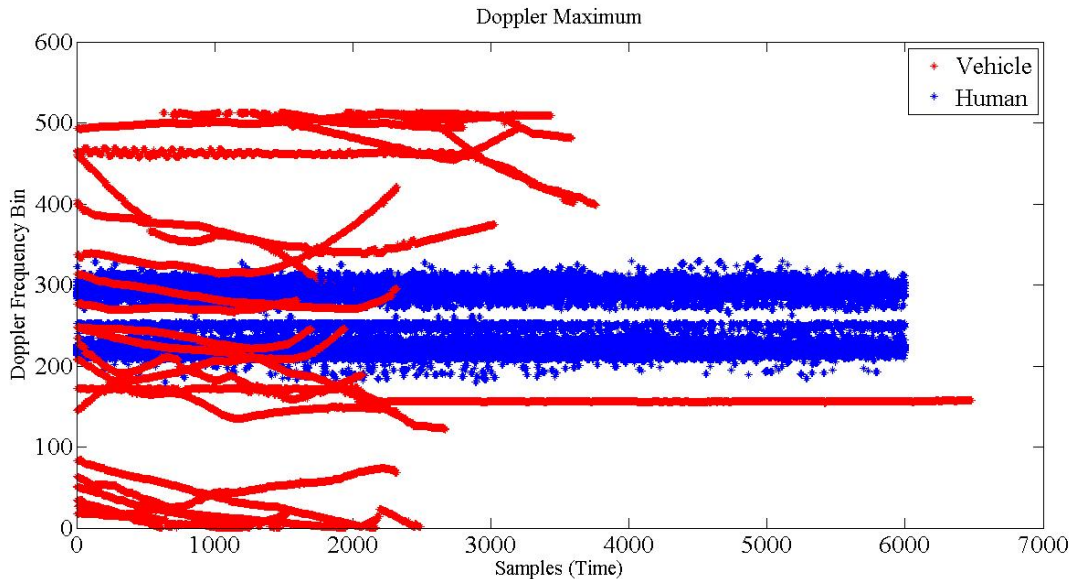
Figure 6.3: Plot of the results of all 41 datasets showing the Doppler maximum. The vehicle data are plotted in red and the humans walking are plotted in blue. Notice the humans walking were generally longer datasets. The vehicle data points occupy the entire region while the human walking data points are bounded.

The Doppler maximum is extracted from all datasets collected using the method previously described. Figure 6.3 is a summary plot of the results obtained from extracting the Doppler maximum from the 41 data sets. Humans walking are plotted in blue and vehicles in red. The x axis is time (samples) and the y axis is the Doppler frequency bin where the maximum occurred. Samples refer to the instance in time that the Doppler maximum was sampled and recorded to be used in the analysis. The middle of region represents the slowest velocity similar to the RDM. The Doppler maximum for humans walking is clustered near the middle. The Doppler maximum for vehicles traveling is spread over the entire range of velocities the radar is measuring. This is a result of the limited velocity that a human can travel versus the wide range of speeds that vehicles can travel.

6.1.1   Doppler Maximum Feature Analysis

One measure of how well the Doppler maximum discriminates between vehicles and humans walking is by how it is able to separate the two classes of objects. The optimal feature provides a measurement that separates the objects so they can easily distinguished. Some analysis can be done to attempt to measure the effectiveness of this feature at separating the two classes of objects.
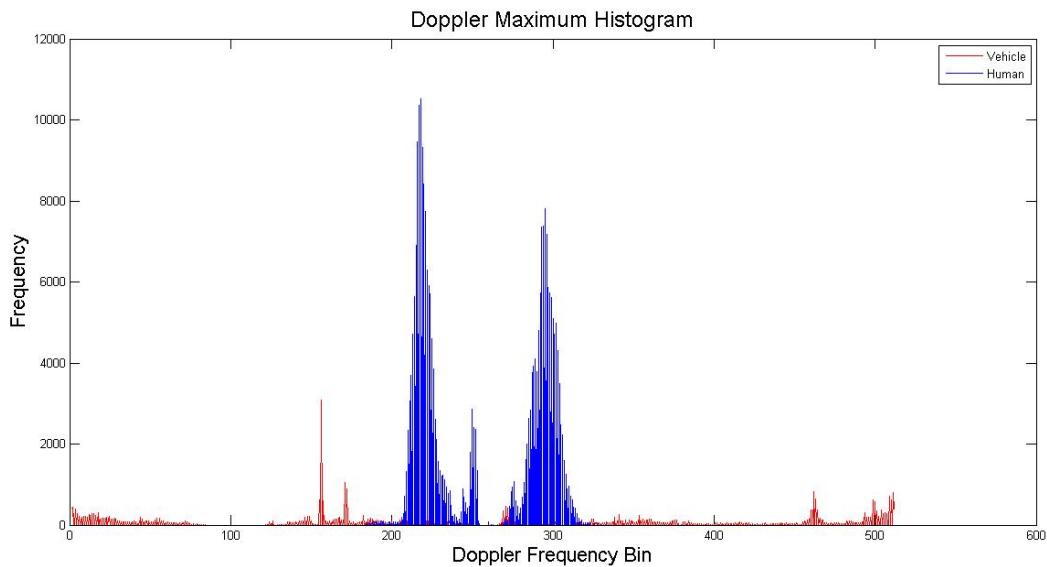
Figure 6.4: Histogram of the the Doppler maximum. Vehicle data is in red and the human walking data is in blue. The human data clusters generally towards the center of the data span representing the slowest velocity.

Figure 6.4 shows the histogram generated of the Doppler maximum from the collected data. The vehicles are plotted in red and the humans walking are plotted in blue. The x-axis is the Doppler bin where the maximum occurred and the y-axis is the frequency of occurrence. There is some clustering for humans walking while vehicles appear to be uniformly distributed over all Doppler frequency bins. From these results it appears there are two main groups of clustering: humans walking towards the radar and humans walking away from the radar.

To better understand this feature and how well it can separate humans walking and vehicles, probability distributions are fit to the data. The probability distribution model for each type
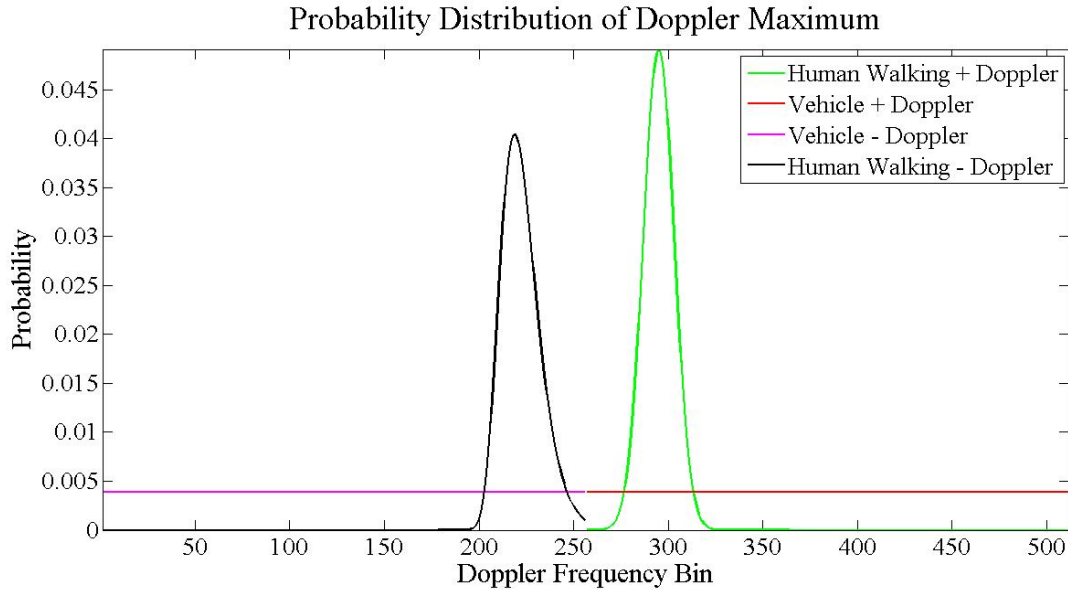
Figure 6.5: The data is fit to four probability distributions. Each describes the classes of objects traveling either towards or away from the radar (-/+ Doppler). The green is the probability distribution for humans walking with a positive Doppler shift, red is vehicles with a positive Doppler shift, black is for humans with a negative Doppler shift, and magenta is for vehicles with a negative Doppler shift.

of object was chosen using a log-likelihood method. A number of arbitrarily selected distributions were tested and the distribution with the greatest likelihood was selected to represent the Doppler maximum data. From the initial observations it seemed like objects with a positive Doppler shift act independently from those with a negative Doppler shift. Probability distributions were fit to each object and the positive and negative Doppler shifts. This resulted in 2 distributions for humans walking and 2 distributions for vehicles. The probability distribution with the greatest likelihood of representing vehicles with positive and negative Doppler shift is the uniform distribution. Humans walking with a negative Doppler shift are best described by the generalized extreme value distribution and humans walking with a positive Doppler shift are best described by a normal distribution. These probability distributions are used to provide a method to analyze how well this feature can separate humans walking from vehicles.

Figure 6.5 shows the four probability distributions fit to the Doppler maximum data. Using these probability distributions, a hypothesis is selected and tested against the probability distributions. The hypothesis was chosen not to put bias on either object. The point where the probability

Table 6.1: Listing of the data sets collected.

Object	Doppler Shift	Probability of Detection (P_D)	Probability of False Alarm (P_{FA})
Human	negative	0.97	0.17
Human	positive	0.97	0.14
Vehicle	negative	0.83	0.03
Vehicle	positive	0.86	0.03

distributions intersect was chosen to be the hypothesis. Once this hypothesis is chosen, estimated probabilities can be calculated indicating how well the feature separates the two classes of objects.

Table 6.3 is a summary of the calculated probabilities. The probability of detection and the probability of false alarm was calculated for each of the objects. With the hypothesis selected, the feature is fairly effective at separating the two classes of objects. There is a high probability of detection with a low probability of false alarm for each of the objects. Figure 6.6 is a plot of the probability distributions highlighting the probabilities measured for each of the objects. The green shows the probabilities of the two objects with a negative Doppler and the magenta shows the probabilities of the two objects containing a positive Doppler shift. The plots are highlighting P_D for humans walking, Fig. 6.6(a), P_{FA} for humans walking, Fig. 6.6(b), P_D for vehicles, Fig. 6.6(c), and the P_{FA} of vehicles, Fig. 6.6(d). The P_D for humans walking with a positive and negative Doppler shift are both 0.97 while the P_{FA} are 0.14 and 0.17 respectively. The P_D for a vehicle with a positive and negative Doppler shift are 0.86 and 0.83 while the P_{FA} for both cases is 0.03. Humans walking are confined to a smaller region so the probability of detection is high. Vehicle's Doppler maximum values are spread over a larger region, consequently the probability of detection is lower.

6.2 Doppler Variability

In addition to the Doppler maximum, the Doppler variability is a feature chosen to analyze the micro-Doppler signature. It was observed in the simulated data that the Doppler maximum has a different amount of variation for humans walking and vehicles. The Doppler variability attempts to measure this difference. It is calculated as previously outlined. To better understand the Doppler
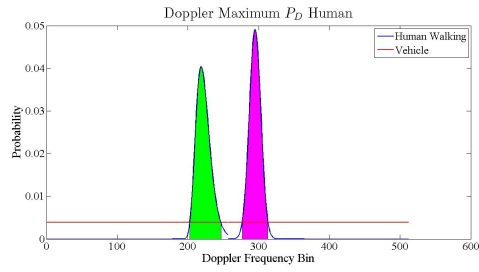
(a) P_D Human Walking
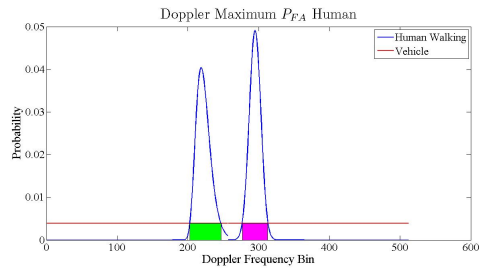
(b) P_{FA} Human Walking
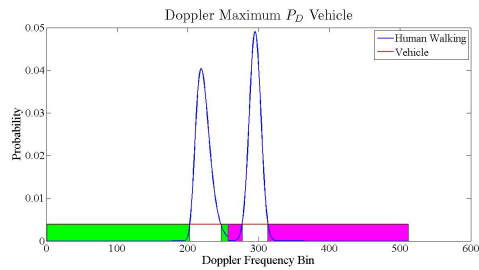
(c) P_D Vehicle

(d) P_{FA} Vehicle

Figure 6.6: By selecting a micro-Doppler maximum hypothesis and with assumed distributions the probability of detection and the probability of false alarm are calculated on all objects. The green show the probabilities with a negative Doppler shift and the magenta is the positive Doppler shift.

variability, two datasets from the collection were chosen to be representative datasets. Figure 6.7 is the representative plot of a human walking. The upper portion of the plot is the time-frequency plot with the Doppler maximum plotted in black. The lower portion of the plot shows the Doppler variance in red and the Doppler variability in blue. In comparing the upper and lower plots of Fig. 6.7, it can be seen, as the Doppler maximum varies, the variance increases. This results in the Doppler variability increasing. The other representative dataset can be seen in Fig. 6.8, which is data from a vehicle traveling. The micro-Doppler profile has no significant variation, therefore the Doppler variability is also low. The two representative datasets have a large discrepancy in the Doppler variability measurement. The variability of the human walking is significantly greater than the vehicle traveling. The Doppler variability of the human walking ranges from 0 to 1200 whereas the vehicle's range is 0 to 12.
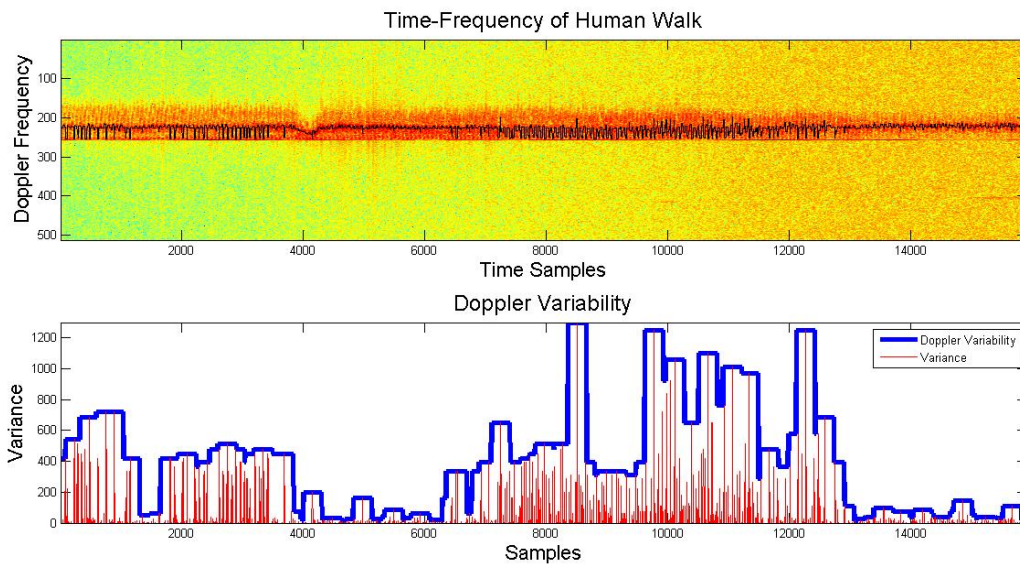
Figure 6.7: The upper portion of the plot is the time frequency plot of a human walking with the Doppler maximum plotted in black. The lower half of the plot is the Doppler variance plotted in red with the Doppler variability in blue.

The Doppler variability was extracted from the 41 collected datasets. Figure 6.9 shows the Doppler variability over time for all datasets. The blue is the Doppler variability of humans walking and the red is the Doppler variability of vehicles. The vehicles are clustered near the bottom of the plot with small Doppler variability measurements while the Doppler variability for
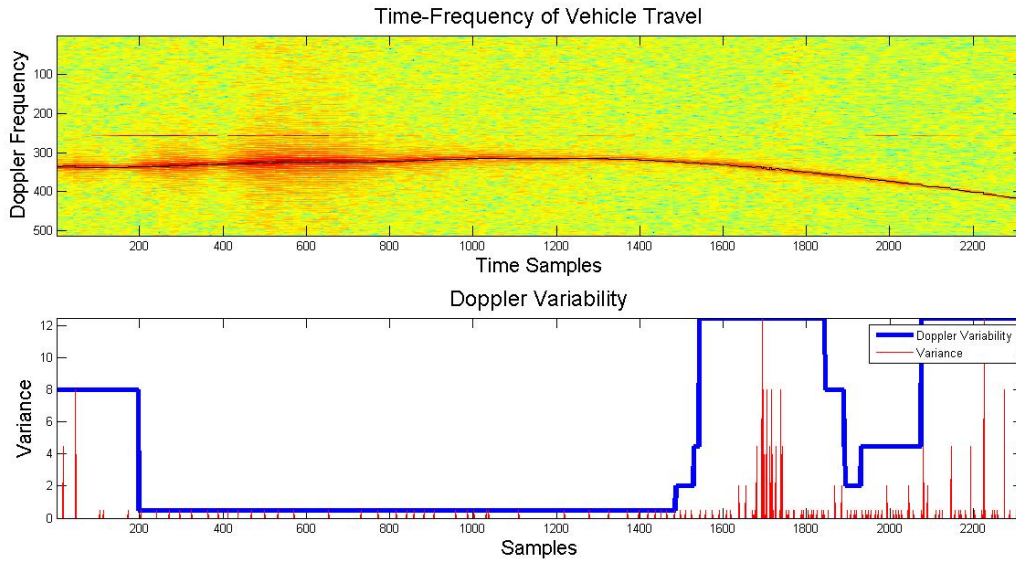
Figure 6.8: The upper portion of the plot is the time frequency plot of a vehicle traveling with the Doppler maximum plotted in black. The lower half of the plot is the Doppler variance plotted in red with the Doppler variability in blue.

humans walking has a significantly broader range. This feature suggests the Doppler variability of vehicles will be limited to a certain bounds while the Doppler variability of humans on average is greater but contains more variance in the measurement.

6.2.1 Doppler Variability Feature Analysis

Similar to the Doppler maximum, the Doppler variability can be assessed as to the quality of the feature. The quality, in this case, is determined by how well the feature can separate humans and vehicles as two distinct classes of objects. Figure 6.10 is the histogram of the Doppler Variability data. Vehicles are plotted in red and humans walking in blue. The vehicles occupy a small cluster of data near the lower Doppler variability measurements. Humans walking are spread over a range of Doppler variability measurements. This is corresponds to the observations made from Fig. 6.9. Using a similar method of determining the log-likelihood, a probability distribution of the Doppler variability for humans walking and vehicles were chosen to describe the collected data. The probability distribution that describes the Doppler variability of humans walking is a

70
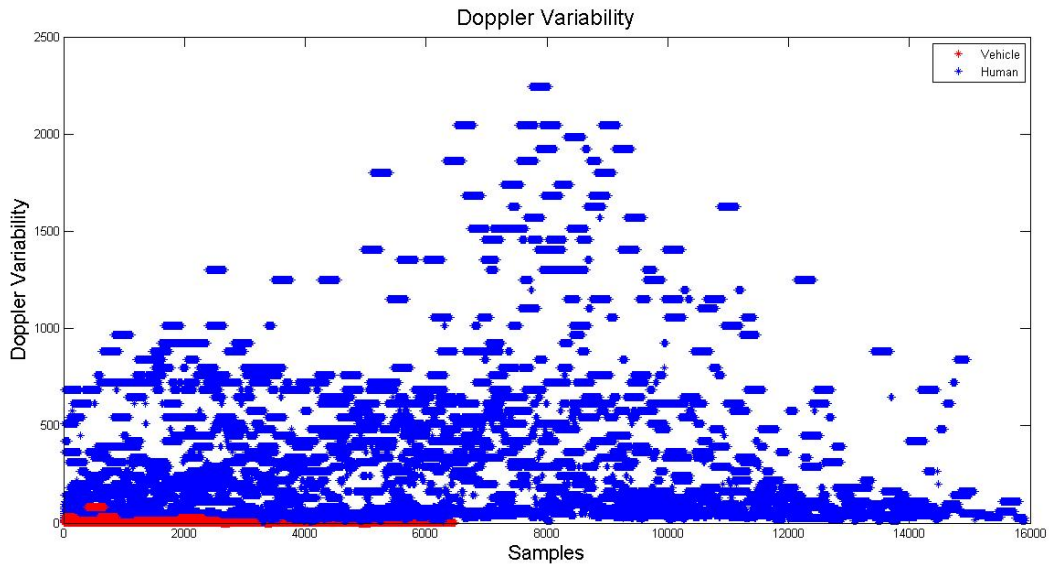
Figure 6.9: This scatter plot shows the Doppler variability versus time. The red are data points for vehicles and the blue are data points for humans walking. Because of swinging arms, hands, legs and feet, a person generally has a greater Doppler variability in the micro-Doppler signature than a vehicle.
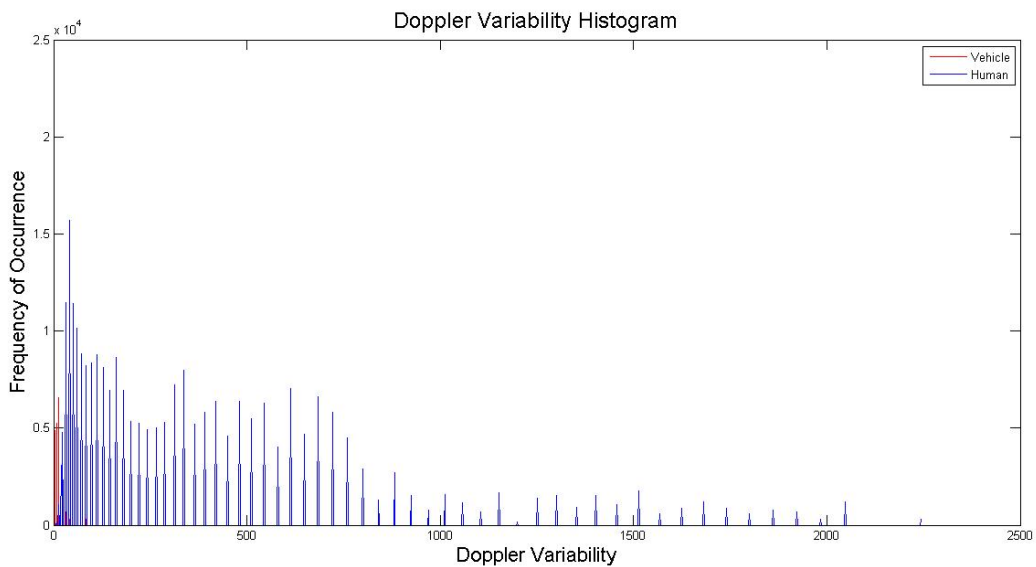
Figure 6.10: Histogram of the Doppler variability for all of the datasets collected. The humans walking are plotted in blue and the vehicles are in red. Vehicles have a small cluster in the front while humans walking spreads over a large section.

71

Probability Distribution of Doppler Variability
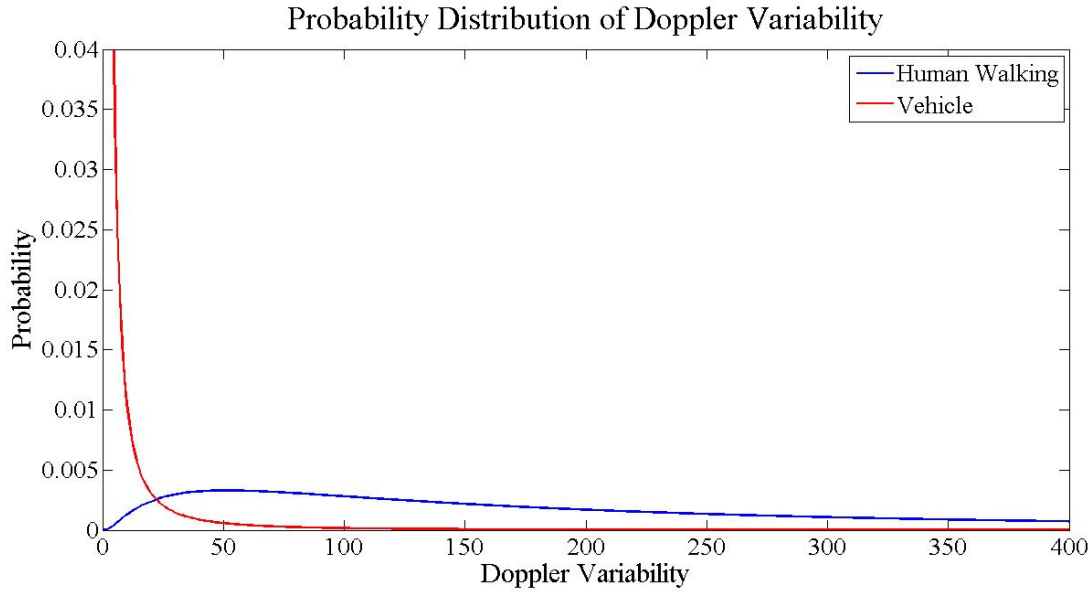
Figure 6.11: The data from the histograms were fit to probability distributions for humans walking and vehicles traveling. The probability distribution for humans walking is a log normal and general extreme value for vehicles. These are the two probability distributions, with the vehicle in red and the human walking in blue.

Table 6.2: Probability of detection and the probability of false alarm for vehicles and humans using the Doppler variability data.

Object	P_D	P_{FA}
Human	0.97	0.07
Vehicle	0.93	0.03

log normal distribution and the distribution that describes the Doppler variability of vehicles is the generalized extreme value distribution.

Figure 6.11 is a plot of the two probability distributions were fit to the data. The blue is humans walking and the red is vehicles. These estimated distributions provide a method of measuring the effectiveness of this feature at distinguishing humans walking and vehicles. Similar to the Doppler maximum the hypothesis is chosen as the point where the probability distributions intersect. In this manner the error is minimized. After the hypothesis was determined, all of the data that occurred on the lower side of the hypothesis is presumed to be from a vehicle and all data on the upper side of the hypothesis is presumed to be from a human walking. The correctness of this assumption can be measured with the probability of detection and the probability of false
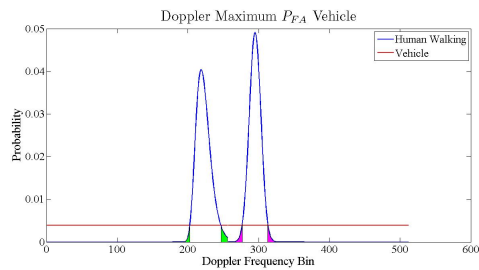
72
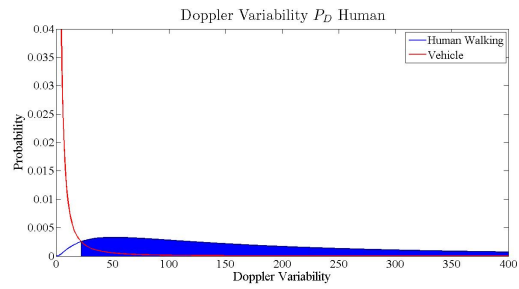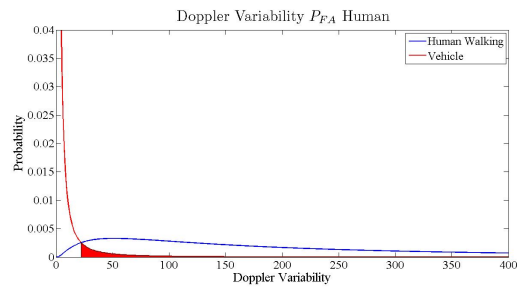
(a) P_D Human Walking

(b) P_{FA} Human Walking
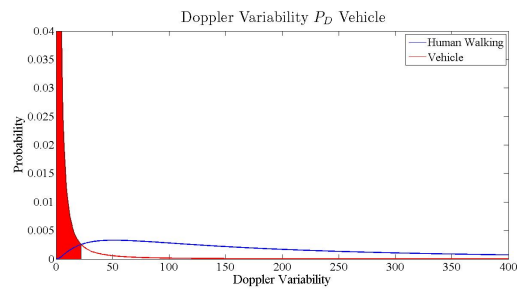
(c) P_D Vehicle
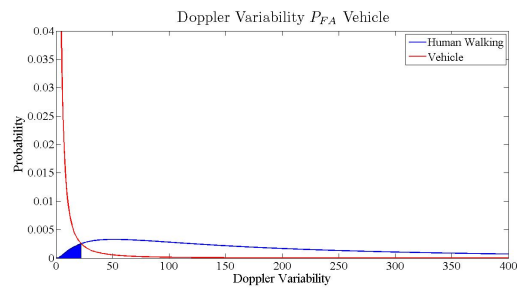
(d) P_{FA} Vehicle

Figure 6.12: By selecting a Doppler variability hypothesis and with known distributions the probability of detection and the probability of false alarm are calculated on all objects.

alarm for each of the objects. Table 6.2 is a summary of the results obtained. The probability of detection for a vehicle and a human walking are 0.93 and 0.97 respectively. The corresponding probabilities of false alarm are 0.03 and 0.07. Figure 6.12 is a plot showing the probability of detection and false alarm for each of the objects. If this feature is used independently of the other micro-Doppler features and the probability distributions are good estimates of the data, this feature may be very effective at distinguishing the two classes of objects.

6.3   Doppler Bandwidth

Doppler bandwidth is another feature of interest. The Doppler bandwidth measures the frequency width of the micro-Doppler signature. Doppler bandwidth is calculated by using the thresholding technique previously outlined. The Doppler bandwidth is calculated using the col-
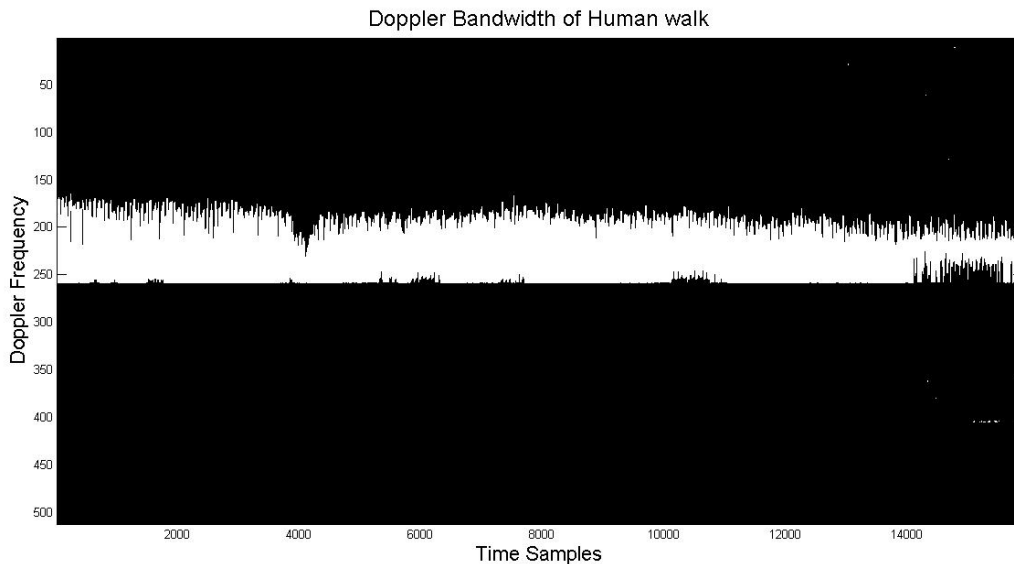
Figure 6.13: The time-frequency plot of a human walking with the threshold applied. This is used to calculate the Doppler bandwidth.

lected radar data. Figures 6.13 and 6.14 are two representative Doppler bandwidth results from the datasets collected. Figure 6.13 is the thresholded time-frequency plot of a human walking and Fig. 6.14 is the thresholded time-frequency plot of a vehicle. The white regions are above the threshold imposed by the Doppler bandwidth calculation. In analyzing the results is can be seen that the

74
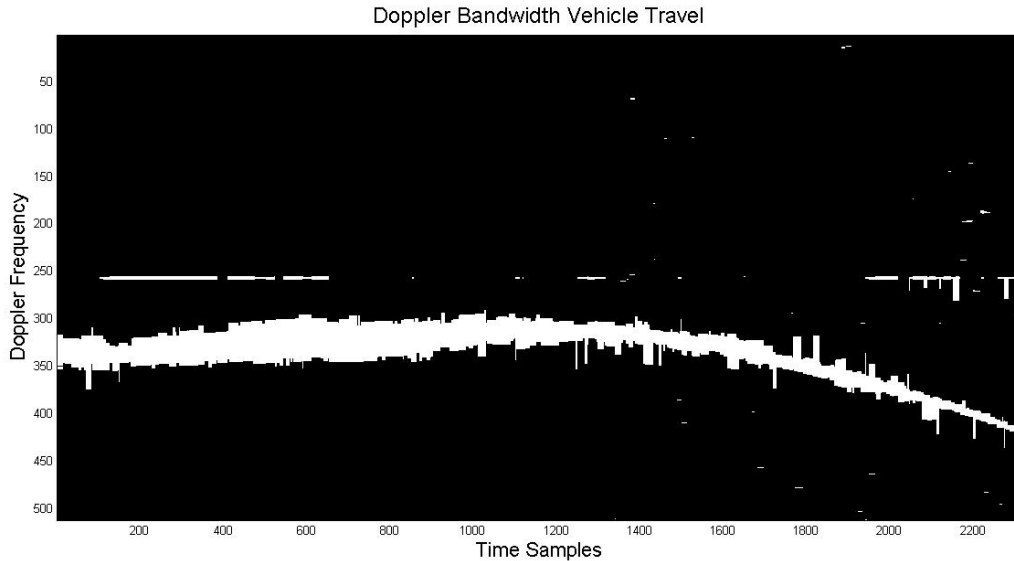
Figure 6.14: The time-frequency plot of a vehicle traveling with the threshold applied. This is used to calculate the Doppler bandwidth.

Doppler bandwidth is attempting to outline the extents of the micro-Doppler radial velocity limits. The Doppler bandwidth is the width of the region above the threshold (white, shown in the plots). It is calculated for every time sample. In comparing the results from these two objects it appears the Doppler bandwidth for the human walking is generally wider than the bandwidth of the vehicle.

The Doppler bandwidth was calculated for all 41 of the datasets. Figure 6.16 is a summary of the results. The blue points are data from humans walking and the red are data points from vehicles. The graph shows the majority of the data points from the vehicle clustering towards the smaller Doppler bandwidth measurements while the data points of humans walking generally have a larger Doppler bandwidth with some overlap of Doppler bandwidth measurements between the two classes of objects.

6.3.1 Doppler Bandwidth Feature Analysis

A similar analysis can be conducted on the Doppler Bandwidth as a feature to measure its effectiveness at distinguishing the two classes of objects. In order to explore this separation a histogram was generated and is shown in Fig. 6.16. The histogram contains a grouping of smaller

75
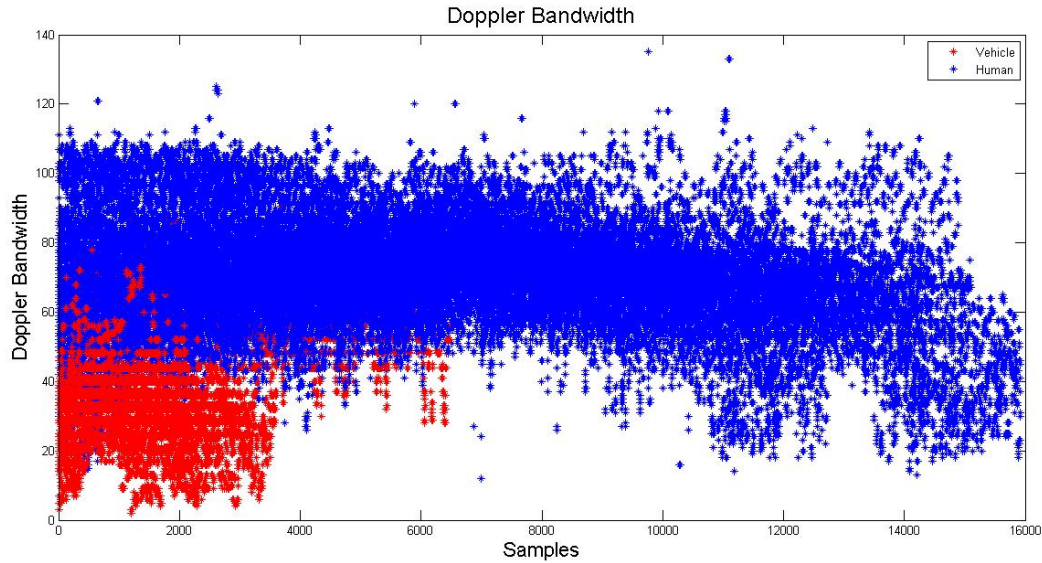
Figure 6.15: Summary of the Doppler bandwidth for all of the datasets collected. The data points for humans walking are plotted in blue and the data points for vehicles are in red. There is a cluster of vehicle bandwidth data samples in the lower portion of the graph and human data samples above that with some overlap between the two.

Table 6.3: Probability of detection and the probability of false alarm for vehicles and humans for Doppler bandwidth.

Object	P_D	P_{FA}
Human	0.91	0.11
Vehicle	0.89	0.09

Doppler bandwidths on the left in red representing the data points for the vehicles and a larger grouping of points on the right in blue representing humans walking. There is some amount of disparity in the number of samples between humans and vehicles because humans tend to stay in the radars FOV longer. Using a method similar to the previous features the log-likelihood was calculated for a select few distributions. The distribution most like the Doppler bandwidth of vehicles is the generalized extreme value distribution and the distribution most like the Doppler bandwidth of humans walking is the normal distribution. Figure 6.17 is a plot of the distributions fit to the data.

To minimize the error, the point where the two distributions intersect is chosen as the hypothesis. Similar to the previous features, the probability of detection and the probability of false

76
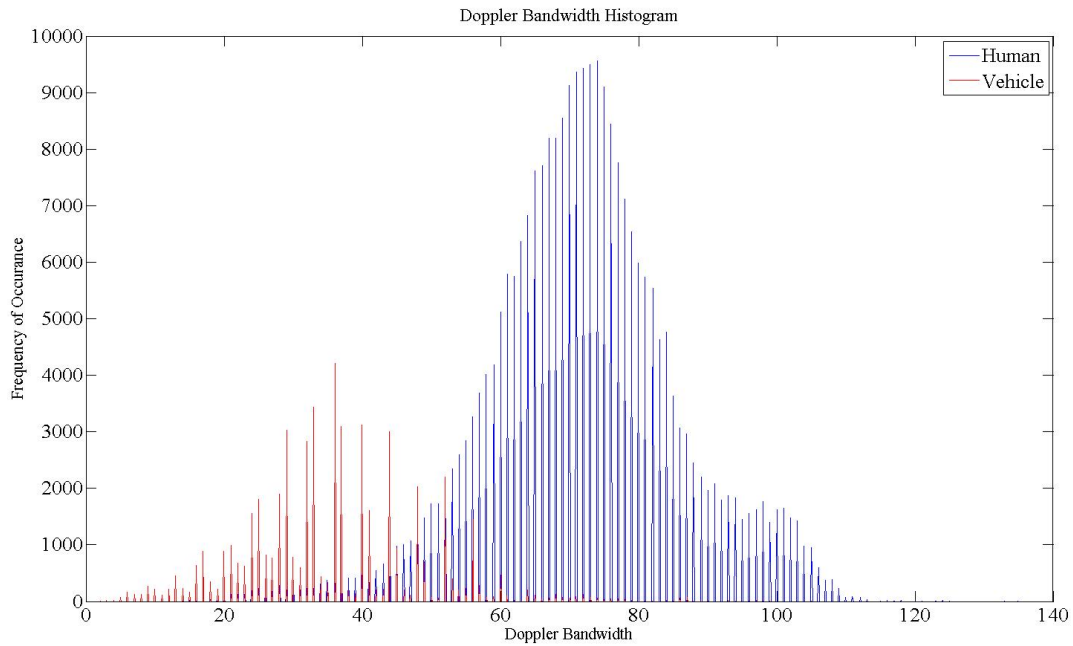
Figure 6.16: Histogram of the Doppler bandwidth data. Blue is the data for humans walking and red is the data for vehicles traveling. There is some clustering occuring with the vehicles and humans walking.
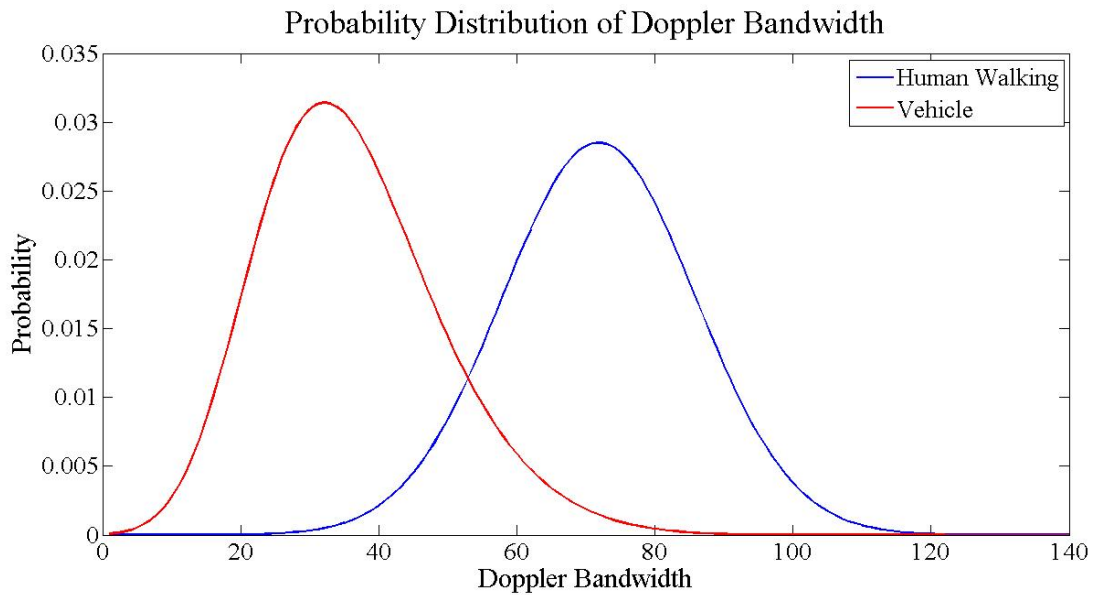
Figure 6.17: The Doppler bandwidth data is fit to two probability distributions. The red is for vehicles and the blue is for humans walking.

alarm can be calculated. Table 6.3 is a summary of the probability of detection along with the probability of false alarm for each of the objects. The probability of detection for humans walking and vehicles are 0.91 and 0.89 respectively. The corresponding probabilities of false alarms are 0.11 and 0.09. Figure 6.18 shows the probability distributions with the probability of detection and the probability of false alarm for each of the objects. The feature seems to provide adequate separation for the two classes of objects.

6.4   Doppler Span

The Doppler span was the final feature chosen to analyze the micro-Doppler signatures of the collected datasets. The Doppler span measures the frequency distance between the high and the low points of the Doppler maximum over time. The Doppler span was calculated on the time-frequency plot using the method previously outlined.

Figure 6.19 is the Doppler span of a human walking extracted and plotted for one representative dataset. The Doppler maximum is in black and the upper and lower thresholds are in red and green. The Doppler span is the distance between the upper and lower limits for all time. Figure 6.20 is a plot of the Doppler span of a vehicle. The Doppler maximum is in black and the upper and lower thresholds are in red and green. It comparing Fig. 6.19 to Fig. 6.20 it can be seen that for these datasets, humans walking have a larger Doppler span than vehicles traveling. This feature is exploiting some of the micro-Doppler motions unique to humans walking that are not found in the micro-Doppler signature of vehicles.

The Doppler Span was extracted from all 41 of the datasets. Figure 6.21 is a plot of the Doppler span results for all data collected. The blue is humans walking and the red is vehicles traveling. The x-axis is samples in time and the y-axis is the Doppler span. The results look somewhat similar to Doppler variability. The data points that are vehicles are grouped near the smaller Doppler span measurements and the data points of humans walking are spread out generally with a greater Doppler span.

Table 6.4: Probability of detection and the probability of false alarm for vehicles and humans using the selected hypothesis and the distribution formed from the Doppler Span data.

Object	P_D	P_{FA}
Human	0.88	0.14
Vehicle	0.85	0.11

6.4.1 Doppler Span Feature Analysis

In a similar manner to the previous features, the Doppler span can be evaluated as a feature by how well it differentiates humans walking and vehicles. The more effective the feature is at differentiating these two groups, the better feature it is.

Figure 6.22 is the histogram of the Doppler span data. Vehicles are plotted in red and humans walking in blue. The vehicle data is concentrated at the smaller Doppler span values while the data for humans walking clusters around larger Doppler span values and contains a larger variance.

Probability distributions were fit to the data in a similar manner as was outlined with the previous features. The Doppler span data of vehicles seem to best fit an exponential probability distribution while the Doppler span data of humans walking seemed to best fit the generalized extreme value distribution. Figure 6.23 is a plot of two probability distributions fitted to the data. The blue probability distribution is the distribution for humans walking and the red is the distribution fit to the Doppler span vehicle data. There is some amount of separation in the two probability distributions.

The hypothesis was selected as the point of intersection of the two probability distributions. Table 6.4 is a summary of the probability of detection and the probability of false alarm. The probability of detection for vehicles is 0.85 and the probability of detection for humans walking is 0.88. The corresponding probabilities of false alarm are 0.11 and 0.14. Over all this feature preforms reasonable with a high probability of detection and a low probability of false alarm.

6.5 Feature Summary

The intent of each feature is to provide a measurement that can be used to separate vehicles from humans walking. Each feature was able to separate these two groups of objects to some

Table 6.5: Summary of the 4 features' probability of detection for a human walking. The probability of detection for Doppler maximum is the average of the positive and negative Doppler shift values.

Feature	P_D Human Walking
Doppler Maximum (+ Doppler)	0.97
Doppler Maximum (- Doppler)	0.97
Doppler Variability	0.97
Doppler Span	0.88
Doppler Bandwidth	0.85

Table 6.6: Summary of the 4 features' probability of detection for a vehicle traveling. The probability of detection for Doppler maximum is the average of the positive and negative Doppler shift values.

Feature	P_D Vehicle Traveling
Doppler Variability	0.93
Doppler Bandwidth	0.89
Doppler Maximum (+ Doppler)	0.86
Doppler Span	0.85
Doppler Maximum (- Doppler)	0.83

degree. Table 6.5 is a summary of each feature and the probability of detection for a human walking using the simple hypothesis test established previously. Table 6.6 is a summary of the probability of detection for a vehicle traveling for each feature. No feature dominates in both the probability of detecting vehicles and humans walking. However the features seem to be able to separate the two classes of objects with a reasonable degree of confidence.

6.6 Chapter Summary

The four features were extracted out of the data collected on the experimental radar system. The results were then analyzed to see how effective the features are at differentiating humans walking and vehicles. From the results obtained it appears the features are adequate at describing these two classes of objects.
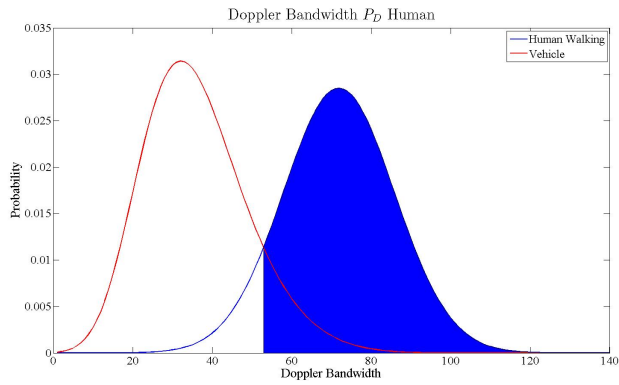
(a) P_D Human Walking
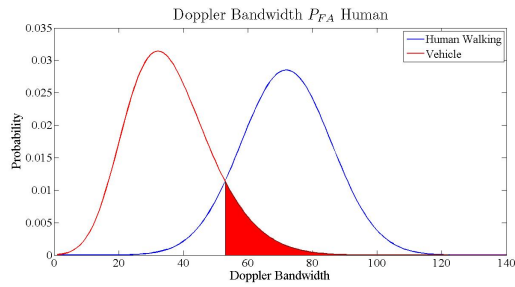
(b) P_{FA} Human Walking
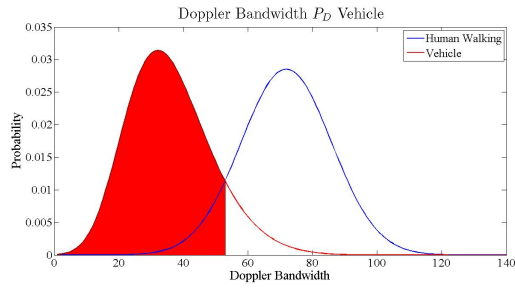
(c) P_D Vehicle
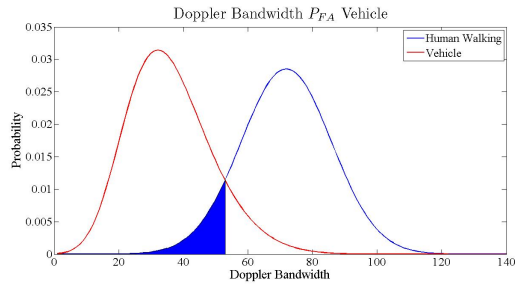
(d) P_{FA} Vehicle

Figure 6.18: By selecting a Doppler bandwidth hypothesis and with known distributions the probability of detection and the probability of false alarm are calculated on all objects.
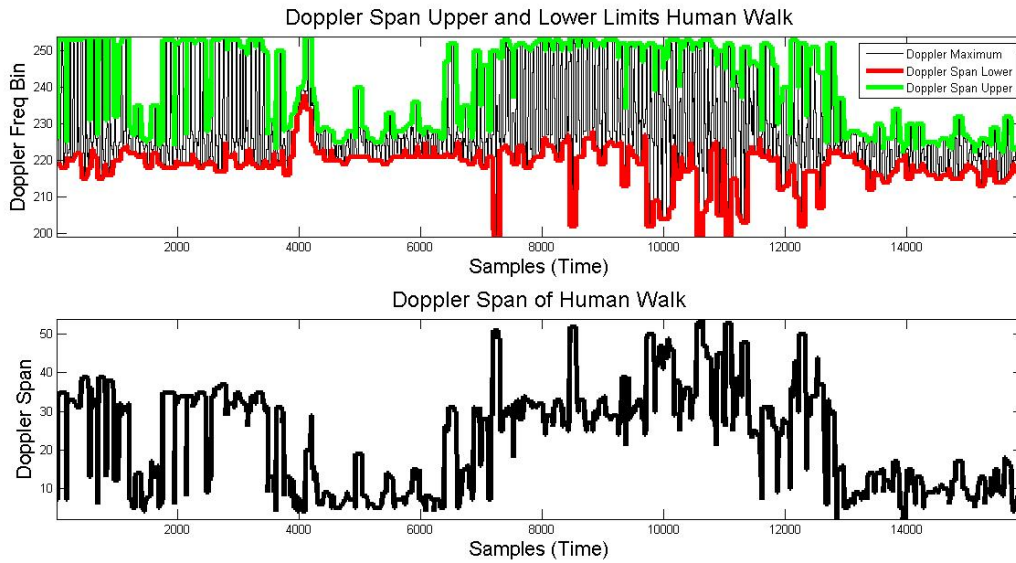
Figure 6.19: Graph of the fundamental components of the Doppler span using data from a human walking. The Doppler maximum is plotted in black, the Doppler Span lower threshold is plotted in green and the upper threshold is in red. The span is the distance between the upper and lower threshold.
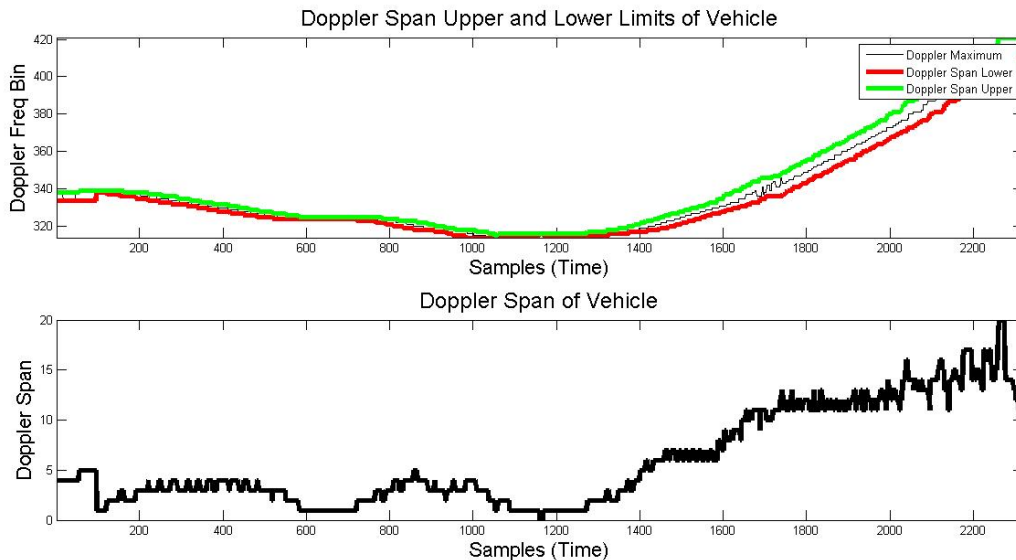
Figure 6.20: Graph of the fundamental components of the Doppler span using data from a vehicle. The Doppler maximum is plotted in black, the Doppler Span lower threshold is plotted in green and the upper threshold is in red. The span is the distance between the upper and lower threshold.
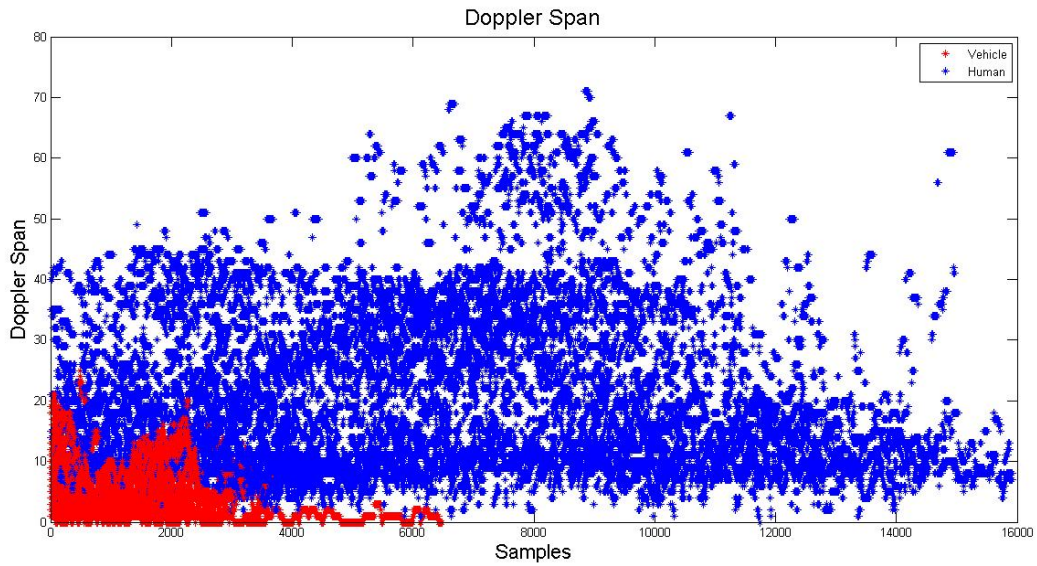
Figure 6.21: Doppler span of all 41 datasets analyzed. The red is data points for vehicles and the blue is for humans walking. The vehicles are grouped near the lower portion of the plot while the humans walking occupy a wider range.
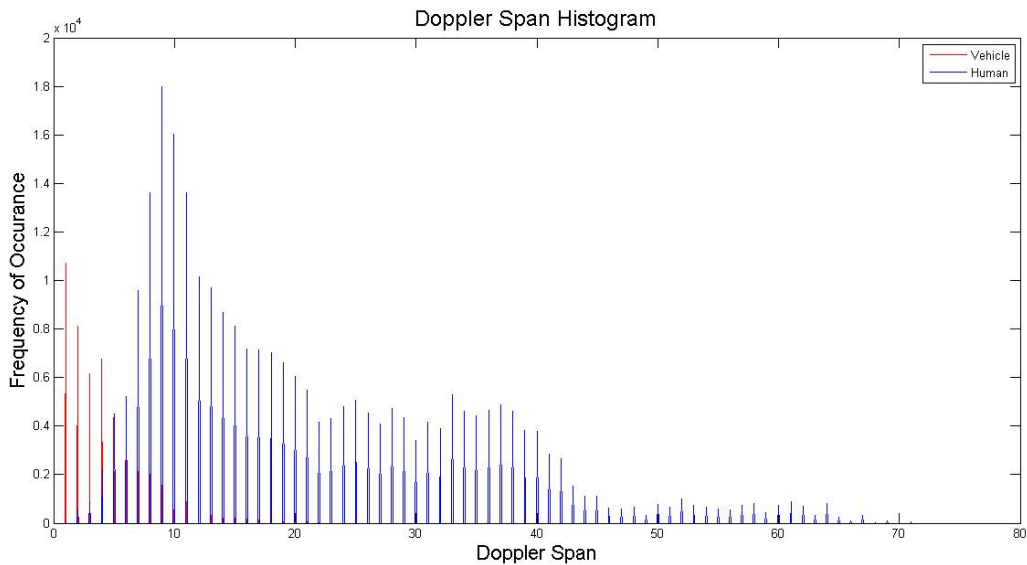
Figure 6.22: Histogram of the Doppler span data. The red is vehicles and blue is humans walking. The vehicle data is concentrated at the smaller Doppler span measurements of the plot while the human walking is spread over a larger area containing a larger span.
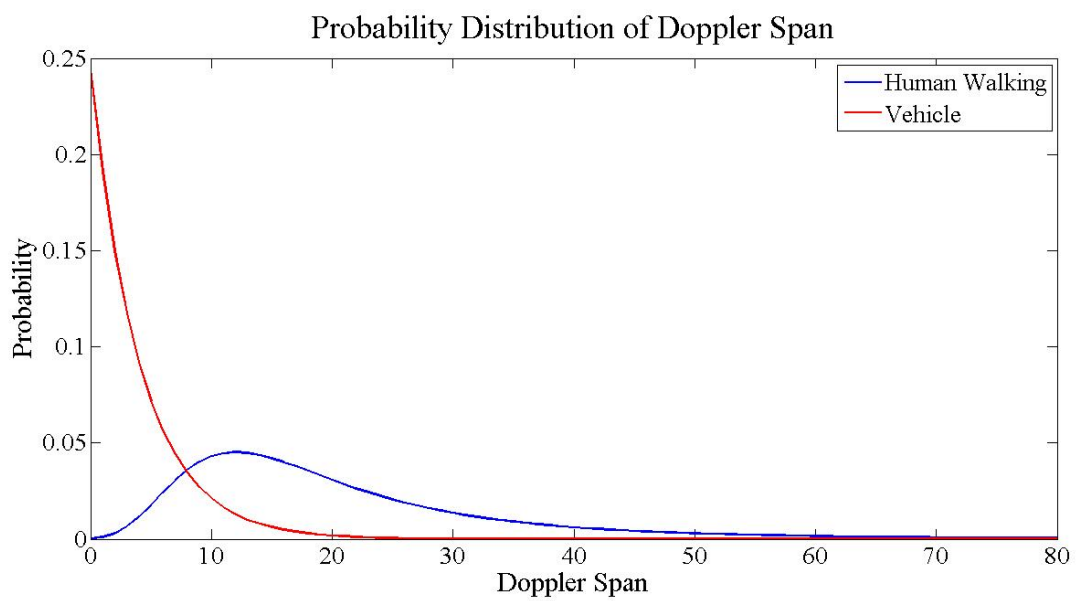
Figure 6.23: The measured data was fit to the two probability distributions shown in the graph.
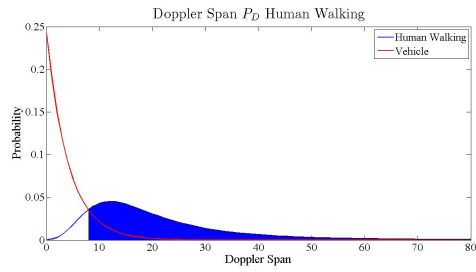
(a) P_D Human Walking
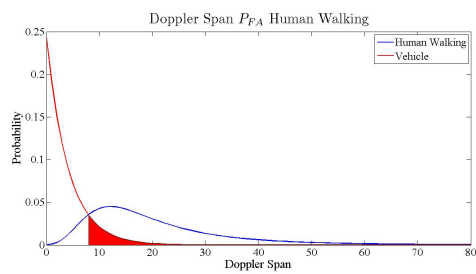
(b) P_{FA} Human Walking
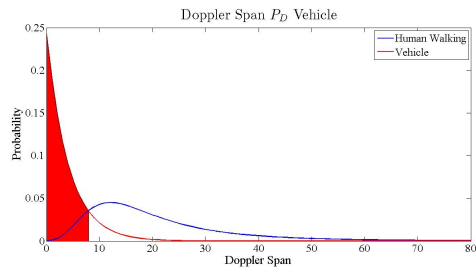
(c) P_D Vehicle
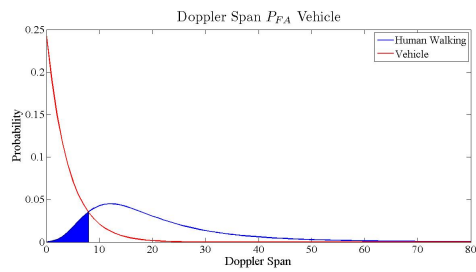
(d) P_{FA} Vehicle

Figure 6.24: By selecting a Doppler span hypothesis and with known distributions the probability of detection and the probability of false alarm are calculated on all objects.

CHAPTER 7. OBJECT CLASSIFICATION

The previous chapter analyzed the four selected micro-Doppler features for each object type. This chapter covers object classification by applying learning algorithms to the micro-Doppler features outlined previously. The learning algorithms are tested with the features extracted from the radar data collected with the experimental radar system. The learning algorithms are also compared to determine their effectiveness at differentiating between humans and vehicles. The micro-Doppler features are analyzed to measure their contribution to the correct classification of the object.

7.1 Training and Test Data

In order to test the learning algorithms, a training set and a test set of data are required. To generate the training and test data the entire collection of data is split into two sections: one for training and the other for testing. Differentiating humans walking from vehicles is the desired outcome in this experiment. The test and training data sets only contain these two classes of objects. To ensure the training and test data have equal points of vehicle and human data, half of the vehicle sample points become part of the training data with the remaining half being designated as the test data. The division process is repeated for the human walking data. The data is divided using a non-repeating random number generator. This ensures no bias is introduced into the selection of the training versus test data sets.

The data consists of 159588 points of training data and 159588 points of test data. In each of the test and training data sets, 26342 of the points are vehicles and 133246 are humans walking. The discrepancy in the amount of vehicle versus human data comes from the earlier explanation that humans move slower than vehicles and are in the radar's field of view longer, which allows the radar to capture more data.

Each data point can be considered a snapshot in time containing the micro-Doppler features used for classification. The extracted features are: micro-Doppler maximum, micro-Doppler variability, micro-Doppler bandwidth, and micro-Doppler span. Each data point is a 4 element vector corresponding to the four features and a designation associated with it, indicating whether the data is either human or vehicle. The designation associated with each point in the training data is used as an input to the learning algorithm to create the classification model. The designation associated with each point in the test data is used to compare the actual object type to the predicted classification. (Note: In most real life cases the designation of the test data is unknown.)

The test and training data are the same for all of the learning algorithms. This is intended so that the learning algorithms can be compared and contrasted to judge their effectiveness against the same data.

7.2 Learning Algorithms

A few common learning algorithms were chosen to test and compare. These algorithms were chosen in part because they are readily available and are part of the Matlab toolbox [14]. The purpose of this test is to use learning algorithms that exist to measure their effectiveness with this micro-Doppler feature set.

7.2.1 Naive Bayes Classifier

The first learning algorithm considered is the naive Bayes classifier. The naive Bayes classifier is a learning algorithm based on probabilities. The naive Bayes classifier estimates probabilities of various features using the frequency of those features in the training data. Then, with these probabilities obtained from the training data, it calculates which outcome is most probable for an unknown feature. The naive Bayes classifier assumes the features are conditionally independent. This may not be true for the micro-Doppler feature data, which may adversely effect the algorithm's ability to classify. One of the benefits of the naive Bayes classifier is that no searching through the training data is required like in other learning algorithms. It forms the classification based on the probabilities obtained through the training process in preprocessing steps [15]. This enhances the speed of future predictions.

7.2.2 K-Nearest Neighbors

K-Nearest Neighbors learning algorithm is also considered. The K-Nearest Neighbors learning algorithm finds K points out of the training data with the least amount of euclidean distance from an unknown point to be classified where the euclidean distance of two n-dimensional vectors $\vec{a}$ and $\vec{b}$ is given by

$$d(\vec{a},\vec{b}) = \sqrt{(a_1 - b_1)^2 + (a_2 - b_2)^2 + \ldots + (a_i - b_i)^2 + \ldots + (a_n - b_n)^2}. \qquad (7.1)$$

The algorithm takes the n-dimensional feature vectors in the training set and computes the distance between those vectors and an unknown vector and locates the K closest points. The K-points in the training that are found to be closest to the unknown point, contain a known label. These K points that are the end result of the algorithm can be used to classify the unknown point. If the unknown point is the closest to the majority of one type of object then the unknown point has the highest probability it is the same type of object. One of the benefits of this algorithm is it is reliable in the presence of noise [15]. One of the drawbacks is with large training data sets it is computationally intensive to classify a new point because the distances for all of the training data points have to be calculated.

7.2.3 Classification Tree

The next type of learning algorithm considered is a classification tree. A classification tree is a sequence of decisions created using the training data. These decisions are structured in a tree data structure. The tree contains a root, nodes, branches and leaves similar to the common tree data structure. The decisions of greater magnitude are made closer to the root rather than the leaves. At the root and each of the nodes, a decision using the information in the feature vector is made. For example, if an unknown point has feature 1 greater than a threshold, the decision is to move to the right branch of the tree, if the feature value is less than the threshold, the decision is to move to the left branch of the tree. The decisions continue traversing the tree with each node deciding its next fate based on the unknown points current feature vector and the decisions at each node. The point traverses the tree and eventually ends at a leaf node. The leaf node is the classifying node or the node where the classification is applied to the unknown point. The unknown point traverses the

tree decisions to end with a classification. Classification trees are a concise way to make decisions about features that lead to classification.

One of the limitations of classification trees is they have a tendency to over-fit the training data. The classification tree can essentially memorize the training data without putting emphasis on the general underlying trends. As a result, the tree fits the training data very well but it may not fit future samples well. To compensate for the tree over-fitting the data, the tree may be pruned to make it more general. Pruning removes some of the lower branches and places more emphasis on the decisions nodes that are higher in the tree.

7.2.4   Bagging Decision Trees

Another type of learning algorithm is called a bagging decision tree. Bagging stands for "bootstrapped aggregating." This type of learning algorithm is similar to the classification tree. The difference is that the training data is used multiple times to create more than one tree. These trees can then be averaged to create a more accurate prediction. Sometimes it is referred to as an ensemble learning algorithm because it is taking the information from all of the trees and combining that into a decision framework with greater accuracy in classification.

7.2.5   Discriminate Classifier

A final type of learning algorithm considered is the discriminate classifier. The discriminate classifier seeks to establish a boundary between the different classes of objects. Once the boundary has been established, then future unknown points can be classified by which side of the boundary they fall on. The boundary can be described as a linear boundary or a quadratic boundary. The quadratic classifier offers greater degrees of freedom in its attempt to fit the training data. In addition to linear and quadratic classification, a third discriminate classifier uses the Mahalanobis distance. The Mahalanobis distance takes into consideration the spread of the object class while calculating the distance. Vectors that measure a large distance are weighted less if their overall variance is also large.

Table 7.1: Confusion matrix showing the results for the Naive Bayes learning Algorithm. The algorithm predicted 25973 out of 26342 vehicles correctly and 130989 out of 133246 humans walking correctly. It misclassified humans as vehicles more often than vehicles as humans.

		Predicted	
		Vehicle	Human
Actual	Vehicle	25973	369
	Human	2257	130989

7.3 Data Results

In order to compare how well each of the learning algorithms preformed on the data, all of the algorithms are run with the same training data. The learning algorithms form a model based on the training data that is used to classify the test data. The true classifications for the test data were known and they are compared to how the learning algorithm classifies the data. The results are presented in a confusion matrix. The major diagonal of the confusion matrix contains the number of correct predictions for each class of objects. The off diagonals contain the number of each object that was misclassified.

7.3.1 Naive Bayes Results

The Naive Bayes learning algorithm was trained on the training data set and then the test data was evaluated using the model generated from the training set. The predicted classification was compared against the actual classification. Table 7.1 shows the results of the Naive Bayes learning algorithm. Naive Bayes predicts the vehicles at a reliability 98.6% and a human at 98.3%. This indicates a human is mistaken as a vehicle more than a vehicle is mistaken as a human. Overall this learning algorithm performs very well with the given training and test data sets.

Table 7.2: Confusion matrix showing results for the K-Nearest Neighbors learning Algorithm.

		Predicted	
		Vehicle	Human
Actual	Vehicle	26338	4
	Human	0	133246

7.3.2   K-Nearest Neighbors Results

In addition to the Naive Bayes algorithm, the K-Nearest Neighbors algorithm was also run on the test data. The K-nearest neighbors algorithm can be run with a varying K-value. The algorithm was run using a K value that seemed to yield the results closest to the truth. This algorithm preforms exceptional with the given data sets and training data. Table 7.2 is the confusion matrix for the the estimates given by the K-Nearest algorithm. It identifies a vehicle correctly 99.9% of the time and a human 100%. Similar to Naive Bayes, K-Nearest Neighbors incorrectly identifies vehicles as humans walking more often than it incorrectly identifies humans walking as vehicles. K-Nearest Neighbors offers an advantage over Naive Bayes when looking at the accuracy of classification.

7.3.3   Classification Tree Results

A classification tree was formed using the same training data set used on the previous learning algorithms. Figure 7.1 illustrates what that tree looks like. The test data was then classified using that classification tree. Table 7.3 are the results from the classification tree. This method has a very low false prediction rate with the ability to predict vehicles with a reliability of 99.9% and humans with a reliability of 99.9%. This is also the first algorithm that miscalculated humans as vehicles rather than vehicles as humans.

As explained earlier, the pruning level has a great effect on whether or not the classification tree over fits the training data and limits the ability of the tree to properly predict new data points. The pruning level was tested to see the effect on the ability of the classification tree to predict future outcomes. Table 7.3 are the results for the classification tree with no pruning. Table 7.4 is a table of confusion matrices for 4 pruning levels. The results show that as the pruning level is
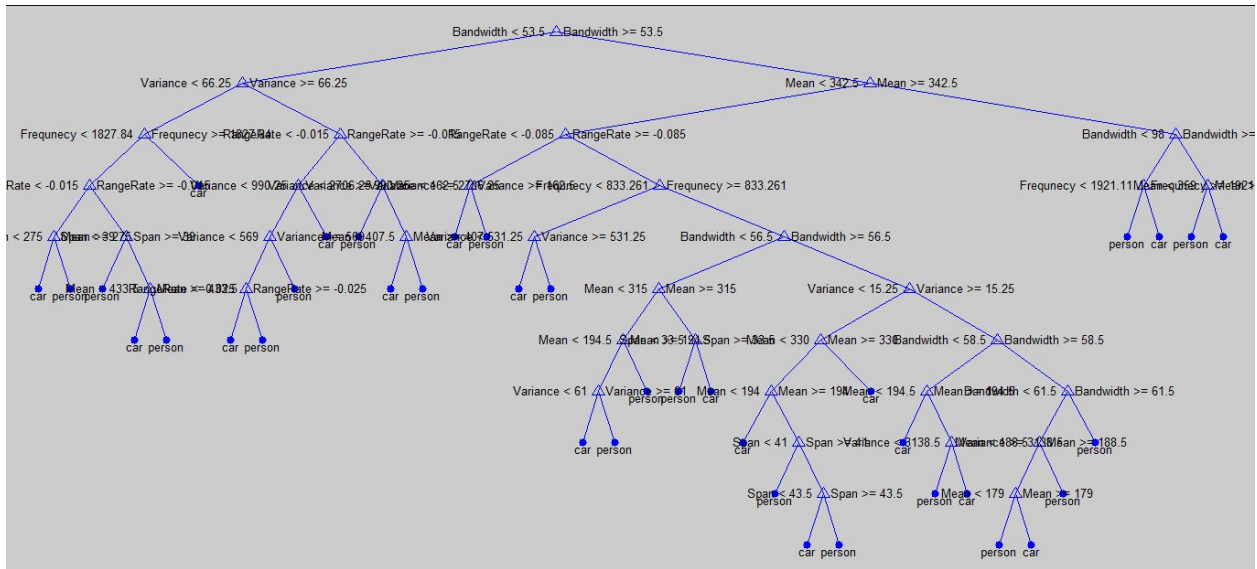
Figure 7.1: An example of a classification tree used in the analysis.

Table 7.3: Confusion matrix showing results for the classification tree learning Algorithm. The algorithm classified 26317 out of 26342 vehicles correctly and 133237 out of 133246 humans correctly.

		Predicted	
		Vehicle	Human
Actual	Vehicle	26317	25
	Human	9	133237

increased the amount of humans that are incorrectly predicted as vehicles also increases, albeit not by much; however the number of vehicles that are incorrectly identified as humans did not change with the pruning level. This indicates that even with a smaller tree, by putting more emphasis on the higher nodes, this classification algorithm preforms well.

7.3.4 Bagged Tree Results

The bagged tree algorithm was also also trained using the same training data set and evaluated using the test data set. Table 7.5 contains the confusion matrix for the bagged tree algorithm. This algorithm preformed the best out of all of the learning algorithms tried. It only mis-classified

Table 7.4: Confusion matrix showing results for the classification Tree learning Algorithm and the effect of pruning. With each pruning level the amount of mis-predictions only slightly increases.

			Predicted	
			Vehicle	Human
Actual	Pruning level 1	Vehicle	26313	29
		Human	9	133237
	Pruning level 2	Vehicle	26319	23
		Human	10	133236
	Pruning level 3	Vehicle	26318	24
		Human	24	133222
	Pruning level 4	Vehicle	26318	24
		Human	30	133216

Table 7.5: Confusion matrix showing results for the Bagged Tree learning Algorithm.

		Predicted	
		Vehicle	Human
Actual	Vehicle	6655	1
	Human	1	69247

1 vehicle and 1 human. This type of algorithm is very effective on this data using the test data and training data.

7.3.5 Discriminate Classifier Results

The training data and test data were also used to evaluate the three discriminate classifiers: linear, quadratic, and Mahalanobis. To illustrate these classifiers consider the 2 dimensional feature vector containing the Doppler span and Doppler Bandwidth. Figure 7.2 shows a plot of Doppler span versus Doppler bandwidth. The vehicles are the red and the humans walking are blue. Higher concentration of data is shown by the darker blue and red. The data is classified with linear classifier and the division that is created is shown by the black line. Notice how the vehicles are mainly to the left of the line and humans walking are to the right. There is however some amount of error
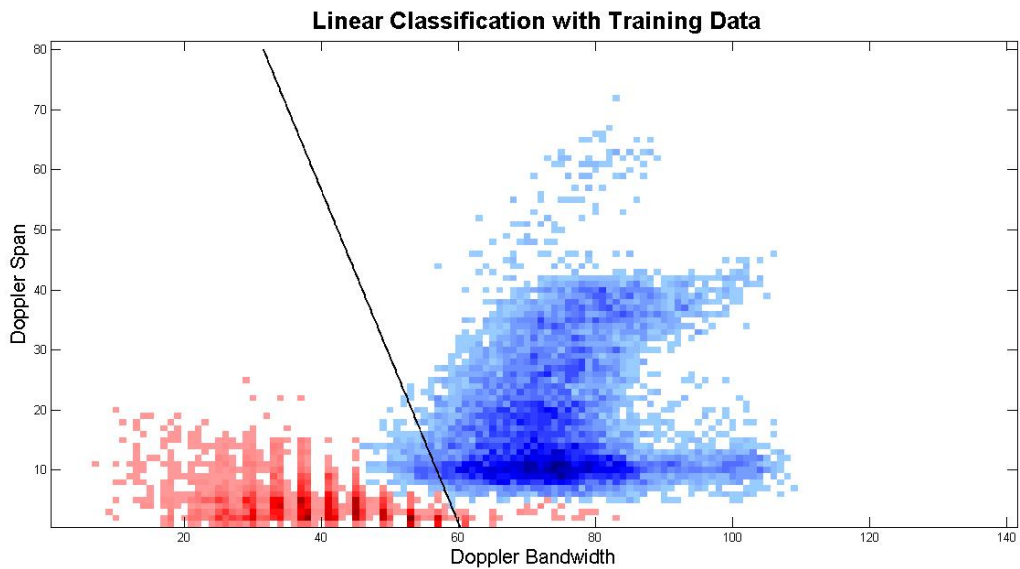
Figure 7.2: 2D linear classification using the Doppler bandwidth and the Doppler span. The blue are vehicle data points and the red are humans walking. Darker blue and darker red represent higher concentrations of data points. The black line represents the dividing line between the two classes of objects. It was created using a linear system of equations.
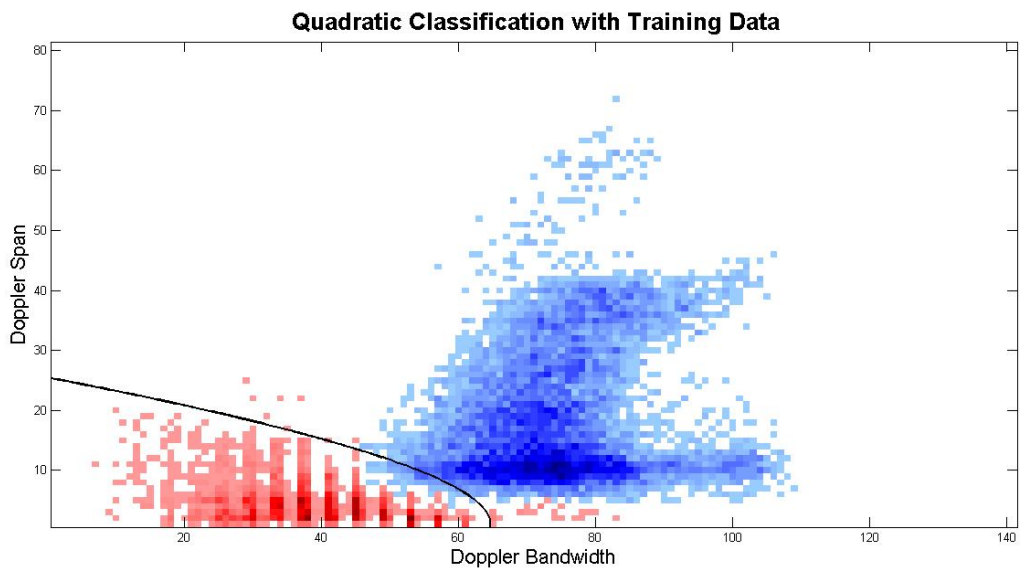
Figure 7.3: 2D quadratic classification using the Doppler bandwidth and the Doppler span. The blue are vehicle data points and the red are humans walking. Darker blue and darker red represent higher concentrations of data points. The black line represents the dividing line between the two classes of objects. It was created using a quadratic system of equations.

94

Mahalanobis Classification with Training Data
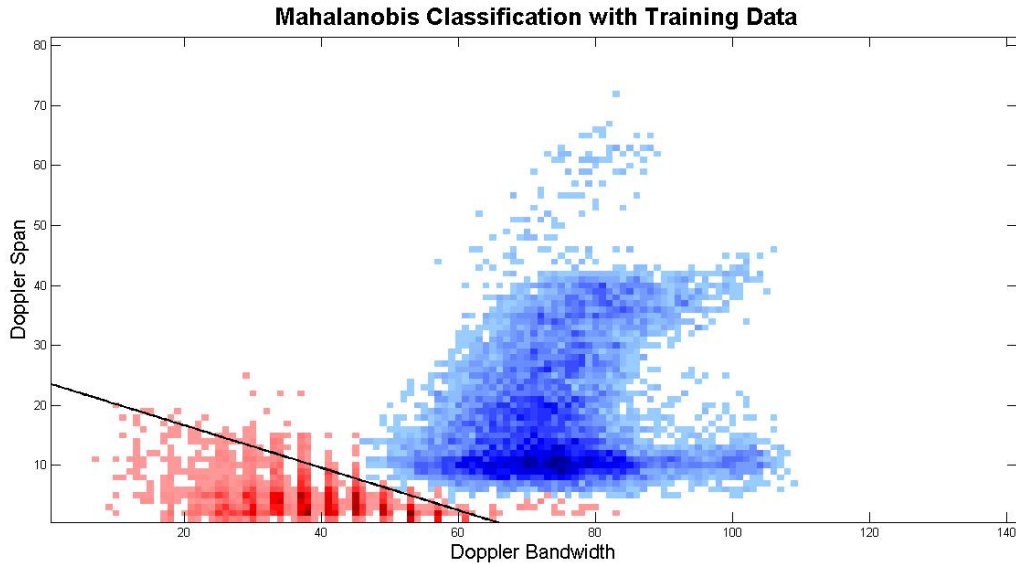
Figure 7.4: 2D Mahalanobis classification using the Doppler bandwidth and the Doppler span. The blue are vehicle data points and the red are humans walking. Darker blue and darker red represent higher concentrations of data points. The black line represents the dividing line between the two classes of objects. It was created using the Mahalanobis distance.

where the line cannot represent the exact boundary. This plot is only showing two dimensions but the linear classifier can be expanded to higher dimensions and in the case of this thesis it was expanded to 4 dimensions to account for the 4 features. Figure 7.3 show the same data but now rather than a linear classifier a quadratic classifier was used. Notice how the quadratic classifier is better able to trace out the two classes of objects in this case. This reduces the classification error. Figure 7.4 show the classification using the Mahalanobis distance.

The three discriminate classifiers were evaluated and the results were tallied. Table 7.6 shows these results. For the training and test data used the linear classifier had the greatest amount of misclassification with the quadratic classifier preforming the next best and Mahalanobis preforming the best with the least amount of misclassification. While these discriminate classifiers seem to preform poorly against the other learning methods used, their overall error in classification is still low.

Table 7.6: Confusion matrix showing results for the different types of discriminate classifier algorithms.

			Predicted	
			Vehicle	Human
Actual	Linear	Vehicle	25318	1024
		Human	8148	125098
	Quadratic	Vehicle	25980	362
		Human	4084	129162
	Mahalanobis	Vehicle	25590	752
		Human	276	132970

7.3.6 Learning Algorithm Summary

After the data was evaluated for each learning algorithm, the accuracy of the learning algorithms can be assessed to measure which algorithms were able to predict classification based on the same training and test data. Table 7.7 shows all of the algorithms organized according to total misclassification. Total misclassification is the combined the misclassification for both humans walking and vehicles. In looking at the table it can be seen that the tree bagger algorithm, the K-Nearest Neighbors and the classification tree preformed far better than the remaining algorithms. The remaining four algorithms had significantly higher error rates however the worst case classifier only had 5% error rate.

The results in table 7.7 only takes into account mis-classification. They are a few other parameters that learning algorithms could be judged by; such as how long it takes to train the data and how long it takes for future predictions.

7.4 Feature Analysis

The previous section explores how the different learning algorithms preform under the same inputs for the full set of features. This section attempts to explore the utility of individual features. As seen in the previous chapter, each feature provides different amount of information that is used to distinguish vehicles from humans walking. We would suspect the features that better separate vehicles from humans walking are the features that are effective in adding valuable information to

Table 7.7: Table showing the total misclassification for the learning algorithms run.

Learning Algorithm	Total Misclassification	Error
Tree Bagger	3	1.8e-5
K-Nearest Neighbors	4	2.5e-5
Classification Tree	34	2.1e-4
Mahalanobis	1028	0.0064
Naive Bayes	2626	0.0165
Quadratic	4446	0.0279
Linear	9172	0.0575

Table 7.8: Summary of the learning algorithms.

			Predicted	
	Learning Algorithm		Vehicle	Human
Actual	Tree Bagger	Vehicle	26340	2
		Human	1	133245
	K-Nearest Neighbors	Vehicle	26338	4
		Human	0	133246
	Classification Tree	Vehicle	26317	25
		Human	9	133237
	Mahalanobis	Vehicle	25590	752
		Human	276	132970

the decision process. This is because the feature provides a means of differentiating the two classes of objects.

To test the effectiveness of an individual feature, the learning algorithm is re-run with the training and test data sets with the feature being evaluated being removed from both. The results are then evaluated against the original results that contained the feature. If the misclassification increases then it is apparent the feature had a significant effect on being able to determine humans walking versus vehicles. For this test the 4 algorithms with the least amount of misclassification are used to evaluate the effectiveness of each feature.

Table 7.9: Confusion matrix showing results for the learning algorithms without the micro-Doppler maximum. Compare the results to Table 7.8.

			Predicted	
	Learning Algorithm		Vehicle	Human
Actual	Tree Bagger	Vehicle	26301	41
		Human	47	133199
	K-Nearest Neighbors	Vehicle	26262	80
		Human	131	133115
	Classification Tree	Vehicle	26274	68
		Human	85	133161
	Mahalanobis	Vehicle	23387	2955
		Human	158	133088

7.4.1 Micro-Doppler Maximum

The micro-Doppler maximum was removed from the feature vector of both the training and test data. The results are shown in Table 7.9. All learning algorithms preformed worse when measured for misclassification. The bagged tree and KNN had extremely low error with all features present. However once the Doppler maximum was removed the prediction error increased many times the original error. This increase in error indicates that the Doppler maximum is a feature that provides significant information the algorithms use correctly classify humans and vehicles.

7.4.2 Micro-Doppler Variability

In a similar manner the micro-Doppler variability was removed from the test and training data sets and the learning algorithms were re-trained and the test data was predicted again. Table 7.10 shows the results for the learning algorithms without this feature. The micro-Doppler variability is similar to the micro-Doppler maximum because the misclassification rate increased for all of the algorithms without this feature. This is an indication that this feature has information that can be used to classify an object.

Table 7.10: Confusion matrix showing results for the learning algorithms without the micro-Doppler variability. Compare the results to Table 7.8.

			Predicted	
	Learning Algorithm		Vehicle	Human
Actual	Tree Bagger	Vehicle	26318	24
		Human	15	133231
	K-Nearest Neighbors	Vehicle	26284	58
		Human	60	133186
	Classification Tree	Vehicle	26283	59
		Human	70	133176
	Mahalanobis	Vehicle	25892	450
		Human	2392	130854

7.4.3 Micro-Doppler Bandwidth

The micro-Doppler bandwidth feature was removed from the feature vector and all of the algorithms were re-trained and re-tested. Table 7.11 shows the classification results without the feature. This feature increased the misclassification rate in every learning algorithm but one. However, the increases in mis-classification are less than occurred when the Doppler maximum and Doppler variability were removed from the feature vector. It is difficult to draw any conclusions about how this feature contributes to the correct classification.

7.4.4 Micro-Doppler Span

Next the micro-Doppler span was removed from the training and test data and the algorithms were re-trained and re-tested. Table 7.12 shows the results of the learning algorithms without the minimum maximum data. This feature produced mixed results with some of the learning algorithms improving prediction and others increasing in error. Bagged tree had the same amount of mis-classification, while classification tree and Mahalanobis had less misclassification and K-Nearest Neighbors had greater misclassification. These trends suggest this is a weak feature.

Table 7.11: Confusion matrix showing results for the learning algorithms without the micro-Doppler bandwidth. Compare the results to Table 7.8.

				Predicted	
	Learning Algorithm			Vehicle	Human
Actual	Tree Bagger		Vehicle	26332	10
			Human	7	133239
	K-Nearest Neighbors		Vehicle	26339	3
			Human	22	133224
	Classification Tree		Vehicle	26331	11
			Human	18	133228
	Mahalanobis		Vehicle	24731	1611
			Human	1200	132046

Table 7.12: Confusion matrix showing results for the learning algorithms without the micro-Doppler min max data. Compare the results to Table 7.8.

				Predicted	
	Learning Algorithm			Vehicle	Human
Actual	Tree Bagger		Vehicle	26342	0
			Human	3	133243
	K-Nearest Neighbors		Vehicle	26338	4
			Human	10	133236
	Classification Tree		Vehicle	26325	17
			Human	14	133232
	Mahalanobis		Vehicle	25763	579
			Human	315	132931

7.4.5 Chapter Summary

Prior to running the feature analysis experiment, it was assumed the performance of all of the learning algorithms would degrade. However, this was not always the case. In some cases degradation occurred and in other cases improvement occurred. From the results each learning algorithm responded slightly different to the information each feature provided. This makes it

Table 7.13: Summary of the total misclassification error that occurs in the learning algorithms when a particular feature is removed from the feature vector.

Algorithm	All Features	Maximum	Variability	Bandwidth	Span
Bagged Tree	3	88	39	17	3
KNN	4	211	118	25	14
Classification Tree	34	153	129	29	31
Mahalanobis	1028	3113	2842	2811	894

difficult to judge the effectiveness of a feature across all learning algorithms. However a few features caused more misclassification among the majority of the algorithms when removed. Those features were: micro-Doppler mean and micro-Doppler variability. These micro-Doppler features provide the most information in classifying between these two classes of objects.

CHAPTER 8.   CONCLUSION

8.1   Summary

A radar system provides sensing capability about an object in its field of view. At its most basic level the radar can measure an object's range and Doppler shift due to motion using the transmitted signal and the received echo.

The radar is able to measure is an object's micro-Doppler signature. Micro-Doppler results from small motions. The micro-Doppler signature of the object is a combination of all small motions of the object. The micro-Doppler signatures of objects differ based how an object moves and the parts of the object in motion. Because objects move in different manners, the micro-Doppler signature is a differentiating characteristic. For example, humans walking and vehicles have different micro-Doppler signatures because they move differently and contain different parts in motion while moving.

The micro-Doppler signature can be used to represent and differentiate objects. Information is extracted out of the micro-Doppler signature using a feature-based technique. This thesis explores a simple set of features that can be used to represent the micro-Doppler signature of humans walking and vehicles. This set of features is the micro-Doppler maximum, micro-Doppler variability, micro-Doppler bandwidth, and the micro-Doppler span. Because the two classes of objects of interest have micro-Doppler signatures that are different, this simple set of features are adequate at differentiating an object's class.

To test and validate this simple feature set, data was collected using an experimental radar system built for experiments in micro-Doppler for this thesis. The micro-Doppler signatures of humans walking and vehicles traveling were captured in the collected radar data and the features of interest were extracted from those signatures. Each feature was analyzed using the data captured from the radar system. Each feature separated humans and vehicles to some degree. That

102

separation was measured through the probability of detection and the probability of false alarm for each of the object classes.

The features are placed in a feature vector for each instance in time. The micro-Doppler signature was used to distinguish a human walking and a vehicle traveling. The information from the features can be used in learning algorithms to predict and classify future objects seen by the radar. Most learning algorithms seem to perform well with the set of four features extracted from the data collected by the experimental radar system. The learning algorithms with the least amount of misclassification error are tree-bagger, KNN, and regression tree.

8.2   Contributions

This thesis offers a different perspective on using micro-Doppler features to differentiate different classes of objects. Many of the schemes to extract information from micro-Doppler signatures are complex. For this thesis with constrained classes of targets, very simple features could be used that yield very good results. This emphasizes the robustness of a radar's ability to measure the micro-Doppler signature and the uniqueness the signature provides. A complex feature set may not be required to provide useful information.

An analysis of the micro-Doppler features considered was presented in this thesis. The micro-Doppler maximum, micro-Doppler variability, micro-Doppler bandwidth, and micro-Doppler span were the simple set of micro-Doppler features. Information is provided on how these features performed on the collected radar data.

The data from an experimental radar system was collected for various objects. Actual data was used as a method of validation and testing.

A variety of commonly used learning algorithms were implemented and tested. These learning algorithms performance are compared. These results provide some insight into the learning algorithms performance with this type of data.

8.3   Future Work

This section outlines possible future work in the area of radar micro-Doppler signature analysis. Future work includes the decomposition of micro-Doppler signatures, increased anal-

ysis of different classes of objects, radar independent learning algorithms and features, and time evolving analysis.

8.3.1 Decomposition of Micro-Doppler Signatures

As described in Chapter 3, the micro-Doppler is comprised of basic micro-motions. Because the signature is a composition of fundamental motions, it might be valuable to attempt to decompose the micro-Doppler signature into the individual motions which created the signature. Some of the four features that were selected for the analysis in this thesis possibly have some relation to the fundamental motions of the micro-Doppler signatures. However, its relation is distant and the information the features provide about the fundamental motions are limited.

If the micro-Doppler signature of a human walking were dissected into its fundamental components, one decomposition would be comprised of four pendulum motions with an articulating trunk representing a simplified model of the arms, legs and torso of a walking human. The decomposition of a micro-Doppler signature becomes difficult due to the complexity of some of the micro-motions. However, this dissection of the signature could prove useful for classification and analysis.

8.3.2 Increased Analysis of Different Classes

This thesis explored a limited a number of objects, constrained to vehicles and humans. There are countless types of objects that have interesting micro-Doppler signatures. Future work to understand the micro-Doppler signatures of a broad class of objects is critical.

8.3.3 Radar Independent Learning Algorithms

One current limitation of the analysis of micro-Doppler is that the some of the features selected and the work performed in training for one particular radar does not carry over to another radar. Every radar is slightly different and the Doppler shift changes as the frequency of the radar changes. These differences make some of the work done on one radar system incompatible with another. This results in time and resources to select features and train a new radar system. New data must be collected and the system re-trained with the new data. This process could potentially

be automated. Future work could be done to address the issue of incompatibility of micro-Doppler analysis from radar to radar.

8.3.4 Time Evolving Analysis

One method of analysis not considered in this thesis is the time evolution of the micro-Doppler signature. Similar to human speech, the micro-Doppler signature evolves over time. Information can be extracted from the evolution with time for an increased understanding of the micro-Doppler signature and the object. The evolution of the signature can be used to increase the accuracy of the analysis and the classification.

REFERENCES

[1] M. A. Richards, *Fundamentals of Radar Signal Processing*, 1st ed.   New York: McGraw-Hill, 2005.

[2] "Time frequency tool box," Online, 2013. [Online]. Available: +http://tftb.nongnu.org/

[3] V. C. Chen and H. Ling, *Time Frequency for Radar Imaging and Signal Analysis*, 1st ed.   685 Canton Street, Norwood, MA 02062: Artech House, 2002.

[4] V. C. Chen, *The Micro-Doppler Effect in Radar*, 1st ed.   685 Canton Street, Norwood, MA 02062: Artech House, 2011.

[5] D. Tahmoush, J. Silvious, and J. Clark, "An ugs radar with micro-doppler capabilities for wide area persistent surveillance," pp. 766 904–766 904–11, 2010. [Online]. Available: +http://dx.doi.org/10.1117/12.848233

[6] M. G. Anderson, "Design of multiple frequency continuous wave radar hardware and micro-doppler based detection and classification algorithms," Ph.D. dissertation, University of Texas at Austin, 2008.

[7] A. Ghaleb, L. Vignaud, and J.-M. Nicolas, "Micro-doppler analysis of pedestrians in isar imaging," in *Radar Conference, 2008. RADAR '08. IEEE*, 2008, pp. 1–5.

[8] V. Chen, F. Li, S. Ho, and H. Wechsler, "Micro-doppler effect in radar: phenomenon, model, and simulation study," *Aerospace and Electronic Systems, IEEE Transactions on*, vol. 42, no. 1, pp. 2–21, 2006.

[9] Y. Li, L. Du, and H. Liu, "Moving vehicle classification based on micro-doppler signature," in *Signal Processing, Communications and Computing (ICSPCC), 2011 IEEE International Conference on*, 2011, pp. 1–4.

[10] Online, 2013. [Online]. Available: +http://www.armyrecognition.com/images/stories/north_america/united_states/main_battle_tank/m1a1_abrams/pictures/m1a1_Abrams_Main_Battle_Tank_USA_united_states_050.jpg

[11] Y. Kim and H. Ling, "Human activity classification based on micro-doppler signatures using a support vector machine," *Geoscience and Remote Sensing, IEEE Transactions on*, vol. 47, no. 5, pp. 1328–1337, 2009.

[12] D. Tahmoush and J. Silvious, "Time-integrated range-doppler maps for visualizing and classifying radar data," in *Radar Conference (RADAR), 2011 IEEE*, 2011, pp. 372–374.

[13] Y. Kim and H. Ling, "Human activity classification based on micro-doppler signatures using an artificial neural network," in *Antennas and Propagation Society International Symposium, 2008. AP-S 2008. IEEE*, 2008, pp. 1–4.

[14] MATHWORKS, "The statistics toolbox for Matlab and Simulink," Online, 24 Prime Park Way, Natick, MA 01760, 2013.

[15] T. M. Mitchell, *Machine Learning*, 1st ed. McGraw-Hill, 1997.